DEFINING A MULTI-PARAMETER OPTICS-BASED APPROACH FOR ESTIMATING CHLOROPHYLL *A* CONCENTRATION USING OCEAN GLIDERS

by

Matthew Beck

Submitted in partial fulfilment of the requirements
for the degree of Master of Science

at

Dalhousie University
Halifax, Nova Scotia
January 2016

DEDICATION PAGE

For my parents

TABLE OF CONTENTS

LIST OF TABLES

LIST OF FIGURES

ABSTRACT

A bio-optical method for increasing the accuracy of chlorophyll *a* estimates from *in situ* fluorometers in the absence of traditional validation methods was implemented for autonomous gliders operating on the Scotian Shelf. The method generates a dynamic fluorescence-to-chlorophyll *a* conversion factor (*F*-factor) designed to account for bio-optical variability in the phytoplankton assemblage. Several changes were made to the method, allowing for the retention and analysis of depth-resolved information in the *F*-factor relationship. Trends in the *F*-factor with depth were driven by the bio-optical properties of the phytoplankton community, while horizontal trends were driven by the influence of coloured dissolved organic matter in the nearshore region of the study site. Variability in the *F*-factor within and between profiles introduced artifactual pattern into estimates of chlorophyll *a*, leading to a recommendation that the bio-optical method under investigation not be implemented for gliders on the Scotian Shelf.

LIST OF ABBREVIATIONS AND SYMBOLS USED

Abbreviation	Description	Units
$a(\lambda)$	Absorption coefficient	m^{-1}
$\overline{a^*_{\mathrm{chl}}}$	Chlorophyll *a*-specific absorption coefficient spectrally-averaged over the PAR wavebands	$\mathrm{m}^2 \cdot (\mathrm{mg\ Chl})^{-1}$
$A(z)$	A variable representing the downwelling irradiance at depth z after accounting for attenuation due to substances other than water	dimensionless
$\hat{A}(z)$	Predicted value of $A(z)$ as determined by the fit of the $A(z)$ vs $C(z)$ regression	
AOP	Apparent Optical Property	-
AUV	Autonomous Underwater Vehicle	-
AZMP	Atlantic Zone Monitoring Program; a long-term study of the Atlantic Ocean surrounding the Eastern coast of Canada, conducted by the Department of Fisheries and Oceans (DFO) Canada	-
$b(\lambda)$	Scattering coefficient	m^{-1}
$b_{\mathrm{b}}(\lambda)$	Backscattering coefficient	m^{-1}
$b_{\mathrm{bp}}(\lambda)$	Particulate backscattering coefficient	m^{-1}
$\beta(124^{\circ}, \lambda)$	Value for the volume scattering function for wavelength λ at 124°	$\mathrm{m}^{-1} \cdot \mathrm{sr}^{-1}$
CDOM	Coloured Dissolved Organic Matter	ppb
$\mathrm{CDOM}_{\mathrm{adj}}$	Remaining CDOM signal after subtracting a mission-specific "background" CDOM value	ppb
$\mathrm{CDOM}_{\mathrm{adj}}\vert_{z_{\mathrm{max}}}^{z_{\mathrm{min}}}$	Remaining CDOM signal after subtracting a mission-specific "background" CDOM value, averaged over the depth interval of z_{min} to z_{max}	ppb
$C(z)$	A variable representing the cumulative attenuation of light from the surface to depth z attributable to $Chla$ and its covarying substances, as represented by $fluor$ counts.	dimensionless
$\chi(\lambda)$	Coefficient describing the empirical relationship between K_{d} and $Chla$ at wavelength λ	units vary with wavelength

$Chla$	Concentration of chlorophyll *a*	$\mathrm{mg\ Chl \cdot m^{-3}}$
$Chla(z')$	$Chla$ assigned to the depth range of $(z' - \Delta z')$ to z' for each depth stratum between the surface and depth z	$\mathrm{mg\ Chl \cdot m^{-3}}$
$Chla\|_{z_{\mathrm{max}}}^{z_{\mathrm{min}}}$	Concentration of chlorophyll *a*, averaged over the depth interval of z_{min} to z_{max}	$\mathrm{mg\ Chl \cdot m^{-3}}$
CV	Coefficient of variation	-
CZCS	Coastal Zone Color Scanner	-
DFO	Department of Fisheries and Oceans, Canada	-
$\mathrm{e}(\lambda)$	Coefficient describing the empirical relationship between K_{d} and $Chla$ at wavelength λ	dimensionless
$E_{\mathrm{d}}(\lambda)$	Downwelling irradiance at wavelength λ	$\mathrm{\mu W \cdot cm^{-2}\ \cdot nm^{-1}}$
$E_{kQ}(490)$	Saturation irradiance for the $\mathrm{NPQ_{corr}}$ versus $E_{\mathrm{d}}(\lambda)$ at z_{min} curve fit	$\mathrm{\mu W \cdot cm^{-2}\ \cdot nm^{-1}}$
$E_0(\mathrm{PAR})$	Scalar irradiance over the PAR waveband	$\mathrm{\mu mol\ photons \cdot m^{-2} \cdot s^{-1}}$
F, F-factor	Conversion factor for *fluor* to *Chla*	$\mathrm{mg\ Chl \cdot m^{-3} \cdot count^{-1}}$
$F(i)$	Full-profile *F*-factor for profile *i*	$\mathrm{mg\ Chl \cdot m^{-3} \cdot count^{-1}}$
$F(i, \zeta)$	*F*-factor for profile *i*, corresponding to optical depth ζ	$\mathrm{mg\ Chl \cdot m^{-3} \cdot count^{-1}}$
$Fluor_{\mathrm{chl}}$	Chlorophyll *a* fluorescence	$\mathrm{\mu mol\ photons \cdot m^{-3} \cdot s^{-1}}$
$fluor$	Chlorophyll *a* fluorescence as measured by an *in situ* fluorometer	counts
$fluor(z')$	$fluor$ assigned to the depth range of $(z' - \Delta z')$ to z' for each depth stratum between the surface and depth z	counts
$\overline{fluor}(z_{\mathrm{min}}, z-1)$	The average chlorophyll *a* fluorescence over the depth interval z_{min} to $(z-1)$	counts
IOP	Inherent Optical Property	-
$K_{\mathrm{bio}}(\lambda)$	The portion of the diffuse attenuation coefficient (K_{d}) attributable to biological constituents	$\mathrm{m^{-1}}$
$K_{\mathrm{d}}(\lambda)$	Diffuse attenuation coefficient for downwelling irradiance	$\mathrm{m^{-1}}$
$\overline{K}_{\mathrm{d}}(\lambda)$	An average, per-profile K_{d} calculated for the depth interval of	$\mathrm{m^{-1}}$

	$z_{\min}$ to $z_{\max}$	
$K_{\mathrm{w}}(\lambda)$	The portion of the diffuse attenuation coefficient (K_{d}) attributable to pure water	m^{-1}
$K_{\mathrm{d}}(\lambda, z')$	The diffuse attenuation coefficient assigned to the depth range of $(z' - \Delta z')$ to z' for each depth stratum between the surface and depth z	m^{-1}
MLD	Mixed Layer Depth	m
MODIS	Moderate-Resolution Imaging Spectroradiometer	-
NPQ	Non-Photochemical Quenching	-
$\mathrm{NPQ}_{\mathrm{corr}}$	The percentage of NPQ calculated at $z_{\min}$ for a given profile	%
$\mathrm{NPQ}_{\max}$	Maximum nonphotochemical quenching for the $\mathrm{NPQ}_{\mathrm{corr}}$ versus $E_{\mathrm{d}}(\lambda)$ at $z_{\min}$ curve fit	%
OTN	Ocean Tracking Network	-
PAR	Photosynthetically Available Radiation, integrated over the 400-700 nm waveband	$\mu\mathrm{mol\ photons} \cdot \mathrm{m}^{-2} \cdot \mathrm{s}^{-1}$
PSI, PSII	Photosystems I and II	-
PQ	Photochemical Quenching	-
Q_a^*	Proportion of fluoresced photons that are reabsorbed by the phytoplankton	dimensionless
qE	Energy-dependent NPQ	-
qI	NPQ associated with the photoinhibition of photosynthesis	-
ϕ_F	Quantum yield of fluorescence	$\mathrm{mol\ photon\ emitted} \cdot (\mathrm{mol\ photon\ absorbed})^{-1}$
RFB(*i*,*z*)	The ratio of $fluor$ to $b_{\mathrm{bp}}(660)$ used to correct for the effects of NPQ in profile *i* at depth *z*	$\mathrm{counts} \cdot \mathrm{m}$
$S(i)$	The slope of the linear, full-profile $A(z)$ versus $C(z)$ relationship for profile *i*	dimensionless
$S(i, \zeta)$	The slope of the linear, per-optical depth $A(z)$ versus $C(z)$ relationship for profile *i* and optical depth ζ.	dimensionless
S08	Sackmann et al. (2008)	-
X11	Xing et al. (2011)	-
z	Depth	m
z'	The depth of the current depth	m

	stratum under consideration in an $A(z)$ versus $C(z)$ profile	
$\Delta z'$	The width of the current depth stratum under consideration in an $A(z)$ versus $C(z)$ profile	m
$z_{\min}$	The minimum depth included in the analysis of a profile	m
$z_{\max}$	The maximum depth included in the analysis of a profile	m
z_ζ	The depth of the lower limit of optical depth ζ	m
ζ	Optical depth; equal to $K_\mathrm{d} \cdot z$	dimensionless

ACKNOWLEDGEMENTS

First and foremost I would like to thank my supervisor, Dr. John Cullen, for all of his critical insight, guidance, advice, and patience through this entire process. I wouldn't be where I am today if he hadn't provided me with this opportunity and I'll always be grateful for his mentorship. An additional thank you goes out to my examining committee, Dr. Marlon Lewis and Dr. Mike Dowd, as well as my external examiner Dr. Emmanuel Devred and reader Dr. Christopher Algar, who provided crucial input on numerous topics in order to improve the quality of this thesis.

I would also like to thank the entire Ocean Tracking Network glider team who have provided invaluable support over the years – most especially Richard Davis, Adam Comeau, and Jonathan Pye, but also Sue L'Orsa, Brad Covey, and all of the individuals who have moved through the glider group over the last few years. They not only managed all of the mission logistics, but contributed in countless other ways including instruction in oceanographic concepts, editing of posters and presentations, and by helping me navigate the wonderful and zany world of MATLAB.

A special thank you goes out to the people who are closest to me – my family, my girlfriend Tonya, and my friends. Your support and motivation kept me going, and somehow managed to keep me sane while doing it. Thank you for keeping me afloat by being the inflatable air bladder to my metaphorical ocean glider.

A final, more formal thank you goes out to Dalhousie University, as well as the providers of funding support for my work – NSERC, through the Ocean Tracking Network and a Discovery Grant to Dr. John Cullen.

CHAPTER 1 INTRODUCTION

1.1 Autonomous Sampling in Oceanography

A significant leap forward for oceanographic research has been the development of sampling platforms that allow for the collection of scientific data without constant on-site supervision by humans. From the launch of the satellite-born Coastal Zone Color Scanner (CZCS) in the 1970s (Hovis et al. 1980), to the deployment of the Argo Lagrangian buoy fleet in the 2000s (Feder 2000), to the development of more versatile Autonomous Underwater Vehicles (AUVs) such as gliders (Eriksen et al. 2001), autonomous platforms are becoming more diverse and more prevalent with each passing year (Dickey and Bidigare 2005; Dickey et al. 2008; Johnson et al. 2009).

The principal advantage of autonomous platforms is the increased spatial- and temporal resolution of sampling regimes when compared with traditional ship-based methods (Dickey et al. 2006; Perry et al. 2008; Johnson et al. 2009). The scales of oceanographic processes range over 10 orders of magnitude, from the molecular to the ocean basin and from milliseconds to millennia (Stommel 1963; Dickey 1991; Karl 2014), and under-sampling due to the logistics of ship-based methodologies has historically imposed fundamental limitations to understanding their patterns (Munk 2000; Dickey and Bidigare 2005; Dickey et al. 2008). By necessity, a research cruise must limit its efforts in space to a transect-based sub-sampling of a region and then use interpolation and extrapolation to describe any spatial patterns in its data. Additionally, ship-based observations are generally constrained in time to scales of hours to days at any one site and possibly up to weeks over a transect; patterns found during those sampling periods are not necessarily representative of other seasons or years for that region. Comparatively, a satellite-based sensor such as the Moderate-Resolution Imaging Spectroradiometer (MODIS) can scan the entire surface of the earth every one to two days and provide a comprehensive snapshot of the state of the world's oceans, but only for a shallow surface layer of the ocean (Lindsey and Herring 2002). In-water autonomous platforms fill a niche between these sampling methods – they provide *in situ* matchup/validation for satellite-borne measurements in the surface layer (for example

Boss et al. 2008), as well as sample the ocean interior at a higher horizontal resolution than traditional ship-based methods. The ability to study our oceans with such enhanced spatiotemporal resolution and scope through the use of autonomous platforms is invaluable. It not only allows us to study known phenomena at higher levels of scrutiny, it also has the potential to reveal phenomena that had previously gone unnoticed, having ‘‘fallen through the loose net of traditional sampling’’(Munk 2000).

Autonomous platforms come with significant inherent drawbacks, however. Biofouling, mechanical failures during extended deployments without maintenance, and the limited number of parameters that can be measured due to space and battery constraints are all difficulties that must be dealt with (Dickey & Bidigare 2005; Dickey et al. 2006 and references contained therein). Additional problems arise when using optical instrumentation to investigate biological properties, as these instruments typically rely on proxies to estimate the variable of interest rather than measuring that variable directly, thereby depending on an optical-biological conversion that is inherently imprecise. An example of this is the use of *in situ* fluorometers to estimate chlorophyll *a* concentration ($Chla$, $\mathrm{mg\,Chl \cdot m^{-3}}$). Chlorophyll *a* fluorescence is a common optical proxy used for bulk estimation of the biomass of phytoplankton in the ocean, and an important measurement when determining the productivity of a body of water despite being a direct measurement of neither $Chla$ nor biomass (Cullen 1982; Bot and Colijn 1996; Huot and Babin 2010). Optical proxies such as chlorophyll *a* fluorescence are widely used because they allow rapid and inexpensive sampling at high spatiotemporal resolution – two traits that are not typical of traditional water sample-based methods for measuring biological variables. The use of optical proxies to obtain high-resolution data has a trade-off however, as it introduces an additional layer of error and uncertainty when calculating the final product (Boss et al. 2008). These uncertainties can be reduced when optical measurements are accompanied by a ship-based sampling regime, as the optical measurements of the proxy can be compared to coincident water-based measurements of the true variable to generate a localised calibration (see for example Cullen and Lewis 1995). The difficulty arises when an autonomous platform operates for extended periods of time without any on-site human supervision, and this traditional approach to validation is not possible.

In order to address the lack of on-site validation when using autonomous platforms, alternative methods of calibration and validation have been developed, involving more intensive pre- and post-mission calibrations (Cetinić et al. 2009; Proctor and Roesler 2010) or the match-up of multiple optical sensors for cross-validation (Boss et al. 2008; Xing et al. 2011; Lavigne et al. 2012). These latter, multivariate optical approaches seem promising for ensuring that high-resolution autonomous sampling platforms are recording bio-optical data as accurately as possible, but considerable development is required before multivariate optical calibration is routine. This thesis focuses on the problem of ensuring the accuracy of bio-optical estimates made by autonomous sampling platforms that operate outside the ranges of traditional validation methods. Specifically, this work addresses the estimation of $Chla$ based on measurements of *in situ* fluorescence using sensors on Slocum electric gliders operating on the Scotian Shelf of the Northwest Atlantic Ocean. The general objectives of this thesis are:

1. To apply an established bio-optical method for increasing the accuracy of fluorescence-based estimates of $Chla$ in the absence of traditional ship-based validation methods to a glider dataset from the Scotian Shelf.
2. To investigate the assumptions inherent to the method when applied in this context and, where necessary, modify the method if flaws in those assumptions are found.

Specific objectives will be presented at the end of this chapter, after the benefits and limits of the fluorometric detection of chlorophyll *a* are outlined in the sections below, along with pertinent background theory and discussion of issues relevant to the implementation and validation of this technique in the context of autonomous sampling.

1.2 Phytoplankton: Their Importance and Method of Estimation

Phytoplankton are photosynthetic aquatic microbes responsible for approximately half of Earth's primary productivity (Behrenfeld et al. 2001). They fill a crucial ecological role as the base of the marine food web and, consequently, measures of phytoplankton biomass are used to describe the status and dynamics of ocean ecosystems. Estimates of phytoplankton concentration are often incorporated into applications such as primary productivity calculations (Ryther and Yentsch 1957; Kolber and Falkowski

1993), biogeochemical ocean general circulation models (Friedrichs et al. 2009), and discussions of how ocean ecosystems have responded to fluctuations in global climate (Boyce et al. 2010; Rousseaux and Gregg 2014). It is therefore critical that estimates of phytoplankton concentration be as accurate as possible in order to increase the confidence of these values when incorporated into the above applications.

The biomass of phytoplankton can be quantified through measurements of nitrogen (Geider et al. 1998), phosphorus (Perry and Eppley 1981), or organic carbon content (Banse 1977; Geider et al. 1998; Sathyendranath et al. 2009). The methods involved in quantifying these elements are typically time consuming however, and it is difficult to isolate the variable contribution of phytoplankton to the total particulate matter for each element without utilising indirect methods (Banse 1977; Cullen 1982; Eppley et al. 1992; Sathyendranath et al. 2009; Graff et al. 2012). Consequently, it is common to estimate phytoplankton biomass by measuring the concentration of chlorophyll *a* (Eppley 1972; Banse 1977; Cullen 1982; Huot et al. 2007; Boyce et al. 2010), a photosynthetic pigment which is found in all phytoplankton but is not produced in other organisms. Chlorophyll *a* is used as a proxy for biomass despite the fact that it represents only a small and variable proportion of the organic carbon content of phytoplankton: the ratio of carbon to chlorophyll can vary by a factor of up to 25 (from a ratio of approximately 10:1 to 250:1 by weight) due to taxonomic influences and the combined effects of environmental factors such as temperature, irradiance and nutrient status (Eppley 1972; Cullen 1982; Cloern et al. 1995; Geider et al. 1998).

There are several ways to measure *Chla* in a laboratory setting, which generally involve collecting particulate material on a filter, extracting it in solvent, and using a detection method to estimate the concentration of pigment based on its optical and chemical properties. Methods include high performance liquid chromatography (HPLC; Ras et al. 2008), spectrophotometry (Lorenzen 1967), and *in vitro* fluorometry (Holm-Hansen et al. 1965). Continuous at-sea measurements of chlorophyll *a* fluorescence, an improvement over the requirement to obtain water samples for later analysis of *in vitro Chla*, became possible when the benchtop fluorometric method was adapted to create a flow-through *in vivo* fluorometry setup that could be used on ships while underway during cruises or in vertical profiles using a pump and hose (Lorenzen 1966). Modern

fluorometers measure chlorophyll *a* fluorescence *in situ* (see for example Derenbach et al. 1979), and compact fluorometers are now deployed routinely on a variety of sampling platforms, including autonomous vehicles (for a review of modern sampling platforms and their associated instrumentation, spanning from ships to gliders, see Dickey et al. 2006). This work will focus on the *in situ* measurement of chlorophyll *a* fluorescence, the principles of which are outlined below in Section 1.3.

1.3 Chlorophyll *a* Fluorescence

1.3.1 Theoretical Background and Determination

There are three fates for a photon once it is absorbed by the photosynthetic apparatus of phytoplankton: it can be utilized in photosynthesis, it can be dissipated as heat, or it can be emitted as fluorescence (see summaries by Krause and Weis 1991; Huot and Babin 2010). Fluorescence occurs when absorbed light stimulates chlorophyll *a*, either directly or through its accessory pigments, exciting electrons to energy levels higher than their resting state. These so-called excitons are passed to the photosynthetic reaction centers PSII and PSI, which are chlorophyll *a*-containing protein complexes within the algal cell, where they can fall back to their initial resting states and emit photons of a lower energy than the photons that were initially absorbed. The re-emission of these photons from the chlorophyll *a* molecule, which are mostly in the red band of the light spectrum and originate primarily from PSII at environmental temperatures (Falkowski and Kiefer 1985), is known as chlorophyll *a* fluorescence (Krause and Weis 1991; Huot and Babin 2010).

The amount of fluorescence emitted by this process ($Fluor_{\mathrm{chl}}$, $\mu\mathrm{mol\ photons\ m^{-3}\ s^{-1}}$) can be described generally using the following equation (Babin et al. 1996b):

$$Fluor_{\mathrm{chl}} = E_0(PAR) \cdot Chla \cdot \overline{a^*_{\mathrm{chl}}} \cdot Q^*_a \cdot \phi_F \qquad (1.1)$$

where $E_0(PAR)$ is the scalar irradiance integrated over the PAR (Photosynthetically Available Radiation) wavebands (400-700 nm; $\mu\mathrm{mol\ photons\ m^{-2}\ s^{-1}}$), $Chla$ is the

concentration of chlorophyll *a* ($\mathrm{mg\,Chl \cdot m^{-3}}$), $\overline{a^*_{\mathrm{chl}}}$ is the chlorophyll *a*-specific absorption coefficient spectrally-averaged over the PAR wavebands ($\mathrm{m^2 \cdot (mg\,Chl)^{-1}}$), Q_a^* is the proportion of fluoresced photons that are reabsorbed by the phytoplankton (unitless), and ϕ_F is the quantum yield of fluorescence ($\mathrm{mol\ photon\ emitted\ (mol\ photon\ absorbed)^{-1}}$). This process occurs naturally in the ocean (sun-induced chlorophyll *a* fluorescence; see Morel and Prieur 1977 and Babin et al. 1996b), but it can be artificially induced using a fluorometer by stimulating chlorophyll-containing organisms with blue light (the fluorometers used in this study excite using light at 470 nm, with a 70 nm bandwidth filter) and then measuring the amount of red light that they emit (the fluorometers used in this study measure light at 695 nm, with a 70 nm bandwidth filter). Since conventional *in vivo* fluorometers measure the fluorescence emitted in response to a constant light source, $E_0(PAR)$ becomes a constant and changes in $Fluor_{\mathrm{chl}}$ relative to *Chla* become attributable to the product $[\overline{a^*_{\mathrm{chl}}} \cdot Q_a^* \cdot \phi_F]$. This product is largely variable in the natural environment (Kiefer 1973a; Falkowski and Kiefer 1985; Babin et al. 1996b), with values for $\overline{a^*_{\mathrm{chl}}}$ and Q_a^* varying by up to an order of magnitude (Bricaud et al. 1995; Babin et al. 1996b), and ϕ_F representing only a small and variable percentage of the fate of absorbed photons (on the order of 1 to 2% of light absorbed; Huot and Babin 2010). However, measurements of artificially-induced fluorescence using an *in vivo* fluorometer alone are insufficient for discerning the independent contributions of the terms in the $[\overline{a^*_{\mathrm{chl}}} \cdot Q_a^* \cdot \phi_F]$ product. In addition, the fluorescence output of an *in vivo* fluorometer is not typically expressed in terms of ($\mathrm{\mu mol\ photons\ m^{-3}\ s^{-1}}$), and therefore the $Fluor_{\mathrm{chl}}$ term from Equation 1.1 is replaced here with the term $fluor$ (with units of counts). Equation 1.1, when rearranged to express $Chla$ as a function of the fluorescence output of an *in vivo* fluorometer, is therefore re-written as:

$$Chla = fluor \times F \qquad (1.2)$$

where *F*, (with units of $\mathrm{mg\,Chl \cdot m^{-3} \cdot count^{-1}}$), now represents the conversion factor between $fluor$ and $Chla$, with its value implicitly including the variability encompassed

in the $[\overline{a^*_{\text{chl}}} \cdot Q^*_a \cdot \phi_F]$ product. It should be noted that utilising a static, single *F*-factor as a constant for the fluorometer (for example, the *F*-factor supplied by the manufacturer from its initial calibration) assumes that this relationship is constant, even between taxonomic groups and variable environmental conditions. This is a necessary but large simplification, as numerous factors, which will be elaborated on below, cause variability in the relationship between $Chla$ and $fluor$ (Kiefer 1973b; Huot and Babin 2010). As a result, it is recommended that users generate their own *F*-factors whenever possible (Zeng and Li 2015). This can be accomplished by using phytoplankton samples collected from the study region to generate a calibration curve before or after a deployment (see for example Cetinić et al. 2009), or to use cross-validation with other measurements made in the field during a deployment (see for example Xing et al. 2011). Care should still be taken with these processes, as the choice of calibration standard can introduce a taxonomic bias if the fluorescence yield characteristics of the phytoplankton community being measured in the field are different than what was used for the calibration (Proctor and Roesler 2010; Lawrenz and Richardson 2010).

1.3.2 Sources of Variability in Fluorescence Yield

Variation in the $fluor$ to $Chla$ relationship is caused by a combination of the adaptive differences between species and the acclimation of individuals to their local conditions and stresses. Pigment composition, and by extension the absorption spectra of phytoplankton, differs between taxa. Therefore not all species of phytoplankton are equally responsive to the excitation and emission wavelengths utilised by a given fluorometer, and this introduces a taxonomic bias (Falkowski and Kiefer 1985; MacIntyre et al. 2010; Proctor and Roesler 2010; Lawrenz and Richardson 2010). Even within a species, acclimation to environmental conditions and stressors can cause variability in fluorescence yield, as the relationship is known to be affected by factors such as nutrient supply (Kiefer 1973b; Cleveland and Perry 1987; Kruskopf and Flynn 2006) and irradiance (Kiefer 1973a; Loftus and Seliger 1975; Falkowski and Kiefer 1985; MacIntyre et al. 2002). Combined, these sources of variation can result in up to 10-fold differences in fluorescence yield in both natural populations (Loftus and Seliger 1975) and laboratory monocultures (Proctor and Roesler 2010).

An aspect of irradiance-driven variability in fluorescence yield that deserves elaboration is non-photochemical quenching (NPQ). NPQ is a photoprotective mechanism that activates under high-irradiance conditions, induced when light absorption by the cell is greater than the rate of light utilization, causing fluorescence yield to decrease as an increasingly larger portion of incoming light energy is dissipated as heat (Krause and Weis 1991; Müller et al. 2001). It can be broken down into two components; energy dependent NPQ (qE), which occurs on the timescale of seconds to minutes and can result in a decrease in ϕ_F of up to 90%, and NPQ associated with the photoinhibition of photosynthesis (qI), which occurs on the scale of minutes to hours and can result in a decrease in ϕ_F of up to 40% (Krause and Weis 1991; Huot and Babin 2010). The first component, qE, involves the rapid conversion of light-harvesting xanthophyll pigments into photoprotective xanthophyll pigments via the xanthophyll cycle. These photoprotective pigments compete with chlorophyll *a* for light energy and dissipate that energy as heat, thereby mitigating damage to the photosynthetic apparatus (Demers et al. 1991; Demmig-Adams and Adams 1996). It should be noted, however, that this mechanism is not present in all species of phytoplankton. Cyanobacteria, cryptophytes and the majority of red algae do not contain xanthophyll pigments and therefore cannot use the xanthophyll cycle for photoprotective purposes (Roy et al. 2011 and references contained therein). The second component, qI, is driven primarily by damage to the photosynthetic apparatus (especially PSII) over prolonged exposure to high levels of irradiance, when the rate of damage is greater than the rate of repair despite photoprotective responses (Adir et al. 2003; Huot and Babin 2010). This too causes an increase in light energy being dissipated as heat. It should be emphasised that NPQ differs fundamentally from photochemical quenching (PQ). PQ is a decrease in fluorescence yield due to competition between the fluorescence and photosynthesis pathways in the cell. PQ can be considered in terms of the proportion of open reaction centres in PSII – where open reaction centres are those available to accept photons for photosynthesis – such that an increase in the proportion of open reaction centres causes an increase in the quantum efficiency of photosynthesis and a proportionate decrease in the quantum efficiency of fluorescence (Krause and Weis 1991; Morrison 2003). The effects of PQ are therefore most pronounced at lower levels of irradiance, when a higher

proportion of reaction centres are open, with PQ decreasing as irradiance increases (Morrison 2003). Beyond a threshold irradiance value where the reaction centres become saturated, the effects of PQ on fluorescence yield tend to be dominated by those of NPQ (Schallenberg et al. 2008). In this work, PQ will not be explicitly considered and instead the analysis will focus on the effects of NPQ.

1.3.3 Correcting for Variability in Fluorescence Yield

Since the introduction of the *in vivo* fluorescence method (Lorenzen 1966), attempts have been made to identify and correct for sources of variability in the *fluor* to *Chla* relationship. These include corrections for fluorescence quenching (Cullen and Lewis 1995; Sackmann et al. 2008; Mignot et al. 2011), methods for isolating any confounding contributors to the signal of the instrument, such as from coloured dissolved organic matter (CDOM; Brown et al. 2004; Proctor and Roesler 2010), determining a proper blank and dark background value for the instrument making the fluorescence measurements (Cullen and Davis 2003), and correcting for the effects of environmental conditions such as temperature on the fluorometer (Proctor and Roesler 2010).

A common practice for compensating for the variability in fluorescence yield is to calibrate a fluorometer through the statistical comparison of fluorescence readings with measurements of the concentration of *Chla* from concurrently collected water samples (see for example Cullen and Lewis 1995; Hersh and Leo 2012). Due to the nature of autonomous platforms and floats, which operate for extended periods of time in remote regions without human supervision, maintaining a coincident water sampling regime is neither logistically nor financially feasible. However, the pairing of *in situ* fluorescence with complementary optical measurements from the same platform to obtain independent estimates of *Chla* is an alternative calibration approach (Boss et al. 2008; Xing et al. 2011; Hersh and Leo 2012; Lavigne et al. 2012; Zeng and Li 2015). This method of cross-validation is particularly relevant, as it can be used to generate a dynamic *F*-factor for a fluorometer (the conversion factor for *fluor* to *Chla* in Equation 1.2) capable of accounting for local variations in the fluorescence yield of the phytoplankton community during deployments (Xing et al. 2011). This is the approach adopted for the analyses

presented here, and is described in more detail in Section 1.6 after an explanation below of the optical properties of the ocean and how light interacts with biology.

1.4 Light and the Optical Properties of the Ocean

There are two fates for a photon of light entering the water column – it can be absorbed (represented by the absorption coefficient, a, m^{-1}), or it can be scattered (represented by the scattering coefficient, b, m^{-1}). These properties are known as inherent optical properties (IOPs), meaning they are determined solely by the water and its constituents and do not vary with the incident light field (Preisendorfer 1961; Kirk 2011). Since IOPs are unaffected by the radiance field and thus can be measured either during the day or at night without introducing any bias from solar irradiance (unlike the fluorometric methods described above), a great deal of research has been conducted to relate biological variables to IOPs over the last several decades (Smith and Baker 1978; Morel 1988; Yentsch and Phinney 1989; Fujii et al. 2007). For example, measurements of phytoplankton absorption have been shown to be a useful indicator of chlorophyll *a* concentration and, by extension of that, phytoplankton biomass (Yentsch and Phinney 1989; Cleveland 1995; Bricaud et al. 1998; Roesler and Barnard 2014). Similarly, phytoplankton and the particles that covary with them can be the dominant source of particulate backscatter in the surface waters of the open ocean (Boss et al. 2008 and the comparative studies listed within), allowing particulate backscatter to be used as a proxy for phytoplankton presence (Ahn et al. 1992; Huot et al. 2007). It should be noted, however, that this approach is complicated significantly when non-phytoplankton particles such as bubbles, detrital matter and sediment/inorganic particles, contribute significantly to the optical properties of the region (Boss et al. 2004; Stramski et al. 2004).

The fate of light in the water can also be described by apparent optical properties (AOPs). AOPs are determined by the optical properties of the water and its constituents, but in contrast to IOPs they are also affected by the angular distribution of the light field. The AOP of relevance for this thesis is the diffuse attenuation coefficient ($K(\lambda)$; m^{-1}), and more specifically the diffuse attenuation coefficient for downwelling irradiance ($K_d(\lambda)$; m^{-1}). In either form, $K(\lambda)$ is a measure of the rate of attenuation of light with

depth (Kirk 2011). Downwelling irradiance ($E_{\mathrm{d}}(\lambda, z)$; $\mu\mathrm{W} \cdot \mathrm{cm}^{-2} \cdot \mathrm{nm}^{-1}$) decays with increasing depth in the water column as a function of $K_{\mathrm{d}}(\lambda)$ which, assuming a constant $K_{\mathrm{d}}(\lambda)$ over that depth interval, can be expressed as:

$$E_{\mathrm{d}}(\lambda, z) = E_{\mathrm{d}}(\lambda, 0) \cdot \mathrm{e}^{-K_{\mathrm{d}}(\lambda) \cdot z} \quad (1.4)$$

where z is depth, $E_{\mathrm{d}}(\lambda, z)$ is downwelling irradiance at depth z and wavelength λ, $E_d(\lambda, 0)$ is downwelling irradiance measured just below the surface of the water at wavelength λ, and $K_{\mathrm{d}}(\lambda)$ is the diffuse downwelling attenuation coefficient at wavelength λ over the depth interval of $0 \rightarrow z$. $K_{\mathrm{d}}(\lambda)$ can then be calculated from $E_{\mathrm{d}}(\lambda, z)$ measurements over this interval by rearranging Equation 1.4 into:

$$K_{\mathrm{d}}(\lambda) = \frac{\ln(E_{\mathrm{d}}(\lambda, 0)) - \ln(E_{\mathrm{d}}(\lambda, z))}{z} \quad (1.5)$$

By studying the spectral patterns of light attenuation it is possible to estimate the concentrations of different constituents in a body of water, due to water and its major constituents preferentially attenuating different wavelengths of light (Baker and Smith 1982; Morel 1988; Ciotti et al. 1999; Brown et al. 2004). Generally, water attenuates strongly in the red part of the spectrum (Morel and Prieur 1977; Pope and Fry 1997), CDOM attenuates strongly in the blue part of the spectrum (see summary of values by Roesler et al. 1989), and phytoplankton have variable attenuation through the visible spectrum dependent on their pigment composition, with strong peaks in the red and the blue caused by the presence of chlorophyll *a* and accessory pigments (MacIntyre et al. 2010). This predictable interaction of the light field with the water and its constituents makes the spectral analysis of attenuation a useful tool in oceanographic research, and allows for a synthesis of the fields of optics and biology.

1.5 The Interaction between Light and Biology

In order to better characterise water masses based on their bio-optical properties, the waters of the ocean were divided into two broad classes: Case 1 waters, where the optical properties are dominated by, and covary with, phytoplankton and their derivatives; and Case 2 waters, where sediments and dissolved organic material contribute significantly to optical patterns and vary independently from phytoplankton (Morel and Prieur 1977; Morel 1988). This division is significant, because the covariance of the optical properties with phytoplankton concentration in Case 1 waters allows empirical relationships to be formulated that link optical proxies based on AOPs with *Chla*, phytoplankton biomass, and primary production. This is in contrast to the optically complex Case 2 waters, where sediment and CDOM interfere with attempts to optically derive phytoplankton-related parameters. Central to the problem of CDOM interfering with *Chla* estimates in Case 2 waters is the overlapping absorption spectra of the two variables, which both absorb strongly in the blue range of the visible spectrum (Bukata et al. 2000)

In order to better quantify the optical influences of specific water constituents, the diffuse attenuation coefficient can be divided into sub-components (Smith and Baker 1978; Baker and Smith 1982; Morel 1988). More specifically, K_{d} (analogous to Baker and Smith's K_{T}) can be said to have the following structure:

$$K_{\mathrm{d}}(\lambda) = K_{\mathrm{w}}(\lambda) + K_{\mathrm{ph}}(\lambda) + K_{\mathrm{DOM}}(\lambda) \qquad (1.7)$$

where $K_{\mathrm{w}}(\lambda)$ is the diffuse attenuation coefficient for downwelling light at wavelength λ by pure water, $K_{\mathrm{ph}}(\lambda)$ is the attenuation from phytoplankton and its covarying derivatives at wavelength λ (analogous to Baker and Smith's K_{C}), and $K_{\mathrm{DOM}}(\lambda)$ is the attenuation from the portion of the dissolved organic matter at wavelength λ that does not covary with phytoplankton (analogous to Baker and Smith's K_{D}). When considering Case 1 waters, with the assumption that the optical signal is dominated by phytoplankton and material covarying with phytoplankton, the equation can be simplified to:

$$K_{\mathrm{d}}(\lambda) = K_{\mathrm{w}}(\lambda) + K_{\mathrm{bio}}(\lambda) \qquad (1.8)$$

where $K_{\mathrm{bio}}(\lambda)$ represents attenuation from phytoplankton and biological components covarying with phytoplankton (namely detritus, viruses, bacteria, and dissolved organic matter; Morel 1988; Morel and Maritorena 2001). It should be noted that the additive nature of the $K_{\mathrm{d}}(\lambda)$ components is not guaranteed, especially in environments with high scattering coefficients (Bukata et al. 2000).

The empirical relationships between phytoplankton concentration and light attenuation in the marine environment were investigated rigorously over the last several decades by multiple research groups, some of which have been mentioned above. Of particular importance to this thesis, however, is the work of André Morel. Morel (1988) determined an empirical relationship between *Chla* and $K_{\mathrm{d}}(\lambda)$ over a range of wavelengths and chlorophyll *a* concentrations in Case 1 (oceanic) surface waters, applied as a depth-average from the surface to the bottom of the euphotic zone (in his work, the euphotic zone was defined as the depth at which PAR was reduced to 1% of its value at the surface. It should be noted that this is not an accurate way to define the euphotic depth; see for example Banse (2004)). In Case 1 waters, where the optical constituents are assumed to vary with phytoplankton concentration, $K_{\mathrm{bio}}(\lambda)$ can be expressed as a function of chlorophyll concentration:

$$K_{\mathrm{d}}(\lambda) = K_{\mathrm{w}}(\lambda) + \chi(\lambda) Chla^{\mathrm{e}(\lambda)} \qquad (1.9)$$

where the last term represents $K_{\mathrm{bio}}(\lambda)$, the attenuation of downwelling light by phytoplankton and its covarying biological elements (m^{-1}). The coefficient $\chi(\lambda)$ and exponent $e(\lambda)$ are descriptors of the nonlinear relationship between $K_{\mathrm{bio}}(\lambda)$ and $Chla$ at each wavelength. It must be emphasised that due to the empirical derivation of this relationship from a global data set, the coefficient values determined by Morel (1988) are statistical averages (that were revised in Morel and Maritorena 2001, and again in Morel et al. 2007). Variation between the optical properties of the phytoplankton community, the overall optical properties of the water column, and the measured attenuation of downwelling light, whether caused by physiological differences between taxonomic groups or by environmental effects such as an increased optical contribution of

independently-varying CDOM, will cause deviations from the expected $Chla$ to $K_{\mathrm{d}}(\lambda)$ relationship implicit in the model (Morel 1988; Bricaud et al. 1998). Importantly, as the Morel relationship is derived as a depth-average over the euphotic zone, any systematic differences that exist in the optical structure of the water column with depth will also cause deviations from Morel's average $Chla$ to $K_{\mathrm{d}}(\lambda)$ relationship if the relationship is applied to anything other than surface-layer averages.

The research proposed here will build on a recent example of this effort to reconcile marine optical properties and phytoplankton ecology and physiology, with the objective of increasing the accuracy of fluorescence-based $Chla$ estimates by incorporating the $Chla$-to-$K_{\mathrm{d}}(\lambda)$ relationship outlined above. The work will be based on a method by Xing *et al.* (2011; hereafter referred to as X11) that makes use of the Morel (1988) relationships between $Chla$ and $K_{\mathrm{d}}(\lambda)$ to generate localised calibrations of fluorometric measurements based on the comparison of K_{bio} retrieved from profiles of downwelling irradiance to $fluor$. The specifics of this methodology and how it will be adapted are explained below.

1.6 The Xing *et al*. (2011) Methodology

An important precaution to take when using any *in situ* optical instrument is to ensure it is calibrated properly. Chlorophyll fluorometers specifically can be calibrated using water samples collected from the intended study site, in order to account for variability in the fluorescence yield of the local phytoplankton populations that can cause estimate errors on the order of several hundred percent (Boss et al. 2008; Cetinić et al. 2009). However calibrations performed before and after deployments cannot account for variability in fluorescence yield caused by changes in the taxonomy or physiology of the phytoplankton assemblage during a mission. During this period the researcher might rely on a static conversion factor (whether supplied by the instrument manufacturer or generated during a pre-mission calibration) for converting raw instrument counts into *Chla* estimates (the "*F*" in Equation 1.2), and this static *F*-factor is incapable of accounting for such variability. This is why *in situ* fluorescence measurements are generally paired with coincident water samples. By utilising Morel's work (Morel 1988; with coefficient values updated by Morel and Maritorena 2001, then again by Morel et al.

2007) the X11 method replaces any static F-factor with a dynamic one that is theoretically capable of accounting for variability in the taxonomy and physiology of the phytoplankton assemblage, therefore obviating the need to do on-site calibrations using coincident water samples. This dynamic F-factor is used to address the problem outlined in Section 1.1 of how to calibrate and validate fluorescence-based estimates of $Chla$ from autonomous platforms operating for extended periods of time where coincident water sampling is not possible.

In the following description of the X11 method some minor changes have been made to the X11 notation in order to maintain consistency with the applications that are addressed in this thesis – for the original structure, see Xing et al. (2011).

1.6.1 Local Calibration of Fluorescence Profiles

In order to achieve a dynamic $fluor$ to $Chla$ conversion factor capable of accounting for local variability, the X11 method generates a unique F-factor for each vertical profile during a mission. To do this, X11 evaluates a profile in iterative layers, from the surface to a depth stratum of order n, where each layer is identified with a subscript (e.g., A_n and C_n) and the thickness of each layer is defined by the vertical resolution of the measurements. For clarity, we have modified the notation so that the relationship is defined by absolute depth values rather than sequential values of n. This allows for a more precise means of referencing specific data points within the X11 relationship, as well as for relating patterns in the X11 relationship to their corresponding locations in the water column. This will become especially relevant in later analyses, where depth-dependent trends in this relationship are investigated.

The core of the method is that it combines two different optical relationships to independently estimate $K_{\mathrm{bio}}(\lambda)$, the coefficient describing attenuation of light due to phytoplankton and its covarying substances. The first incorporates the equation for deriving $K_{\mathrm{d}}(\lambda)$ from changes in downwelling irradiance (see Equation 1.4). This allows for a calculation of the cumulative attenuation of downwelling irradiance due to phytoplankton and its covarying substances as one moves down through the water column, based on measurements of $E_{\mathrm{d}}(\lambda)$. This can be expressed in a manner consistent with a natural-log transform of Equation 1.4, where irradiance at depth z, $E_{\mathrm{d}}(\lambda, z)$, is

determined by the irradiance just below the surface, $E_{\mathrm{d}}(\lambda, 0)$, as well as from the accumulated attenuation from the surface to depth z:

$$\ln E_{\mathrm{d}}(\lambda, z) = \ln E_{\mathrm{d}}(\lambda, 0) - \sum_{z' = \Delta z'}^{z} K_{\mathrm{d}}(\lambda, z') \cdot \Delta z' \qquad (1.10)$$

where z' is the depth of the bottom of the current depth stratum, $\Delta z'$ is the width of the current depth stratum, and $K_{\mathrm{d}}(\lambda, z')$ is the diffuse attenuation coefficient assigned to the depth range from $(z' - \Delta z')$ to z' for each depth stratum between the surface and depth z. Note that the summation of z' begins at depth $\Delta z'$ – this is because the method requires an initial interval over which to calculate the first iteration of the equation, therefore the summation cannot begin at the surface (z' = 0 m).

The second optical relationship is Morel's chlorophyll-based equation for deriving $K_{\mathrm{d}}(\lambda)$ (see Equation 1.9). This allows for a calculation of the cumulative attenuation of downwelling irradiance due to phytoplankton and its covarying substances as one moves down through the water column, based on estimates of $Chla$. Following Equation 1.9, we can now replace $K_{\mathrm{d}}(\lambda, z')$ with an estimate of K_{d} based on the concentration of $Chla$ from the Morel relationship:

$$\ln E_{\mathrm{d}}(\lambda, z) = \ln E_{\mathrm{d}}(\lambda, 0) - \sum_{z' = \Delta z'}^{z} \left[K_{\mathrm{w}}(\lambda) + \chi(\lambda) Chla(z')^{\mathrm{e}(\lambda)}\right] \cdot \Delta z' \qquad (1.11)$$

where $Chla(z')$ is $Chla$ over the depth interval of $(z' - \Delta z')$ to z', for each depth from the surface to depth z. Replacing the term for integrated attenuation by water from the surface to depth z with its equivalent, $K_{\mathrm{w}}(\lambda) \cdot z$, and replacing $Chla(z')$ with $fluor(z') \cdot F$ according to Equation 1.2, and then rearranging, we get:

$$\ln E_{\mathrm{d}}(\lambda, z) + K_{\mathrm{w}}(\lambda) \cdot z = \ln E_{\mathrm{d}}(\lambda, 0) - F^{\mathrm{e}(\lambda)} \sum_{z' = \Delta z'}^{z} \chi(\lambda) fluor(z')^{\mathrm{e}(\lambda)} \cdot \Delta z' \qquad (1.12)$$

where F is the $fluor$ to $Chla$ conversion factor, with units of $(\mathrm{mg\ Chl\ m^{-3} count^{-1}})$. In order to simplify Equation 1.12, and to elucidate the relevant fact that it is in the form of a linear equation, the terms can be grouped and the notation presented as:

$$A(z) = A(0) - S_{0,z} \cdot C(z) \qquad (1.13)$$

where by definition, $A(0) = \ln E_{\mathrm{d}}(\lambda, 0)$, and the only unknown is $S_{0,z}$, which represents the slope of the $A(z)$ vs. $C(z)$ relationship for the depth interval from the surface to depth z. $A(z)$ and $C(z)$ values are then calculated from the $fluor$ and $E_{\mathrm{d}}(\lambda)$ data for each of n depth intervals in the profile, where n is the number of independent depth strata between the surface and some maximum depth, $z_{\max}$, generating n similar equations for each profile. Each of the n equations will have a unique $A(z)$ value, the same $A(0)$ value, an empty/unsolved $S_{0,z}$ value, and a unique $C(z)$ value. A single regression is then conducted for each profile, plotting the $A(z)$ versus $C(z)$ data for that profile, where a linear relationship is expected when evaluating over the full range of depths for the profile from the surface to $z_{\max}$ (Figure 1.1). For this relationship, $A(0)$ is the y-intercept and $S_{0,z_{\max}}$ is the slope of the regression line over that interval. Since $S_{0,z} = F^{\mathrm{e}(\lambda)}$, this allows us to calculate the $fluor$ to *Chla* conversion *F*-factor for a profile from the surface to depth $z_{\max}$:

$$F_{0,z_{\max}} = \left(S_{0,z_{\max}}\right)^{\frac{1}{e(\lambda)}} \qquad (1.14)$$

where $F_{0,z_{\max}}$ is now a profile-specific calibration factor capable of accounting for local variability in the phytoplankton community.

Note that $S_{0,z_{\max}}$ can be derived directly from Equation 1.13 when evaluating at the surface and at $z_{\max}$, without the need for a regression over that interval (assuming that $A(0)$ remains constant over this interval):

$$S_{0,z_{\max}} = \frac{A(0) - A(z_{\max})}{C(z_{\max})} \qquad (1.15)$$

This method of calculating $S_{0,z_{\max}}$ would be preferable if the slope was the only relevant piece of information obtainable from the $A(z)$ vs. $C(z)$ profile. However by calculating Equation 1.12 iteratively for each depth in the profile, we are able to observe patterns and anomalies in the $A(z)$ vs. $C(z)$ relationship. Specifically, the interim data points can be used to identify and correct for anomalous changes in $A(z)$ caused by variability in $E_{\mathrm{d}}(0)$ (see Section 1.6.2), as well as explore depth-resolved variability in the $A(z)$ vs. $C(z)$ relationship once the anomalous $A(z)$ have been corrected (see Section 2.6). Change in $E_{\mathrm{d}}(0)$ is one of three sources of variability in the overall $A(z)$ vs. $C(z)$ relationship; the other two being changes in the fluorescence yield properties of the phytoplankton ($fluor$ to $Chla$), and changes in the attenuating properties of the plankton relative to $Chla$ ($Chla$ to K_{bio} via the Morel relationship in Equation 1.9). It should be noted that variability in instrument performance is another source of variability in the aforementioned measurements; this issue will be discussed in more detail in Section 4.5.

This notation can be generalized further to accommodate profiles whose upper limits do not reach the surface of the water column, contained in a depth stratum from a minimum depth, $z_{\min}$, to $z_{\max}$. First, the minimum depth replaces all explicit and implicit incidences of $z = 0$ in Equation 1.12:

$$\ln E_{\mathrm{d}}(\lambda, z) + K_{\mathrm{w}}(\lambda) \cdot (z - z_{\min}) = \ln E_{\mathrm{d}}(\lambda, z_{\min}) - F^{\mathrm{e}(\lambda)} \sum_{\substack{z'=z_{\min} \\ +\Delta z'}}^{z} \chi(\lambda) fluor(z')^{\mathrm{e}(\lambda)} \cdot \Delta z' \qquad (1.16)$$

which, after moving $(-K_{\mathrm{w}}(\lambda) \cdot z_{\min})$ to the right hand side, simplifies to:

$$A(z_{\max}) = A(z_{\min}) - S_{z_{\min},z_{\max}} \cdot [C(z_{\max}) - C(z_{\min})] \qquad (1.17)$$

Equation 1.15 can now be written as:

$$S_{z_{\min},z_{\max}} = \frac{A(z_{\min}) - A(z_{\max})}{C(z_{\max}) - C(z_{\min})} \qquad (1.18)$$

and thus, the *F*-factor for the profile delineated by $z = z_{\min}$ to $z_{\max}$ can be determined using:

$$F_{z_{\min},z_{\max}} = \left(S_{z_{\min},z_{\max}}\right)^{\frac{1}{e(\lambda)}} \quad (1.19)$$

It is worth reiterating that the X11 method was derived to describe the average relationship over the photic zone, and as such there is only a single *F*-factor for a given profile. Therefore, when referring to the X11 *F*-factor as applied to a given profile, *i*, the notation used will be:

$$F(i) = S(i)^{\frac{1}{e(\lambda)}} \quad (1.20)$$

This version of the *F*-factor equation, used for converting $fluor$ into $Chla$ for a profile spanning a depth range from $z_{\min}$, to $z_{\max}$ via Equation 1.2, will be used for the remainder of this thesis. It is also worth stating for clarity at this point that the "e" in e(λ) is a wavelength-specific constant determined by Morel et al. (2007); it is not the Eulerian constant.

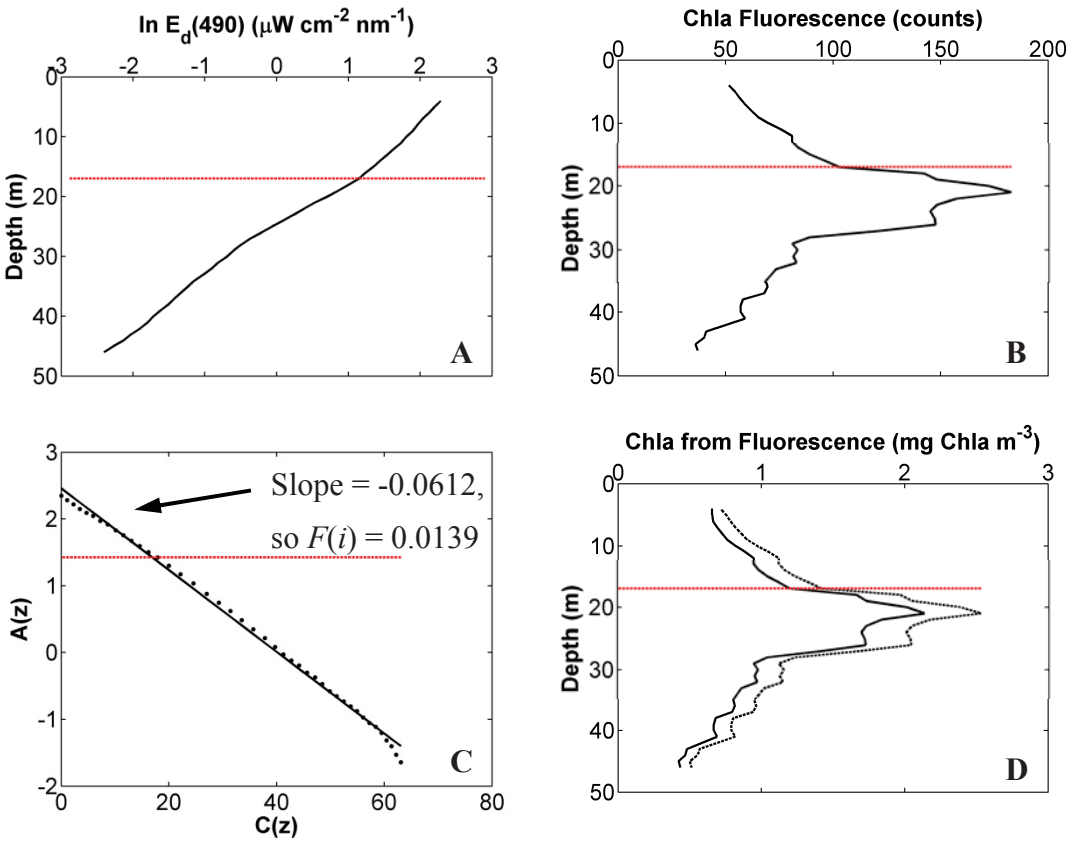

Figure 1.1. A glider profile showing the inputs of the X11 method and the change in *Chla* from applying the X11 $F(i)$, from Mission #1 (2011-07-26). The red horizontal line is the pycnocline (the depth where the change is density between data points, in kg m^{-3}, is largest). **(A)**: Depth profile of ln-transformed downwelling irradiance at 490 nm. **(B):** Depth profile of chlorophyll *a* fluorescence, in raw counts. **(C)**: An X11 $A(z)$ vs. $C(z)$ curve calculated using the data from A and B as inputs. Each point on the curve is a consistent with an evaluation of Equation 1.16. Consistent with X11, the slope of this relationship (the black line) is converted into the profile-specific *F*-factor, $F(i)$, via the relationship $F(i) = S(i)^{1/e(\lambda)}$. This *F*-factor, with units of mg Chla $m^{-3}count^{-1}$, is then used to convert all measured fluorescence counts for this profile into estimated *Chla* via Equation 1.2. **(D)**: Depth profile of *Chla* estimated from raw fluorescence counts (from B) using both the *F*-factor from C calculated using the X11 method ($F(i)$ = 0.0139 mg Chla $m^{-3}count^{-1}$; dashed black line), as well as the *F*-factor supplied by the fluorometer manufacturer (F = 0.0117 mg Chla $m^{-3}count^{-1}$; solid black line).

1.6.2 Smoothing and Correction of Downwelling-Irradiance Profiles

An aspect of the X11 method is the correction of perturbations in the $E_{\mathrm{d}}(\lambda, z)$ data caused by intermittent cloud cover (Figure 1.2.C. Clouds circled in red). Transient changes in cloud cover during a profile will lead to deviations in $E_{\mathrm{d}}(\lambda, 0)$ that cannot be detected directly by the sensor, but will influence $A(0)$ and hence $A(z)$ in Equation 1.13 while having no direct influence on $C(z)$. Data points affected by these changes in $E_{\mathrm{d}}(\lambda, 0)$ should appear as statistical outliers from the general $A(z)$ vs. $C(z)$ trend, which need to be corrected before the calculation of $F(i)$ proceeds (how this is accomplished will be discussed in Methods, Section 2.4). This removal of outliers serves multiple purposes. The first is that it obviates a major problem in the determination of the attenuation coefficient from a profiling instrument that does not have a reference sensor at the surface (cf. Brown et al. 2004). Removal of error associated with $E_{\mathrm{d}}(\lambda, 0)$ means that any remaining trends in the $A(z)$ vs. $C(z)$ profile can be attributed to changes in fluorescence yield or changes in the relationship between $Chla$ and $K_{\mathrm{bio}}(\lambda)$. The second purpose that outlier correction serves is that it allows for a more accurate calculation of $F(i)$, as the cloud-affected points will affect the slope of the relationship if not removed.

It should be noted that there are some differences between the X11 study and the work presented here, as well as some assumptions in the X11 method that warrant additional investigation. First, the X11 method was developed using data from profiling floats conducting noon-time profiles in Case 1 waters. This is in contrast to our dataset, which contains data from Slocum gliders collecting data 24 hours per day in both Case 1 and Case 2 waters. Second, the X11 method was intended as a depth-integrated application over the photic zone (as was the underlying Morel model used in the method), preventing any explicit investigation of patterns with depth in the $A(z)$ vs. $C(z)$ relationship. Finally, the way in which outliers are detected and corrected for in X11 is not as comprehensive as it could be, allowing for anomalous data points to affect the linear fit to the $A(z)$ vs. $C(z)$ relationship under certain conditions. These differences introduce sources of potential error that will be discussed in more detail in the following chapters.

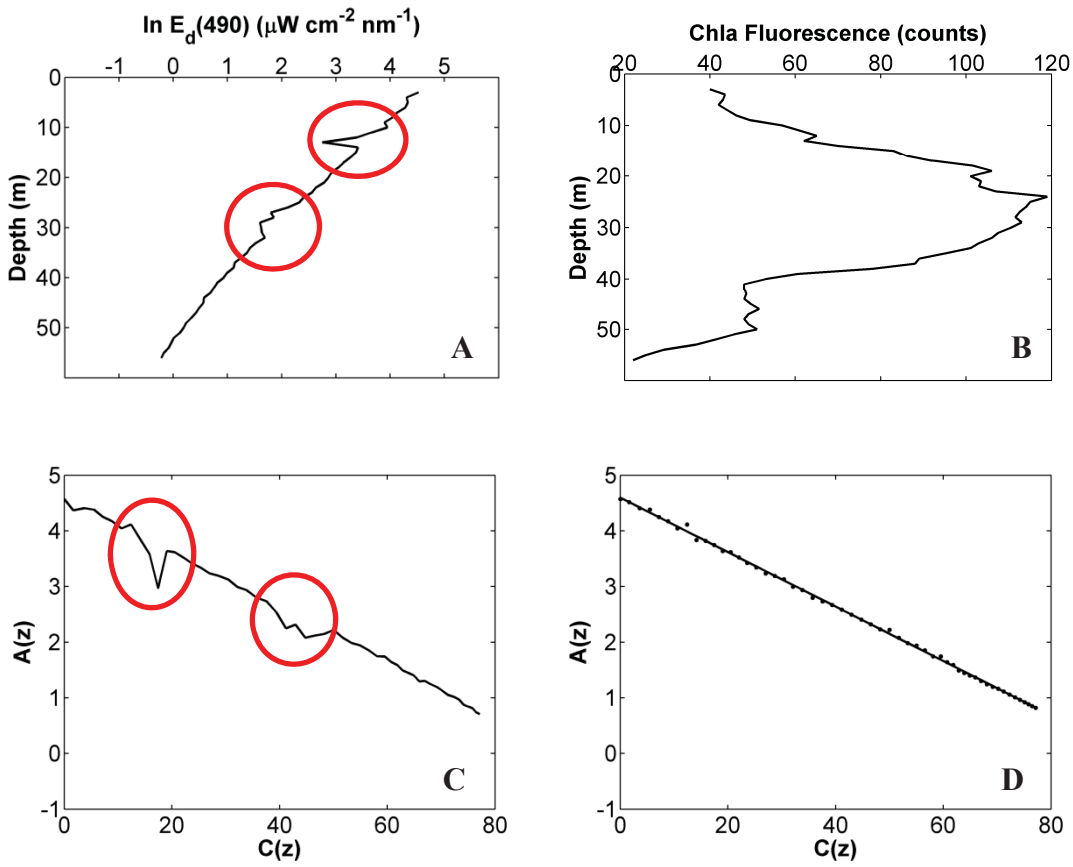

Figure 1.2. A glider profile contaminated by passing cloud cover from Mission #7 (2013-03-29). **(A)**: Depth profile of ln-transformed downwelling irradiance at 490 nm. Note the two sudden drops in ln $E_d(490)$ at approximately z = 12 m and z = 30 m (circled in red). **(B):** Depth profile of chlorophyll *a* fluorescence, in raw counts. **(C)**: An X11 $A(z)$ vs. $C(z)$ curve calculated using the data from 1.2.A and 1.2.B as inputs. The sharp deflections in $A(z)$, circled in red, are consistent with passing cloud cover depressing incident irradiance at the surface, and consequently $A(z)$ at depth, independent of changes in cumulative attenuation of irradiance above that depth as inferred from fluorescence (see Equation 1.16). **(D)**: $A(z)$ vs. $C(z)$ relationship after the cloud-affected points have been removed and the properly fitting slope calculated (described in Methods Section 2.4). This slope (black line) is then used to calculate the unique, profile-specific conversion factor ($F(i)$) for converting fluorescence counts to *Chla*.

1.7 Overall Objective and Scientific Rationale

This thesis addresses the problem of how to ensure the accuracy of $Chla$ estimates when using an *in situ* fluorometer mounted on an autonomous glider platform, in the absence of traditional ship-based validation methods. It will focus on the application and modification of an established method for increasing the accuracy of optics-based

estimates of $Chla$ (Xing et al. 2011), that complements the chlorophyll *a* fluorescence ($fluor$) measurements with downwelling irradiance. Specifically, the method determines an optically derived $fluor$-to-$Chla$ conversion factor capable of accounting for taxonomic and physiological changes in the phytoplankton assemblage. This thesis aims to address some questions that remain unanswered surrounding the work of Xing et al. (2011):

1. Can the Xing et al. (2011) method be easily and reliably generalised from its original application of single, noon-time profiles by a buoy in Case 1 waters to the context of ocean gliders doing continuous horizontal transects through Case 1 and Case 2 waters?

2. Are there any systematic weaknesses or shortfalls to the method that can be identified, and can they be improved upon?

From these questions, the specific objectives of this thesis can be outlined:

1. To investigate the applicability of an optics-based approach for estimating in-situ $Chla$, developed for Argo floats in the open ocean by Xing *et al*. (2011), when using ocean gliders deployed off the coast of Nova Scotia.

2. To identify and address any flaws inherent to the method when applied in this context and, where possible, modify the method in order to correct them.

3. To determine, using the modified method, if there are any consistent patterns of variability in the $fluor$-to-$Chla$ relationship (as inferred from attenuation) either spatially or temporally in the study zone of the Scotian Shelf.

4. To recommend a calibration procedure for the Ocean Tracking Network's fleet of Slocum gliders operating on the Scotian Shelf.

CHAPTER 2 METHODS

2.1 Data Collection, Study Site, and Data Sources

2.1.1 Data Collection: the Slocum Glider

Data for this thesis were collected by a Teledyne Webb Slocum electric glider (North Falmouth, MA, USA) — an autonomous underwater sampling platform that moves through the water column in a vertical saw-tooth pattern measuring a range of oceanographic variables every 1-2 seconds. The gliders consist of a torpedo-shaped body with attached wings and tail section (Simonetti 1992; Webb et al. 2001). It has a length of approximately 1.5 m and can dive to depths of up to 200 m. Instead of using an energy-demanding source of propulsion like a propeller, the glider controls its buoyancy by displacing a portion of its internal volume and controls its pitch by moving its battery forwards and aft. The result of these two low-energy movements is vertical motion and a change in pitch. When combined with the wings that are attached to the glider's hull this vertical motion is partially translated into horizontal motion, with the end result being a diagonal trajectory through the water column with a vertical speed of ~0.15 m s^{-1} and a horizontal speed of ~0.25 m s^{-1}. The low-energy, slow-speed design of the glider makes it ideal for two reasons. First, a slow-moving and stable platform is ideal for providing reliable measurements. Second, the low energy demands of this propulsion system allow the gliders to be deployed for much longer periods of time than if they were driven by propellers. A standard propeller-driven AUV may be deployed for hours over a range of tens of kilometers, whereas glider can be deployed for months over a range of thousands of kilometers (Eriksen et al. 2001).

The instrument payload is customisable for each glider, making it a versatile platform capable of addressing different research objectives. The gliders specific to this project are equipped with a Sea-Bird (Sea-Bird Electronics. Bellevue, WA, USA) CTD to record depth, temperature and salinity, an Aanderaa (Aanderaa Data Instruments, Bergen, Norway) oxygen optode, a Satlantic (Satlantic, Halifax, NS, Canada) OCR-504 downwelling irradiance sensor (measuring at wavelengths 412, 444, 490 and 555 nm with a bandwidth of 10 nm full width at half maximum [FWHM]; only data from the 490 nm

channel was used for analysis), and two WET Labs (WET Labs, Philomath, OR, USA) ECO Puck sensors configured to measure *Chla* fluorescence (exciting at 470 nm and measuring at 695 nm with a 70 nm bandwidth FWHM), coloured dissolved organic matter (CDOM) fluorescence (exciting at 370 nm and measuring at 460 nm with a 120 nm bandwidth FWHM) and optical scattering (measuring scattering at an angle of 124 degrees for wavelengths 470, 532, 660 and 880 nm with a 20 nm bandwidth FWHM; only data from the 660 nm channel was used for analysis). Sampling rates are 0.5 Hz for the CTD and 1 Hz for the ECO sensors and irradiance sensor, translating into approximately 4 data points and 8 data points respectively per vertical meter travelled by the glider.

Several operational decisions were made regarding the sampling protocols for the gliders in order to balance sampling resolution with battery life and mission duration. First, although the duration of a saw-tooth profile is on the order of 10 minutes, the gliders were programmed to return to the surface only once every six hours for communication purposes. While at the surface, glider propulsion temporarily ceases and a subset of the recorded data is transmitted via Iridium satellite communication (Iridium Communications Inc., McLean, VA, USA) for real-time analysis. Minimising surface time is important for maximising the amount of time sampling as well as reducing the amount of battery power used to make transmissions (instead of being conserved for sampling). A consequence of this decision is that most of the profiles do not reach depth z = 0 m; instead, the shallowest point reached per profile, $z_{\min}$, averaged over the dataset of n = 5362 profiles was 2.30 ± 0.80 m S.D., leading to uncertainty in estimates that require a reference value from just below the surface (z = 0 m). Second, it was decided that the gliders would only sample scientific data (data non-crucial for navigation purposes, such as downwelling irradiance, chlorophyll *a* fluorescence, CDOM fluorescence, and optical scattering) during an "upcast" – the portion of the glider's diving pattern where it is ascending from its deepest point to $z_{\min}$. In addition to balancing the demands of high resolution against battery life, this decision was made because the downwelling irradiance ($E_{\mathrm{d}}(\lambda)$) sensors are mounted on the glider to be parallel to the surface during the upcast, whereas during the downcast they are not. Having a properly oriented irradiance sensor is important for accurate measurements due

to the cosine effect, where $E_{\mathrm{d}}(\lambda, z)$ measured on a flat plane decreases as a function of the cosine of the average angle of incoming light (Mobley 1994; Berwald et al. 1995; Kirk 2011).

2.1.2 Data Collection: Water Samples

When there was sufficient time and weather conditions permitted it, water samples were collected simultaneously with glider launches and recoveries to obtain measurements of $Chla$ using laboratory-based procedures. Water was sampled from several depths using Niskin bottles in an attempt to capture the defining features of the $Chla$ profile, which was pre-determined using an *in situ* profiling package. These samples were made as close as possible to a coincident glider profile in both space and time, with disparities ranging from 0 h to 23 h (with 37 of 39 samplings being made within 6 h of a coincident glider profile). Avoiding exposure to direct sunlight, samples were dispensed into dark bottles, placed in a cooler, and transported to the laboratory for analysis within 1-2 h. Laboratory analysis involved collecting triplicate samples on 25mm Whatman GF/F filters using a vacuum pump filtration rig, followed by overnight extraction in 90% acetone at -20 ℃. Fluorescence of the extracted chlorophyll *a* was then measured using the Welschmeyer method (Welschmeyer 1994) on a Turner 10-005 benchtop fluorometer.

2.1.3 Research Study Site and Data Set

The gliders were operated by the Ocean Tracking Network (OTN) – an international research group focused on the tagging and tracking of marine animals, and the interaction of those animals with the marine habitat. Data and operational information for all glider deployments included in this thesis, including visualisations such as Figure 2.2, can be found on their website (OTN 2015).

The study site for this thesis was the Scotian Shelf in the northwest Atlantic, sampled on a transect from the coast of Nova Scotia, Canada near the mouth of the Halifax Harbour to the edge of the continental shelf. This transect corresponds, where possible, with the “Halifax Line” section of the Atlantic Zone Monitoring Program

(AZMP; Therriault et al. 1998; Petrie 2004). Figure 2.1 shows an example of a glider mission track along this transect.

Figure 2.1. Google Earth image showing the transect sampled by a glider over a 1-month mission (July 26 to August 8 2011). The solid white line shows the glider's track, light blue squares near the shore show the start- and end-points of the mission, and black squares show the location of sampling stations for the "Halifax Section" portion of the Atlantic Zone Monitoring Program. The turnaround point of this mission (HL6) is approximately 230 km from the point of mission origin.

Gliders were deployed along this section from May 2011 until the present day, with the data for this thesis collected during from July 2011 through December 2013. Efforts were made to ensure continuous collection of data during that period, but mechanical and logistical problems led to interruptions (Figure 2.2).

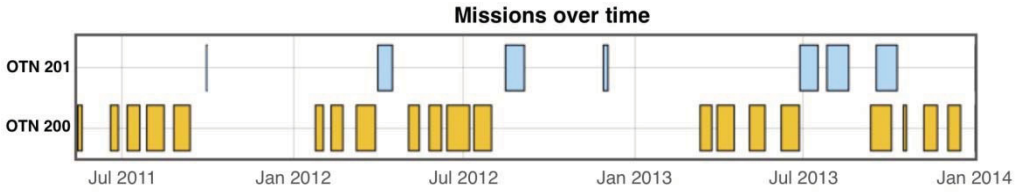

Figure 2.2. A representation of time spent collecting data for the two gliders operated by OTN used in this thesis, for the period of July 2011 to December 2013. There are gaps in the data collection due to logistical and mechanical difficulties that resulted in gliders being unable to conduct sampling (modified with permission from Ocean Tracking Network Canada).

From the available missions, transects selected for analysis were required to have 1.) travelled along or close to the Halifax Section, and 2.) traversed the majority of the distance across the continental shelf to the shelf break. A complete list of the missions during the 2011-2013 period, as well as the criteria that excluded any missions from analysis, is shown in Table 2.1. A data set of twelve missions was selected for analysis.

Table 2.1. Glider missions conducted between July 2011 and December 2013, with an explanation of why a mission was excluded from analysis, if applicable. For missions that were included in the analysis, a Mission Number is provided for reference.

Mission Number	***Mission Start***	***Mission End***	***Statement of Exclusion/Inclusion for Mission***
	2011-05-13	2011-05-19	Test mission
	2011-06-17	2011-06-27	Did not cover enough distance across the shelf
	2011-07-05	2011-07-20	Transect backtracked/overlapped too often
1	2011-07-26	2011-08-15	Included
	2011-08-24	2011-09-12	Transect backtracked/overlapped too often. Aborted due to glider leak.
	2011-09-28	2011-09-30	Aborted due to glider leak
	2012-01-23	2012-02-02	WET Labs ECO Pucks removed for repairs
	2012-02-09	2012-02-23	WET Labs ECO Pucks removed for repairs
	2012-03-07	2012-03-29	WET Labs ECO Pucks removed for repairs
	2012-03-30	2012-04-16	Did not cover enough distance across the shelf
2	2012-05-02	2012-05-15	Included
3	2012-05-24	2012-06-08	Included
4	2012-06-12	2012-07-08	Included
5	2012-07-11	2012-08-01	Included
	2012-08-14	2012-09-05	Test mission. Iridium communication issues.
	2012-11-27	2012-12-04	Did not cover enough distance across the shelf. Aborted mission.
6	2013-03-11	2013-03-25	Included
7	2013-03-29	2013-04-18	Included
8	2013-05-03	2013-05-21	Included
9	2013-06-06	2013-06-27	Included
	2013-06-26	2013-07-17	Did not cover enough distance across the shelf
	2013-07-25	2013-08-19	Did not cover enough distance across the shelf
	2013-09-10	2013-10-04	Mission was not along the Halifax Transect (Roseway Basin)
10	2013-09-16	2013-10-10	Included
	2013-10-15	2013-10-20	Mission was not along the Halifax Transect (Roseway Basin)
11	2013-11-06	2013-11-22	Included
12	2013-12-02	2013-12-17	Included

2.2 Data Management, Creation of Preliminary Variables, and Quality Control

2.2.1 Level 1 Processing

While operating, the glider's on-board computers convert the raw digital signatures from some of the instruments into scientifically relevant units using factory set conversion equations and calibration factors. These equations are in a format similar to the one below:

$$\text{Scientific Units} = (\text{Digital counts} - \text{Digital offset}) \times \text{Conversion factor} \qquad (2.1)$$

where "Digital counts" are the direct measurement from the instrument (units of counts), "Digital offset" is a value provided by the instrument manufacturer representing the instrument output in the absence of the signal to be quantified (units of counts), and "Conversion factor" is the calibration constant that the is used to convert the raw signal from the instrument into relevant scientific units. For the OTN gliders, conversions were automatically calculated for downwelling irradiance, chlorophyll *a* fluorescence and CDOM fluorescence using calibration values determined by the manufacturer from tests done in a laboratory. Other variables are calculated as described in the sections below.

At the end of each glider mission, which usually lasts 3-4 weeks, the glider is retrieved and brought back to the laboratory for cleaning, calibration, and data collection. Data are downloaded from the glider and uploaded to a central database. Both the raw counts and the converted measurements in relevant scientific units are stored. Minimal processing and quality control is done at this stage – GPS coordinates are interpolated for all data time stamps based on known GPS coordinates that are obtained when the glider surfaces approximately once every six hours, and time-lag corrections are made so that the logs of all instruments are synchronised. The end-user is responsible for any further data manipulation. For this thesis, we will refer to this geo-referenced, time-stamped data as Level 1.

2.2.2 Level 2 Processing

Level 1 data were reorganised and subjected to quality control procedures, as well as used to generate new variables to support the research goals of this thesis as outlined in the steps below.

Salinity and Density

Practical salinity (unitless) and potential density ($\mathrm{kg\,m^{-3}}$) were calculated from measurements of conductivity, temperature and pressure from the CTD using the Gibbs Seawater Toolbox package for MATLAB (version 2012a). The steps required for generating these products can be found in the Intergovernmental Oceanographic Commission manual for the international thermodynamic equation of seawater (McDougall et al. 2010).

Particulate Backscatter

The raw output from the WET Labs ECO puck fluorometers were calibrated by subtracting the dark offset and multiplying by the scaling factor supplied on the calibration sheet in order to convert the raw instrument signal (counts) into the volume scattering coefficient (β; $\mathrm{m^{-1}\ sr^{-1}}$) measured at an angle of 124° for each of four wavelengths (this thesis only uses the data from the 660 nm waveband; $\beta(124^{\circ}, 660)$). Particulate backscattering ($b_{\mathrm{bp}}(660)$; $\mathrm{m^{-1}}$), the component of scattering caused by particles and integrated over 180° in the backwards direction, was then calculated from $\beta(124^{\circ}, 660)$ using equations provided by the WET Labs Eco BB User's Guide (WETLabs 2011), which were derived from the work of Boss and Pegau (2001), Zhang et al. (2009), and Sullivan et al. (2013).

Chlorophyll *a* from Fluorescence

The raw output from the WET Labs ECO puck was calibrated by subtracting a dark offset and multiplying by the scaling factor supplied on the instrument calibration sheet in order to convert the raw signal (counts) into a chlorophyll *a* concentration ($\mathrm{mg\,Chla\,m^{-3}}$). The scaling factor was determined by the manufacturer using a

laboratory monoculture of phytoplankton of the diatom species *Thalassiosira weissflogii*. The chlorophyll *a* fluorescence data were then blanked on a per-mission basis in order to correct for any residual non-zero values at depth after the application of the manufacturer's dark offset, where the concentration of chlorophyll *a* should be approaching zero. This was accomplished using the 1st percentile value of the data between 150-200m for each mission (the deepest data available with these gliders; see Table 2.2 for the blank values for each mission). No mission required a correction larger than 3 counts (the equivalent of 0.0351 $\mathrm{mg\ Chla\ m^{-3}}$). Any data points that were below zero after this correction were set to zero.

When possible, corrections like the one described above should be determined in addition to any manufacturer calibrations, and ideally it should done while an instrument is operating in the study site (Cullen and Davis 2003). This is done so that the environmental conditions that can affect instrument measurements such as temperature and pressure are the same during the blank calculation as during sampling (Roesler and Boss 2008; Proctor and Roesler 2010). The method with which the blank calculation is made also has an effect. According to the provided calibration sheet, the dark offset for the WET Labs ECO Puck fluorometers is determined while the instrument is in "clean water with black tape over the detector". The dark offset obtained in this manner can by 30% lower than a dark offset obtained by placing the instrument in filtered sea water and leaving the face of the detector uncovered (Proctor and Roesler 2010). Acknowledging that the choice of using the 1st percentile value of the 150-200 m data may have error associated with it, due to any non-zero fluorescence signal at that depth and any differences in instrument response between that depth and the depth of shallower measurements, this blank estimate is considered to be more applicable than the dark offset determined in a laboratory by the instrument manufacturer.

Downwelling Irradiance at 490 nm

The data for downwelling irradiance at 490 nm were blanked using the median value of the data between 150-200 m depth for each mission. This depth range was chosen due to the negligible $E_{\mathrm{d}}(490)$ signals present there, even during the day (see Table 2.2 for the blank values of each mission). Additional blanks should be conducted

for irradiance sensors for the same reasons as those outlined above for fluorometers. When downwelling irradiance data is improperly blanked, "tails" are evident in plots of $\ln(E_d(\lambda))$ vs. depth (Cullen and Davis 2002). Underestimation of the blank results in deeper portions of the $\ln(E_d(\lambda))$ profile deviating from linearity in the vertical direction, creating a "tail" that asymptotically approaches a residual $\ln(E_d(\lambda))$ value. Overestimation of the blank results in deeper portions of the $\ln(E_d(\lambda))$ profile deviating from linearity in the horizontal direction, creating a "tail" to the left as untransformed irradiance values decrease to zero (or below) at a residual depth value (Figure 2.3). In order to qualitatively determine if an appropriate blank had been chosen, a $\ln(E_d(490))$ vs. depth plot was generated on a per-mission basis of every profile used in that mission and visually inspected for "tails".

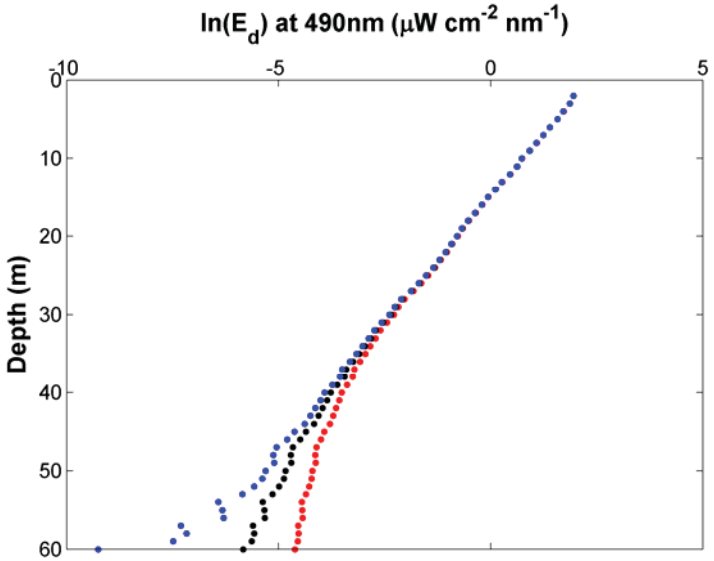

Figure 2.3. A glider profile from Mission # 12 (2013-12-02) showing the effect of the blank value on the shape of the vertical profile. In waters of uniform optical properties with depth, this profile should be linear. Black points represent data after the mission-specific deep water blank was applied, with the profile maintaining an approximately linear shape with depth. Underestimating this blank by 0.007 μW cm^{-2} nm^{-1} results in the data deviating from linearity in the vertical direction (red points), and overestimating this blank by 0.003 μW cm^{-2} nm^{-1} results in the data deviating from linearity in the horizontal direction (blue points). Note that this effect is only evident when the data values are quite small (less than approximately $\ln(E_d(490))$ = -3, which corresponds to approximately 0.05 μW cm^{-2} nm^{-1}), below approximately 35 m depth.

Acknowledging that our choice of using the median value of the 150-200 m data may have error associated with it, due to any differences in instrument response between that depth and the depth of shallower measurements, bulk visualisation of blank-corrected $\ln(E_{\mathrm{d}}(490))$ vs. depth plots did not reveal any noticeable deviations from linearity and this blank estimate is therefore considered to be more applicable than the offset determined in a laboratory by the instrument manufacturer.

Table 2.2. Field blank values for downwelling irradiance ($E_{\mathrm{d}}(490)$; $\mu\mathrm{W\ cm^{-2}\ nm^{-1}}$), and chlorophyll *a* estimated from chlorophyll *a* fluorescence ($Chla$; $\mathrm{mg\ Chla\ m^{-3}}$), after the factory-determined dark offset and conversion factor supplied on the instrument calibration sheets had been applied to the raw instrument data. Negative values mean that the factory-determined dark offset was too large of a correction.

Mission Number	***Mission Date***	***Sample Size***	***Blank Values***	
			$E_{\mathrm{d}}(490)$ ($\mu\mathrm{W\ cm^{-2}\ nm^{-1}}$)	***Chla*** **($\mathrm{mg\ Chla\ m^{-3}}$)**
1	2011-07-26	59,649	0.0056	0
2	2012-05-02	32,019	-0.0037	-0.0234
3	2012-05-24	36,058	0.0054	0
4	2012-06-12	67,800	0.0051	0
5	2012-07-11	50,139	-0.0291	-0.0351
6	2013-03-11	34,361	-0.0047	-0.0234
7	2013-03-29	38,711	-0.0049	-0.0234
8	2013-05-03	51,861	-0.0048	-0.0234
9	2013-06-06	54,040	-0.0048	-0.0351
10	2013-09-16	67,735	0.0102	0
11	2013-11-06	37,577	0.0101	0
12	2013-12-02	33,886	0.0102	0

Binning of Data and Division of Profiles

Generally, 3 to 8 data points were collected per metre for each instrument, dependent on the sampling frequency of that instrument and the vertical velocity of the glider. The data were assigned to 1 m vertical resolution bins and the median was used as the nominal value for each bin (data for depth z were binned over the interval from z to all depths up to, but not including, z + 1 m).

As explained in Section 2.1.1 data were only collected on upcasts, which will be referred to as profiles for the remainder of this thesis. The lower limit of a profile was the deepest recorded data point as the glider began an ascent towards the surface. The upper limit of the profile was determined using a MATLAB algorithm developed by Adam Comeau, a glider technician with OTN. It analyses the data in the upper 2m of a profile, and sets $z_{\min}$ to be the depth at which the glider's vertical speed decreases to where there is less than 0.01 m difference between depth measurements. This indicates that the glider has reached the peak of its upcast and was preparing to dive again (as reference, the glider ascends at a rate of approximately 0.15 m s^{-1} during sampling). Visual inspection of several thousand profiles confirmed that these criteria were not erroneously trimming profile end-points.

Pycnocline and Mixed Layer Depth

The pycnocline was defined as the depth in the profile at which the density exceeded that at $z_{\min}$ by at least 0.125 kg m^{-3} (Monterey and Levitus 1997). This varies slightly from the accepted practice of comparing density at depth to that of the surface, but is necessary because most profiles did not extend to the surface. The use of $z_{\min}$ rather than the surface as a reference point could result in overestimation of pycnocline depth, but only when the density at $z_{\min}$ exceeds that of the surface, i.e., in stratified water.

Consistent with the assumption that mixing prevents the formation of discontinuities in any variable that changes slowly compared the mixing time (Cullen and Lewis 1988), the mixed layer depth (MLD) was defined as the shallower of either the pycnocline or the discontinuity of $b_{\mathrm{bp}}(660)$. The $b_{\mathrm{bp}}(660)$ discontinuity was defined as the depth in the profile at which $b_{\mathrm{bp}}(660)$ differed from its value at $z_{\min}$ by at least 2.5 x

10^{-4} m^{-1}. This threshold value was determined empirically, based on comparisons made with the density-based criterion for the MLD over several hundred profiles.

Diffuse Attenuation Coefficient of Downwelling Irradiance and Optical Depth

The diffuse attenuation coefficient for downwelling irradiance at 490 nm ($K_{\mathrm{d}}(490)$) was calculated based on Equation 1.5 for each profile. A whole-profile $K_{\mathrm{d}}(490)$ was calculated for the interval z_{min} to z_{max}, denoted $\overline{K}_{\mathrm{d}}(490)$:

$$\overline{K}_{\mathrm{d}}(490) = \frac{\ln(E_{\mathrm{d}}(490, z_{\mathrm{min}})) - \ln(E_{\mathrm{d}}(490, z_{\mathrm{max}}))}{z_{\mathrm{max}} - z_{\mathrm{min}}} \qquad (2.2)$$

This $\overline{K}_{\mathrm{d}}(490)$ can then be used to determine the number of optical depths for each profile, under the assumption that the average $\overline{K}_{\mathrm{d}}(490)$ applies over the whole profile (Kirk 2011):

$$\zeta = \overline{K}_{\mathrm{d}}(490) \cdot (z_{\mathrm{max}} - z_{\mathrm{min}}) \qquad (2.3)$$

This equation was rearranged to determine the geometric depth, in metres, of an optical depth (z_ζ) within a profile, where ζ corresponds to the desired optical depth:

$$z_\zeta = \frac{\zeta}{\overline{K}_{\mathrm{d}}(490)} \qquad (2.4)$$

Equation 2.4 was then used to vertically delineate strata within each profile, as multiples of ζ, in order to investigate trends with depth. It should be noted that the geometric depths for each optical depth were calculated starting at depth z = 0 m.

Quality Control Criteria

Several quality control criteria (QCC) were applied to exclude inappropriate data from the analysis, and to ensure that the remaining data were both of high-quality and

relevant to the investigation of bio-optical interactions between phytoplankton and the ambient light field.

The first was the exclusion of any profiles that were not collected within 4 hours of local apparent noon. The X11 study only included profiles conducted at local apparent noon, due to the sampling nature of their profiling float platform. This wider window was chosen to avoid eliminating unnecessary glider profiles, while maintaining the requirement for sufficient downwelling irradiance to conduct the X11 method.

The minimum depth for a profile, z_{min}, was set as the depth with the largest $E_{\mathrm{d}}(490)$ value once the data had been binned into 1m intervals. This was done to exclude noisy near-surface irradiance values, which would occasionally result in a decrease in downwelling irradiance as the glider approached the surface. These noisy irradiance values were likely caused by near-surface wave action, which resulted in instability in the sensor orientation as well as focusing/defocusing of the downwelling light field (Zaneveld et al. 2001). This approach is not completely robust, as noisy near-surface irradiance values resulting in an increase in downwelling irradiance will still be included.

Several conditions were applied to determine the maximum useable depth of the profile, z_{max}. The objective was to focus the analysis on the surface layer, where interaction of phytoplankton and the light field are most important. The condition which resulted in the shallowest termination of the profile was used for z_{max}. The first condition was that no profile would extend beyond the fifth optical depth, i.e., z_5 (see Equation 2.4). This depth was chosen because downwelling irradiance is reduced to 1% of its surface value at 4.6052 optical depths (Lorenzen 1972), a value which can be used as a rough first approximation for the bottom of the euphotic zone despite well recognized inaccuracies in this assumption (see Banse 2004; Cullen 2015). The second condition was a lower limit for $E_{\mathrm{d}}(490)$ of 0.08 $\mu\mathrm{W\,cm^{-2}\,nm^{-1}}$ above the deep-water field blank; a value approximately 10x the detection limit of the instrument, according to the manual provided by the manufacturer (Satlantic 2011). The final condition was a limit based on measurements of $fluor$ to exclude data from below the surface layer of relatively high concentrations of phytoplankton. This limit was used to detect if $fluor$ at depth z ($fluor(z)$) had decreased to insignificant levels relative to the magnitude of the average $fluor$ signal in the intervening waters between $z = z_{\mathrm{min}}$ to $z = (z - 1)$, denoted as

($\overline{fluor}(z_{\min}, z-1)$). The profile reached this condition at the depth where the relationship of $\frac{fluor(z)}{\overline{fluor}(z_{\min}, z-1)}$ first fell below a threshold value of 0.15.

A final quality control criterion was applied after all of the preceding QCC were implemented, requiring that ($z_{\max} - z_{\min}$) must be equal to or greater than 10m in order to ensure that enough data points existed in the profile to resolve meaningful patterns. For this thesis, we will refer to 1m-resolution binned data that had successfully fulfilled all of the preceding quality control criteria as Level 2. Table 2.3 shows summary information for each of the missions, detailing the data available after the application of all QCC. Level 2 data were used for all analyses for the remainder of the thesis, which were completed using the programming package MATLAB. These analyses are outlined in Sections 2.3 – 2.6 below.

Table 2.3. Number of data points and profiles for each of the missions at three stages of processing: Original number of data points from the raw glider measurements (n), the number of data points (n_{binned}) and profiles (i_{binned}) after the data had been binned and split into profiles, and the number of data points (n_{QCC}) and profiles (i_{QCC}) after implementation of quality control procedures. Only the data in the "Quality Controlled" columns, representing the final Level 2 data, were used for analysis.

Mission Number	***Mission Date***	***Original***	***Binned***		***Quality Controlled***	
		n	n_{binned}	i_{binned}	n_{QCC}	i_{QCC}
1	2011-07-26	836,994	113,986	1,429	42,522	515
2	2012-05-02	511,533	82,381	875	30,847	327
3	2012-05-24	596,878	88,285	945	32,569	355
4	2012-06-12	987,887	156,850	1,754	57,079	638
5	2012-07-11	828,036	125,161	1,334	48,261	490
6	2013-03-11	524,595	86,239	845	33,309	338
7	2013-03-29	827,018	130,353	1,345	49,442	526
8	2013-05-03	769,838	119,571	1,212	42,787	441
9	2013-06-06	886,585	133,571	1,340	50,956	507
10	2013-09-16	971,801	137,331	1,242	51,855	470
11	2013-11-06	718,465	91,011	1,004	32,684	374
12	2013-12-02	662,963	89,301	1,018	31,968	381

2.3 Correction of Non-Photochemical Quenching (NPQ) Effects using the Methodology of Sackmann *et al*. (2008)

As stated in Section 1.3, nonphotochemical quenching of fluorescence can lead to errors in the estimation of $Chla$ from *in situ* fluorescence measurements in the upper water column where the fluorescence yield of phytoplankton is reduced in bright light. Following the method of Sackmann et al. (2008) (hereafter referred to as S08), this problem was addressed by using a ratio of fluorescence (a proxy for phytoplankton concentration which is affected by NPQ), to backscatter (a proxy for particle abundance which is not affected by NPQ; cf. Fennel and Boss 2003) to correct for the reduction of fluorescence yield in surface waters in order to get more accurate estimates of $Chla$. For this thesis, this relationship will be referred to as *RFB*, and it can be expressed as $RFB = fluor : b_{bp}(660)$, with units of $(\text{counts} \cdot \text{m})$. By examining the ratio of these two independent proxies for phytoplankton presence it is possible to determine if a reduction in fluorescence near the surface is caused by NPQ or by a decrease in plankton biomass with greater confidence than by looking at fluorescence data alone (Figure 2.4). This approach differs marginally from that of X11, which extrapolated $fluor$ from the mixed layer depth to shallower depths in the water column without any specific regard for changes in particle abundance over that interval. However, if particle distributions are uniform in the empirically determined mixed layer, then both approaches yield the same result.

It should be noted that in stratified waters, physiological and taxonomic differences between strata can affect the fluorescence to biomass relationship (Cullen, 1982), confounding the effects of NPQ as reflected in *RFB*. Therefore a core requirement for the application of the S08 method is the presence of a mixed layer in which phytoplankton biomass is close to uniform and not differentiated vertically with respect to biomass or any physiological acclimation that proceeds more slowly than fluorescence quenching (cf., Cullen and Lewis, 1988). Analyses of stratified waters are outside of the scope of this method, and any data that has experienced NPQ in stratified waters remains uncorrected. As a result of this assumption that biomass is not differentiated vertically with depth, it should also be noted that the differences between the X11 method for

correcting for NPQ and the method utilised here will be small.

The S08 correction for NPQ used in this analysis is outlined in Equation 2.5 and demonstrated in Figure 2.4. The proportional reduction of fluorescence due to quenching at a given depth within the mixed layer is assumed to be equal to *RFB* at that depth divided by *RFB* at the bottom of the mixed layer (termed the Mixed Layer Depth; MLD). Modifying Equation 1.2, we can therefore express a NPQ-corrected *Chla* estimate as:

For $z <$ MLD:

$$Chla(i,z) = fluor(i,z) \times F(i) \times \left[\frac{RFB(i,z)}{RFB(i,z_{MLD})}\right]^{-1} \quad (2.5)$$

For $z >=$ MLD:

$$Chla(i,z) = fluor(i,z) \times F(i) \quad (2.6)$$

where z_{MLD} (m) is the depth of the bottom of the mixed layer, $Chla(i,z)$ (mg Chl m^{-3}) is the estimated concentration of chlorophyll *a* at depth z for profile i, $fluor(i,z)$ (counts) is raw fluorescence counts at depth z for profile i, $RFB(i,z)$ is the ratio of $fluor{:}\, b_{bp}(660)$ (counts $\cdot$ m) at depth z for profile i, $RFB(i,z_{\mathrm{MLD}})$ is the ratio of $fluor{:}\, b_{bp}(660)$ (counts $\cdot$ m) at depth z_{MLD} for profile i, and $F(i)$ is the conversion factor between fluor and Chla (mg Chl m^{-3} count^{-1}) for profile *i*.

Once the corrected $Chla$ values were obtained, $Chla$ at z_{min} after the NPQ correction was compared to $Chla$ at z_{min} from before the NPQ correction to obtain a per-profile estimate of the percent-NPQ at z_{min}. The magnitude of the NPQ correction at z_{min}, in percent, will be referred to as $\mathrm{NPQ_{corr}}$. This was calculated using the following equation:

$$\mathrm{NPQ_{corr}} = \left(1 - \frac{Chla \text{ at } z_{\mathrm{min}} \text{ before the NPQ correction}}{Chla \text{ at } z_{\mathrm{min}} \text{ after the NPQ correction}}\right) * 100\% \quad (2.7)$$

The S08 methodology was applied to the Level 2 data. The NPQ-corrected data resulting from this were used from this point onwards for all analyses requiring chlorophyll *a* fluorescence unless otherwise stated.

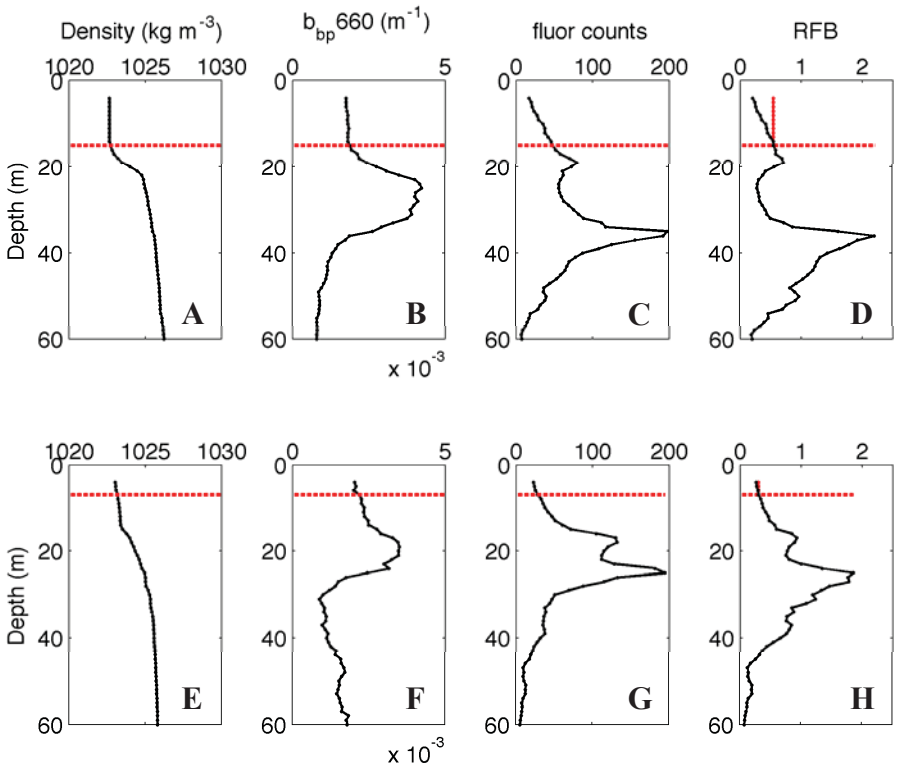

Figure 2.4. Correction for nonphotochemical quenching of fluorescence for two types of profiles: one with a uniform surface mixed layer (A-D), and one with weak stratification (E-H). **(A-D)**: Plots for a cast in which the NPQ correction was successfully applied. Note that both density and $b_{\mathrm{bp}}(660)$ are constant with depth down to the MLD, defined by the shallower of either a density difference of 0.125 kg m^{-3} from the value at z_{min}, or a $b_{\mathrm{bp}}(660)$ difference of $2.5\mathrm{x}10^{-4}\ \mathrm{m}^{-1}$ (horizontal dashes) implying a well-mixed surface layer. In contrast, $fluor$ decreases towards the surface, resulting in a similar decrease in *RFB*, implying that the decrease in $fluor$ is due to NPQ rather than any drop in phytoplankton biomass. The vertical red line in 2.6.D extrapolates the *RFB* from the MLD to the surface. **(E-H)**: Plots for a cast in which the application of the NPQ correction was impeded by stratification in the surface layer, resulting in an MLD estimate of approximately 7m. Note the gradients in density, backscatter, and fluorescence. A stronger pycnocline, with associated changes in the phytoplankton assemblage, occurs at approximately 17m. For this profile the drop in $fluor$ is matched by a similar drop in $b_{\mathrm{bp}}(660)$, suggesting the decrease in $fluor$ is caused by a reduction in phytoplankton biomass rather than NPQ.

2.4 Implementation of the Xing *et al*. (2011) Methodology

The X11 method was developed to be applicable at multiple wavelengths, based on the relationship determined by Morel (1988) and the updated coefficients by Morel et al. (2007). The X11 study examined three wavelengths specifically (412, 490, and 555 nm) to determine which would provide the most accurate estimate of $Chla$ from $K_{\mathrm{bio}}(\lambda)$, based on each wavelengths' sensitivity to attenuation caused by variations in *Chla*. Of these wavelengths, 412 nm was determined to be too strongly influenced by the attenuating effects of CDOM and 555 nm was determined to lack sensitivity to changes in $Chla$. Therefore 490 nm was chosen as the optimal wavelength for the study, being sensitive to changes in $Chla$ while minimising (although not eliminating) the influence of CDOM concentration on total attenuation (Xing et al. 2011). The same rationale was used for adopting 490 nm as the wavelength of choice for this study. For 490 nm, the values for the coefficients used in Equation 1.9 are: $\chi(490)$ = 0.0825, and e(490) = 0.6529. The value for $K_{\mathrm{w}}(490)$, which is also a constant, is 0.0166 m^{-1}.

2.4.1 Outlier Detection and Determination of *F*(i)

Once the Level 2 data were corrected for NPQ effects using S08, they were incorporated into Equation 1.16 and $A(z)$ vs. $C(z)$ values were calculated for each profile in each mission for $z = z_{\mathrm{min}}$ to z_{max}. Once all $A(z)$ and $C(z)$ values were calculated, the slope (*S*) of the relationship was determined using an iterative linear regression procedure to remove and correct for outliers associated with the $A(z)$ profile (see Figure 1.2). The intention of this was to detect anomalous deviations of $A(z)$ (a measure of cumulative light attenuation in the water column) that were not associated with corresponding deviations in $C(z)$ (a measure of cumulative $fluor$ in the water column). As recognized by X11, a common cause of these deviations is the passage of clouds during a profile (Figure 1.2.C), which affects $E_{\mathrm{d}}(490,0)$ and therefore all values of $A(z)$ that are recorded during the event. Recall that the three sources of variability in the X11 relationship are variability in $E_{\mathrm{d}}(\lambda,0)$, in the $fluor$ to $Chla$ relationship, and in the $K_{\mathrm{d}}(\lambda,z)$ to $Chla$ relationship (see Section 1.6.2). In order to relate variability in the light field with variability in $Chla$ (via measurements of $fluor$), it is important to remove any sources of

variability in $E_{\mathrm{d}}(490,z)$ that are not attributable to phytoplankton – cloud-induced changes in $E_{\mathrm{d}}(490,0)$ are an important source of such variability.

In the X11 method, outlier removal was accomplished by comparing the observed values of $A(z)$ to the values predicted from the regression of $A(z)$ on $C(z)$, $\hat{A}(z)$. Values of $A(z)$ < 98% of the regression-predicted value (i.e., $\frac{\left(\hat{A}(z)-A(z)\right)}{\hat{A}(z)} > 0.02$) were considered to be outliers and were removed. A new $A(z)$ vs $C(z)$ regression was conducted with the remaining points, and outliers were removed based on the same criterion. This iterative process continued until no outliers remained. The slope of the final regression was then calculated via linear regression and used to interpolate any missing values of $A(z)$, using $\hat{A}(z)$. This slope, $S(i)$, was also used to calculate the profile-specific *F*-factor, $F(i)$, according to Equation 1.20. It should be noted that the X11 method only made reference to $A(z)$ values greater than zero, and the above definition of an outlier is not appropriate for $A(z)$ values less than zero. To handle the latter case, for $A(z)$ values less than zero, outliers were redefined using absolute values, represented as $\left|\frac{\left(\hat{A}(z)-A(z)\right)}{\hat{A}(z)}\right| > 0.02$. This provided an identical outlier criterion to the one used for positive values of $A(z)$.

2.5 Modification of the Xing *et al*. (2011) Methodology

During the implementation of the X11 methodology, it was determined that the procedure to identify and correct for the effects of cloud cover could introduce bias into the estimation of $F(i)$. Further, it was noted that the $A(z)$ vs $C(z)$ relationship was often curved, suggesting possible inconsistencies with the linear assumptions of the analysis that might lead to errors in the estimation of a profile-specific $F(i)$. Consequently the outlier correction procedure was modified, and the curvature with depth of the $A(z)$ vs. $C(z)$ relationship was explored to determine the suitability of a depth-dependent calibration factor for routine analysis.

2.5.1 Outlier Correction

The X11 method for outlier correction is subject to biases from two possible sources. The first is that the X11 method only detects outliers below the regression line. The authors of X11 stated, correctly, that their outlier-removal process is targeted at removing the effects of cloud-induced variability in $E_d(0)$, and therefore $A(0)$. However they only considered the condition of intermittent cloud clover during a predominantly sunny profile (Figure 1.2). This scenario can be identified by sharp drops in $A(z)$, where all anomalous data points are below the general trend of the profile (Figure 1.2). They did not consider the condition of intermittent sunlight during an otherwise cloudy profile, a scenario that can be identified by sharp upward spikes in $A(z)$ where all anomalous data points are above the general trend in the data (Figure 2.5). This issue was resolved by modifying the X11 definition of an outlier to include anomalous points in $A(z)$, presumably caused by variability in $E_d(0)$, both above and below the regression line.

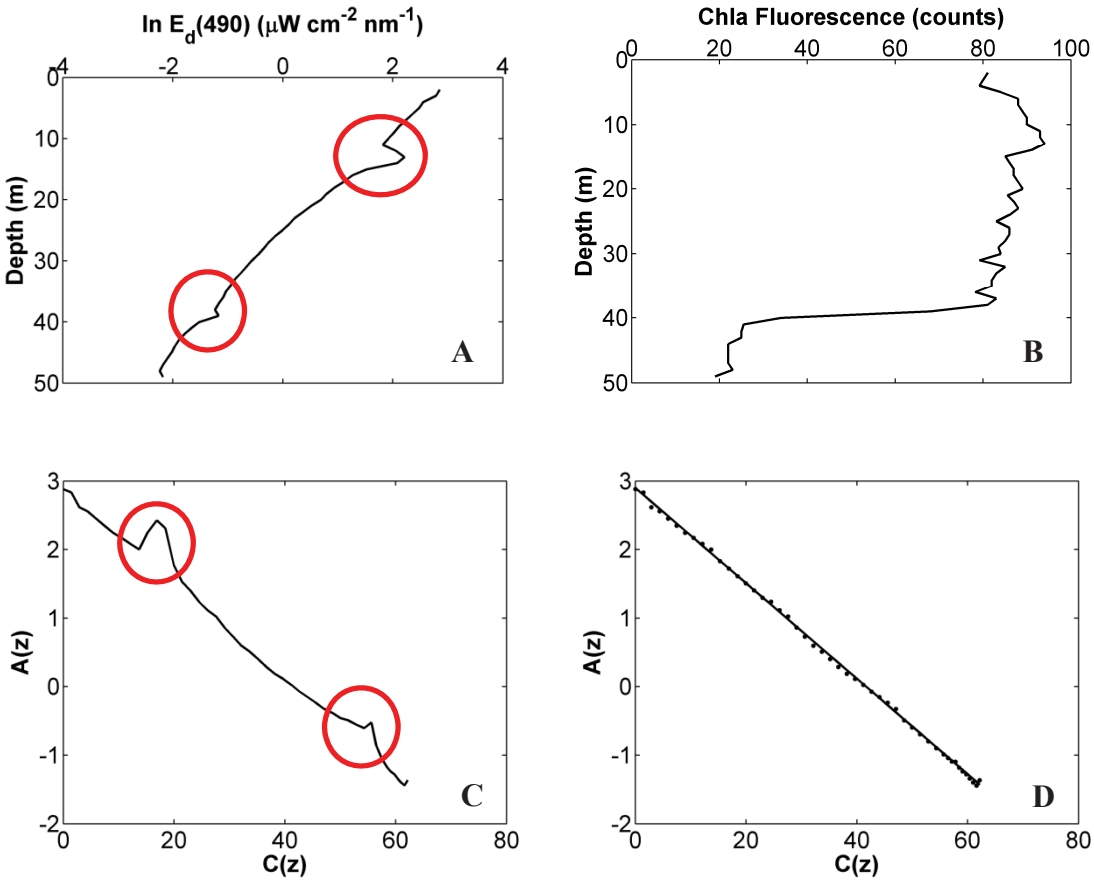

Figure 2.5 (Previous Page). A glider profile contaminated by short periods of sunlight during an otherwise cloudy period, from Mission #12 (2013-12-02). **(A)**: Depth profile of ln-transformed downwelling irradiance at 490 nm. Note the two spikes in $\ln E_{\mathrm{d}}(490)$ at approximately z = 12 m and z = 38 m (circled in red). **(B):** Depth profile of chlorophyll *a* fluorescence, in raw counts. **(C)**: An $A(z)$ vs. $C(z)$ curve calculated using the data from 2.7.A and 2.7.B as inputs. The sharp deflections in $A(z)$, circled in red, are consistent with transient sunny patches affecting incident irradiance at the surface, and consequently at depth z, independent of changes in cumulative attenuation of irradiance above that depth as inferred from fluorescence (see Equation 1.16). **(D)**: $A(z)$ vs. $C(z)$ relationship after the affected points have been removed using the modified outlier criteria. The slope (black line) is then used to calculate the unique, profile-specific conversion factor ($F(i)$) for converting fluorescence counts to $Chla$.

The second source of error is that by defining an outlier as $\frac{\left(\hat{A}(z)-A(z)\right)}{\hat{A}(z)} > 0.02$, the acceptable range within which $A(z)$ can deviate from $\hat{A}(z)$ without being identified as an outlier shrinks as $\hat{A}(z)$ decreases (Figure 2.6.A). When $\hat{A}(z)$ = 0, a solution for this value cannot be obtained. Additionally, visualisation of the outlier removal process of the X11 method revealed that this criterion was unnecessarily stringent and was identifying points as outliers that were not noticeably anomalous (Figure 2.6.A). This resulted in a high proportion of points being discarded as outliers and a final $A(z)$ vs. $C(z)$ profile that rigidly conformed to the linear fit of the slope, regardless of the initial shape of the profile. This issue was resolved by modifying the X11 definition of an outlier to be any value of $A(z)$ outside of the 90% prediction interval for $\hat{A}(z)$ at a given value of $C(z)$ (Figure 2.6.B). This provided a wider acceptable deviation for values of $A(z)$ from $\hat{A}(z)$, allowing for greater retention of original data points and the information retained therein. Prediction intervals were calculated using the "polyfit" and "polyconf" functions in MATLAB (version 2012a).

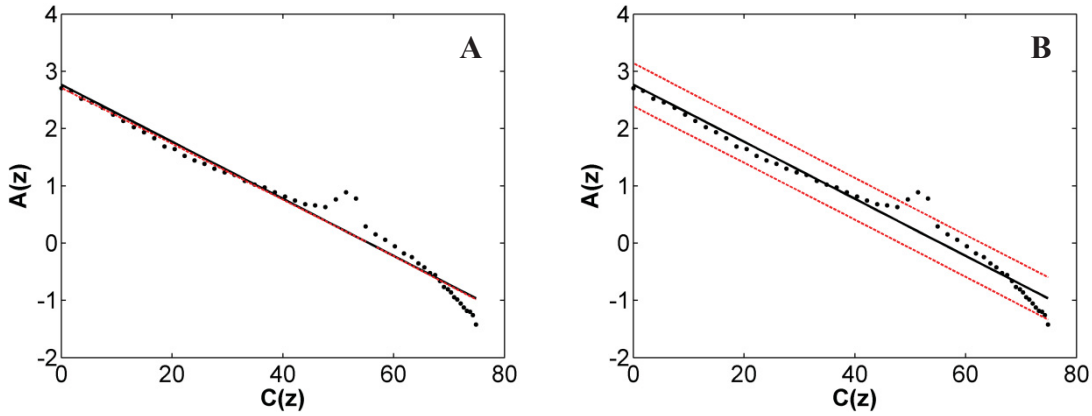

Figure 2.6. Comparison of the original (2.8.A) and modified (2.8.B) X11 outlier identification criterion as applied to an $A(z)$ vs. $C(z)$ glider profile, showing the linear fit (solid black line) and outlier threshold range around that fit (dashed red lines). **(A):** the original X11 outlier detection threshold, where a data point is identified as an outlier if $A(z)$ is less than 98% of the value of $\hat{A}(z)$, is almost indistinguishable from the slope. Note that for this profile a large portion of the data points would be identified as outliers and removed by this process. **(B):** the modified X11 outlier detection threshold, where a data point is identified as an outlier if $A(z)$ is outside of the 90% prediction interval of $\hat{A}(z)$. Note that for this profile only the data at approximately 50 m would be identified as outliers and removed by this process.

2.5.2 Retaining Depth-Dependent Information in the $A(z)$ vs. $C(z)$ Relationship

The X11 method fits a single linear function to the $A(z)$ vs. $C(z)$ relationship, thereby implicitly assuming that the bio-optical properties of the phytoplankton community that drive this relationship are constant with depth. The authors acknowledge this assumption as a methodological simplification, and state that it is probable that the relationship actually varies with depth (Xing et al. 2011). Initial visual inspection of glider profiles used in this thesis demonstrate depth-dependent variability in the relationship. However, by fitting a single linear function to the $A(z)$ vs. $C(z)$ relationship and excluding any data that doesn't conform to linearity as an outlier, any depth-dependent information contained in the profile is lost and any variability in the $A(z)$ vs. $C(z)$ relationship with depth cannot be explored. Therefore if there is any depth-dependent curvature to the relationship, an alternative to the linear fit needs to be investigated.

Systematic deviation from linearity in an $A(z)$ vs. $C(z)$ profile can be tested, with the null hypothesis being that there is no systematic deviation from linearity and therefore deviations from a linear fit are random. To investigate this hypothesis a runs test was performed on each $A(z)$ vs. $C(z)$ profile before the outlier-removal process was conducted, using the "runstest" MATLAB function (version 2012a). This function was used to determine whether the residuals around the regression fit were randomly distributed in the depth-dependent sequence, or whether there were runs of consecutive residuals above or below the fit. Randomly-distributed residuals would not reject the null hypothesis at a significance level of alpha = 0.05, and would indicate in this context that a linear fit was appropriate for the data. Residuals that contain fewer than expected runs, indicating systematic deviation around the fit, would lead to a rejection of the null hypothesis at a significance level of alpha = 0.05, suggesting that a linear fit was not appropriate for the data (Figure 2.7.A).

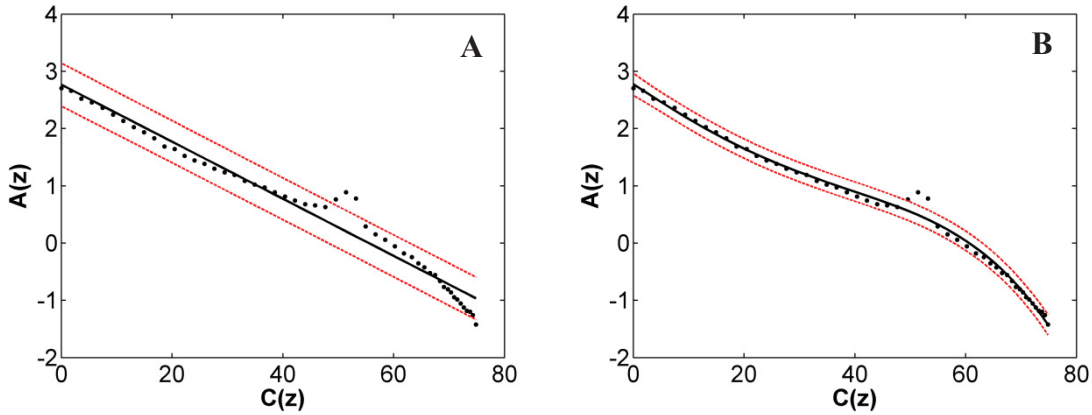

Figure 2.7. Comparison of fits to the same $A(z)$ vs. $C(z)$ profile used in Figure 2.6. Both plots show the fit (solid black line) and the 90% prediction interval around each value of $\hat{A}(z)$ used to detect outliers (dashed red lines). **(A):** a linear fit to the $A(z)$ vs. $C(z)$ profile that failed the runs test. Note that the data points are not randomly distributed around the fit due to the difference in shape between the data and the fit – sequential points run together below the fit ($C(0)$ to $C(35)$), then above the fit ($C(35)$ to $C(65)$), then below the fit again ($C(65)$ to $C(75)$). **(B):** a 4th order polynomial fit to the $A(z)$ vs. $C(z)$ profile that didn't fail the runs test. Note that the fit line more closely resembles the natural shape of the data than does the linear fit. Also note that the transient increase in $A(z)$ seen at approximately $C(50)$, consistent with a break in cloud cover, would still be identified as outliers by the outlier-detection process.

As a metric for determining whether a linear fit was the most appropriate fit for the $A(z)$ vs. $C(z)$ relationship, each profile was fitted with five polynomial fits of successively increasing order, from 1st (linear) through 5th order. The following parameters were then collected for each $A(z)$ vs. $C(z)$ curve to determine how appropriate each degree of fit was for the profile: the adjusted r^2 coefficient, the root mean square error (*RMSE*), and whether or not the profile failed a runs test at $p = 0.05$. For the higher order polynomials, the implication for the outcome of the runs test is the same as those for the linear fit: if there are systematic patterns of deviation in the residuals around the fit then the fit is an oversimplification of the pattern in the data set. A problem remains, because higher-order fits will conform to departures associated with cloud cover, defeating the purpose of the outlier correction. So, in addition, each profile was inspected visually for a subjective determination of overfitting and inadvertent retention of points that might have been identified as outliers. The objective of these processes was to determine a fit that consistently maintained the original curvature of the profile so that any depth-dependent variability in the $A(z)$ vs. $C(z)$ relationship could be explored in more detail, while still identifying cloud- and sun-induced anomalies in $A(z)$ as outliers as described in Section 2.5.1 (Figure 2.7).

2.5.3 Modified Full-Profile *F*(i)

As discussed in Chapters 3 and 4, although nonlinearities in the $A(z)$ vs. $C(z)$ relationship may exist a full-profile *F*-factor, $F(i)$, can still be a relevant estimate of the $fluor$ to $Chla$ relationship capable of accounting for local variation in the bio-optical properties of the phytoplankton population. Thus, following the outlier-detection method outlined above in 2.5.1 and 2.5.2, a second linear, full-profile $F(i)$ was calculated for each profile. To distinguish it from the $F(i)$ generated using the original X11 methodology, the $F(i)$ generated using the methodology outlined in this thesis will be denoted BC15 $F(i)$, for Beck and Cullen 2015.

2.6 Vertical Division of the $A(z)$ versus $C(z)$ Relationship: Generating Depth-Resolved F-factors ($F(i,\zeta)$)

Once a profile had its outliers identified, removed, and replaced using a fit appropriate for retaining any curvature with depth (Section 2.5.1 and 2.5.2), then depth-dependent trends in the $A(z)$ vs. $C(z)$ relationship, if present, could be explored for consistency between profiles and missions. This was accomplished by dividing the surface layer into strata delineated by optical depth (ζ; Equation 2.3) with the lower limit of each optical depth represented by z_ζ (units of m; Equation 2.4) (cf. Babin et al. 1996a; Woźniak et al. 2003). The water column was thereby divided into layers based on levels of irradiance relative to $E_\mathrm{d}(\lambda, 0)$, where, for reference, $E_\mathrm{d}(\lambda, z_\zeta)$ at $\zeta = 4.6$ corresponds to 1% of $E_\mathrm{d}(\lambda, 0)$ (Lorenzen 1972; Kirk 2011).

Once the water column was divided into optical layers a linear regression was conducted for the $A(z)$ vs. $C(z)$ relationship within the stratum defined by the upper limit of each layer ($z_{\zeta-1}$) and the lower limit of each layer (z_ζ). The slope of each linear regression in profile i in optical layer ζ, $S(i,\zeta)$ was then converted into an F-factor for that optical depth, $F(i,\zeta)$, using Equations 1.16 through 1.19, but replacing z_min and z_max with z_upper and z_lower. In order to maintain consistency with Equation 1.20, the operational notation for the optical-depth-specific F-factor used for the duration of this thesis will be expressed by:

$$F(i,\zeta) = S(i,\zeta)^{\frac{1}{e(\lambda)}} \qquad (2.10)$$

where $F(i,\zeta)$ is the F-factor for optical layer ζ in profile i, and $S(i,\zeta)$ is the slope for that same layer.

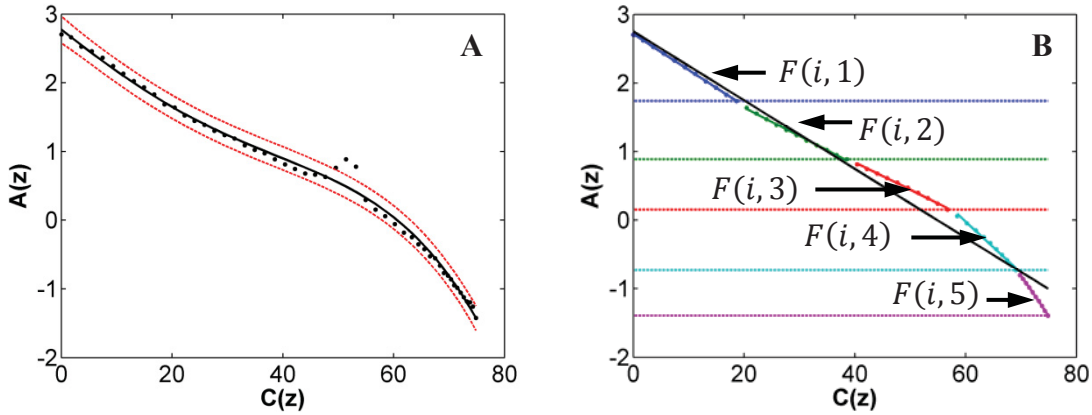

Figure 2.8. Comparison of an $A(z)$ vs. $C(z)$ profile, the same profile used in Figures 2.8 and 2.9, before and after the removal of outliers. **(A):** original profile data points, with a 4th order polynomial fit (black line) and 90% prediction intervals (red dashed lines) showing the acceptable range for $A(z)$ values, outside of which any values will be identified as an outlier. Note the outliers at approximately $C(50)$. **(B):** the same profile after being corrected for outliers using a 4th order polynomial fit. Note that the inflated values of $A(z)$ at approximately $C(50)$ from 2.10.A are no longer present. The profile has also been subdivided into five optical layers (delineated by colour) between $z_{\min}$ and $z_{\max}$. Linear regressions were conducted for each optical layer (solid coloured lines), and the slope of those regressions converted into $F(i,\zeta)$, with units of (mg Chla $\mathrm{m}^{-3} \cdot \mathrm{count}^{-1}$). These depth-resolved F-factors are: $F(i,1) = 0.0109$, $F(i,2) = 0.0077$, $F(i,3) = 0.0072$, $F(i,4) = 0.0189$, and $F(i,5) = 0.0373$. These F-factors can be compared to the BC15 $F(i)$ value obtained from the overall linear slope for the whole profile (solid black line), which converts to an $F(i) = 0.0102$ (mg Chla $\mathrm{m}^{-3} \cdot \mathrm{count}^{-1}$). Notice the depth-dependent variability in the $F(i,\zeta)$ of the $A(z)$ vs. $C(z)$ relationship when optical layers are considered independently of the whole profile.

By dividing the surface layer into strata it is possible to test the hypothesis that there is consistent variability in the underlying bio-optical relationships of the X11 method with depth. Specifically, variability in the relationship between $fluor$ and $Chla$ or between K_{bio} and $Chla$ as represented by changes in $F(i,\zeta)$ with optical depth (note: the unique contributions of these two sources of variability cannot be separated using this method). The null hypothesis in this case would be that there is no consistent variability with optical depth in the aforementioned bio-optical relationships, and therefore there will be no significant difference in the $F(i,\zeta)$ between optical depths.

In order to compare the F-factors calculated per optical layer ($F(i,\zeta)$) to the F-factors determined per profile using the X11 method ($F(i)$), each $F(i,\zeta)$ was expressed

as a percent difference from its corresponding X11 $F(i)$. This was accomplished using the following formula:

$$\text{Percent Difference} = \left(1 - \frac{F(i,\zeta)}{F(i)}\right) * 100\% \qquad (2.11)$$

This provided a measure of the relative difference between the *F*-factor at each optical depth calculated by the modified BC15 method and the overall *F*-factor for the profile calculated using the X11 method. The data for each optical depth was then pooled for all profiles across all missions, and the MATLAB function "boxplot" (version 2012a) was used to compare whether there were any differences in the pooled, normalised BC15 $F(i,\zeta)$ values between each optical depth. This allowed for the analysis of any systematic, depth-specific trends in the depth-resolved *F*-factors relative to the full-profile *F*-factor estimated using X11, in order to test the hypothesis that there is variability in the underlying bio-optical relationships of the X11 method with depth.

2.7 Investigating the Effects of CDOM on the Modified X11 Method

The model relating chlorophyll concentration to the rate of attenuation of downwelling light that underlies the X11 method, developed for Case 1 waters by Morel (1988) and modified by Morel et al. (2007), attributes all of the variability in the diffuse attenuation coefficient to chlorophyll-containing particles and their covariates (Equation 1.9). When light-attenuating water constituents are present that do not covary with the phytoplankton assemblage as described in Morel's model for Case 1 waters, such as sediment or coloured dissolved organic matter (CDOM) in Case 2 waters, Equation 1.9 still attributes this change in attenuation directly to chlorophyll *a* and will provide an inaccurate $Chla$ estimate. When this $Chla$ estimate is incorporated into the X11 method (Equation 1.11) the result is a similarly inaccurate *F*-factor estimate. This potential for inaccuracy implies that that X11 method cannot reliably be applied to Case 2 waters, where phytoplankton are not the only significant contributors to the optical properties of the water column and where these other contributors do not covary with phytoplankton

concentration. However that is not to say that the method does not account for a certain degree of attenuation caused by non-phytoplankton constituents, as the coefficients calculated by Morel (1988) relating $K_{\mathrm{bio}}(490)$ to $Chla$ implicitly include an attenuating effect of the CDOM concentration and detritus that does covary with the phytoplankton assemblage. It is therefore important to emphasize that it is not simply a change in CDOM concentration that will cause inaccuracies in the $Chla$ estimates, and therefore the *F*-factor estimates, of the X11 method. Instead, it is a change in CDOM relative to $Chla$ other than what is implicitly accounted for by the underlying Morel model. X11 acknowledges this theoretical limitation of the method; this is not a novel observation. They also mention that a qualitative assessment of the relative contribution of CDOM to overall attenuation can be accomplished through the comparison of $K_{\mathrm{bio}}(490)$ to $K_{\mathrm{bio}}(412)$, which is more sensitive to the presence of CDOM. They do not, however, propose any direct correction for the effect of CDOM on $Chla$ estimates from $K_{\mathrm{bio}}(490)$ using the methods outlined in X11. Since the gliders used in this study move from near-shore to off-shore through both Case 1 and Case 2 waters, there is an opportunity to study the effects of applying the modified X11 method to Case 2 waters (Figure 2.9). It can therefore be tested whether or not CDOM that varies independently of $Chla$ has a significant effect on estimates of the *F*-factor, in either the horizontal or vertical dimensions, with the null hypothesis being that there is no significant effect.

The possible influence of CDOM on the estimation of $Chla$ from $K_{\mathrm{bio}}(490)$, and thus on the *F*-factor, is illustrated by the horizontal patterns in X11 $F(i)$ during Mission #7 in the spring of 2013 (Figure 2.9). For this mission it can be observed that there are greatly increased $Chla$ values nearshore (0 – 50 km) in the return transect. Notice the correspondingly large decrease in the X11 $F(i)$ values over the same interval, while the CDOM concentrations and density structure are roughly similar. The large nearshore $F(i)$ values during the outgoing transect are consistent with the influence on the *F*-factor of a combination of a high CDOM concentration with low concentrations of $Chla$. The ratio of CDOM to $Chla$ here is likely higher compared to the Case 1 conditions assumed by the Morel model underlying the X11 method, which would result in any increased attenuation from CDOM being interpreted as increased attenuation from $Chla$. When this increased attenuation is combined with a lack of $Chla$ signal, this would result in inflated

X11 $F(i)$ values. During the return transect $Chla$ is higher nearshore, meaning phytoplankton are contributing more to $K_{\text{bio}}(490)$. It can be proposed that the ratio of CDOM to $Chla$ is closer to the covarying relationship implicit in the Morel relationship, and the X11 $F(i)$ would likely be more representative of the phytoplankton community's $fluor$ to $Chla$ relationship.

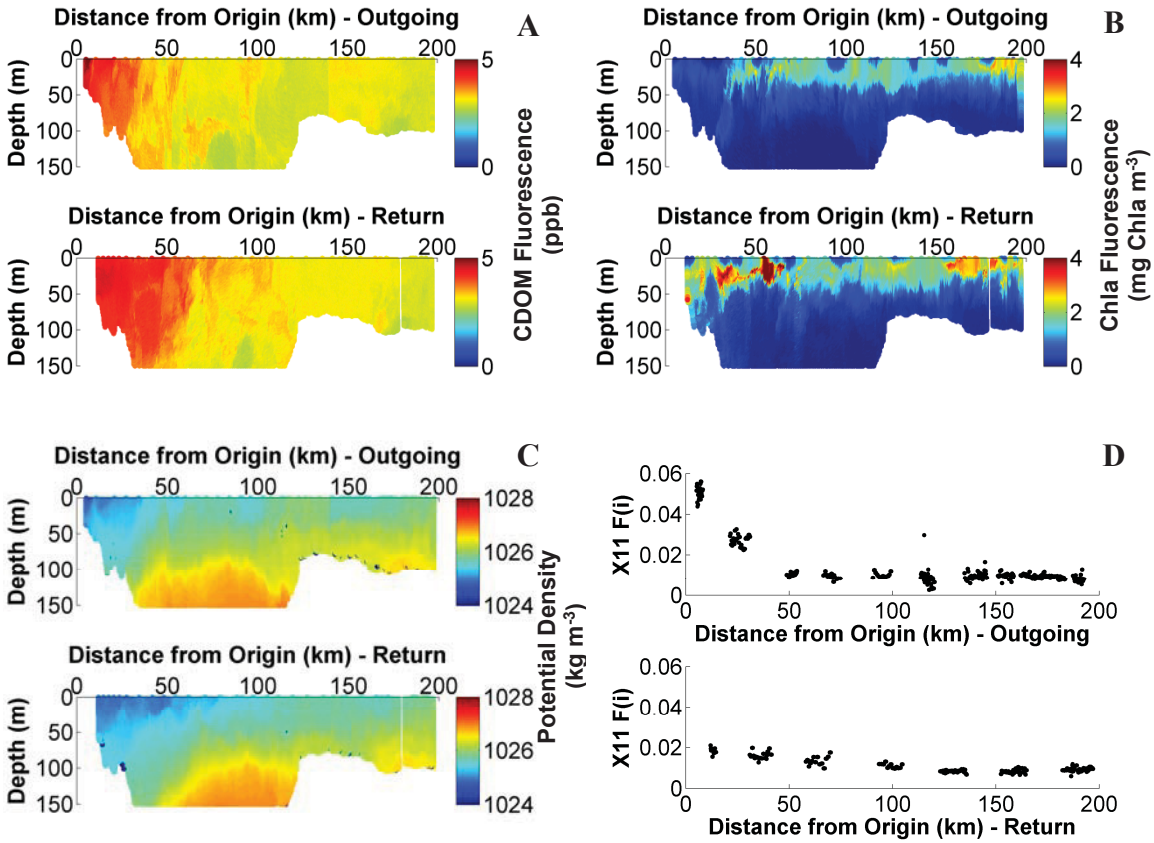

Figure 2.9. Outgoing (originating at the mouth of the Halifax Harbour, Nova Scotia; 0 km) and return (ending at the edge of the continental shelf; 200 km) transects for Mission #7 running from 2013-03-29 to 2013-04-18. The glider was deployed for approximately 3 weeks and travelled a distance of approximately 400 km. Each variable here is plotted as a function of depth and distance offshore: **(A)** CDOM fluorescence (ppb), **(B)** chlorophyll *a* estimated from fluorescence (mg Chla m^{-3}), **(C)** potential density (kg m^{-3}), and **(D)** the X11 $F(i)$ for all profiles available after Level 2 QC processing (mg Chla $m^{-3} \cdot count^{-1}$).

In order to more directly compare the varying concentrations of CDOM and $Chla$, and to determine whether this relationship had a significant effect on the calculation of the F-factor, patterns in F were related to the ratio of CDOM to $Chla$. For this

investigation $Chla$ was calculated from the NPQ-corrected $fluor$ data and the manufacturer's F-factor, so that estimates of $Chla$ were not affected by the same bio-optical issues as the BC15 $F(i)$ currently under investigation. The CDOM values were also adjusted for a background value (Figure 2.10) due to the ubiquitous non-zero CDOM signal in the data set (CDOM – mission specific background = $CDOM_{adj}$). The background value for each mission was calculated as the 1st percentile value of the Level 2 data. It served as a baseline above which variability in CDOM could be related to variability in $Chla$. Consequently, the $CDOM_{adj}$:$Chla$ relationship has an origin corresponding to the minimum $Chla$ fluorescence and baseline CDOM values for the surface waters.

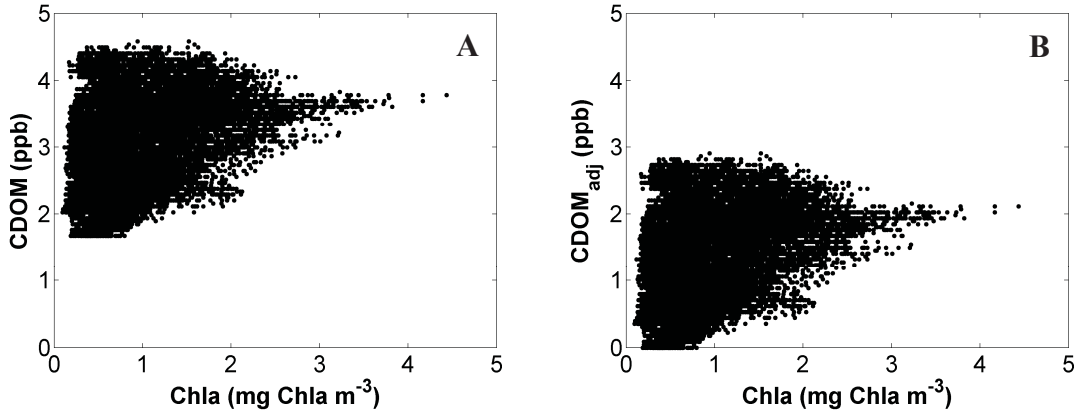

Figure 2.10. CDOM and $Chla$ data from Mission #4 running from 2012-06-12 to 2012-07-07, both **(A)** before and **(B)** after removing the mission-specific CDOM background value of 1.67 ppb (n = 30,638). After this correction, the data shown in panel B were used to calculate the per-data-point ratio of $CDOM_{adj}$:$Chla$.

Using this rough measure of the concentration of CDOM relative to an inferred background it was possible to investigate the influence of $CDOM_{adj}$:$Chla$ on the F-factor by conducting a linear regression for each mission of the F-factor on this ratio (Figure 2.11; results should be interpreted with caution as some underlying assumptions of regression were violated). This was done in two ways. The first approach evaluated the relationship on a per-data-point basis, where the BC15 $F(i,\zeta)$ for each data point in a mission (which was determined using the profile number, i, and optical depth, ζ, for the data point) was paired with the ratio of $CDOM_{adj}$ to $Chla$ values for that data point

($\mathrm{CDOM_{adj}}$:$Chla$; units of ppb $\cdot$ (mg Chla $\mathrm{m^{-3}})^{-1}$). The second approach evaluated the relationship on a per-profile basis, where the BC15 $F(i)$ for each profile was paired with the ratio of the average $\mathrm{CDOM_{adj}}$ value over the interval $z_{\min}$ to $z_{\max}$ to the average $Chla$ value over the same interval ($\mathrm{CDOM_{adj}}|_{z_{\max}}^{z_{\min}}$: $Chla|_{z_{\max}}^{z_{\min}}$; units of ppb $\cdot$ (mg Chla $\mathrm{m^{-3}})^{-1}$).

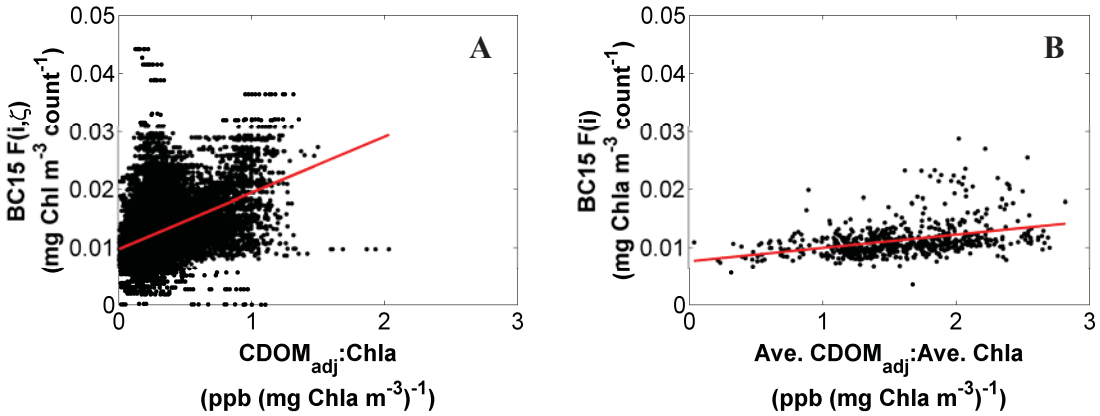

Figure 2.11. (A): Linear regression of BC15 $F(i,\zeta)$ on the per-point $\mathrm{CDOM_{adj}}$:$Chla$ ratio for the same glider mission as in Figure 2.10 (n = 30,638; y = 0.0097x + 0.0097; r^2 = 0.17). From these regressions, residuals of BC15 $F(i,\zeta)$ around the fit are calculated to isolate variability in the F-factor caused by factors other than the contribution of CDOM, relative to $Chla$, on the rate of attenuation of light in the water column. **(B)**: Linear regression of BC15 $F(i)$ on the per-profile $\mathrm{CDOM_{adj}}|_{z_{\max}}^{z_{\min}}$: $Chla|_{z_{\max}}^{z_{\min}}$ ratio for the same mission as in 2.13.A (n = 639; y = 0.0024x + 0.0076; r^2 = 0.14). Residuals of BC15 $F(i)$ around the fit are also calculated for this relationship. For the regression equation, slopes have units of $(\mathrm{mg\ Chla\ m^{-3}})^2 \cdot (\mathrm{count} \cdot \mathrm{ppb})$ and y-intercepts have units of $\mathrm{mg\ Chl\ m^{-3}\ count^{-1}}$. Results should be interpreted with caution as some underlying assumptions of regression were violated

Once the linear regressions were conducted, the residual F-factor values around the fit were obtained. These residuals are significant, because they represent variability in the BC15 F-factor that cannot be attributed to the increasing contribution of CDOM, relative to $Chla$, on the rate of attenuation of light in the water column as estimated with a linear regression. They therefore allow for the analysis of trends in the F-factor that may be caused by changes in the $fluor$ to $Chla$ relationship and the K_{bio} to $Chla$ relationship. The residuals were plotted as a function of distance from shore, to determine if there were any horizontal trends in the BC15 F-factors once $\mathrm{CDOM_{adj}}$, relative to $Chla$, was

accounted for. These trends were compared to the results of the same analysis that were made before accounting for $CDOM_{adj}$:$Chla$ (Sections 2.5.3 and 2.6). For the depth-resolved BC15 $F(i,\zeta)$, the residuals were also grouped by optical layer for each mission, and the MATLAB function "boxplot" was used to determine if there were any systematic variations in the residuals of $F(i,\zeta)$ with optical depth. These results were then compared to the patterns in BC15 $F(i,\zeta)$ with optical depth from before $CDOM_{adj}$, relative to $Chla$, was accounted for (Section 2.6).

2.8 Comparison of *Chla* Estimates from Glider Measurements to *Chla* Values Extracted from Water Samples

When available, *Chla* data from water samples collected during the deployment or retrieval of a glider were plotted as a function of depth (n = 39 samples, from 14 separate days). The values obtained from these samples (see Section 2.1.1 for $Chla$ extraction methods) were compared to the $Chla$ values estimated from the glider's $fluor$ readings, at the same depths but separated in time by up to 23 hours (see Section 2.1.1), using four different conversion factors: the manufacturer's static *F*-factor, the X11 profile-specific *F*-factor, X11 $F(i)$, our profile-specific *F*-factor, BC15 $F(i)$, and our depth-resolved *F*-factors, BC15 $F(i,\zeta)$. This was done to determine whether the X11 method, or our modifications to it, were an improvement over the static *F*-factor in regards to the final *Chla* estimates generated using each method.

CHAPTER 3 RESULTS

3.1 Correction of Non-Photochemical Quenching (NPQ) Effects using the Methodology of Sackmann *et al*. (2008)

NPQ_{corr}, calculated using the S08 method (Equation 2.7), was quantified for each of the 12 missions. NPQ_{corr} was binned into 10% intervals and the percent of profiles in each interval, relative to the total number of mission profiles, was calculated (Figure 3.1).

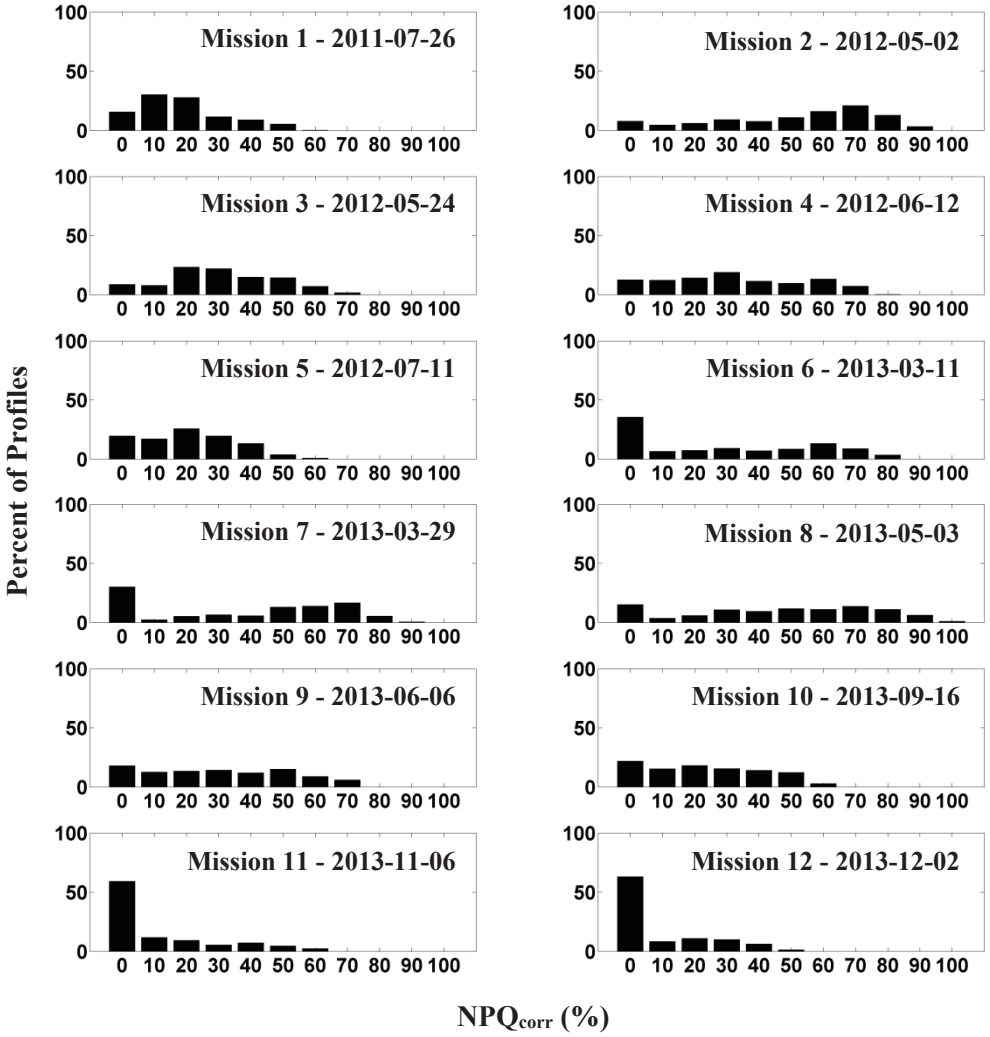

Figure 3.1. NPQ_{corr} (Equation 2.7) for each of the 12 missions. NPQ_{corr} was binned into 10% intervals and the percent of profiles in each interval relative to the total number of mission profiles was calculated. X-axis values denote the largest NPQ percentage for that bin. Notice the high proportion of profiles that experience very little (< 20%) NPQ.

Since it is expected that periods of sustained high irradiance should correlate with higher NPQ (Kiefer 1973a; Krause and Weis 1991; Cullen and Lewis 1995; Müller et al. 2001; Huot and Babin 2010), $\mathrm{NPQ_{corr}}$ was plotted as a function of $E_\mathrm{d}(490, z_\mathrm{min})$ to test whether there was a significant relationship and one was found (Figure 3.2). This relationship can be quantified using a non-linear curve fit, of the form:

$$\mathrm{NPQ_{corr}} = \mathrm{NPQ_{max}} \cdot \left(1 - \exp\left(\frac{-E(490, z_\mathrm{min})}{E_{kQ}(490)}\right)\right) \qquad (3.1)$$

where $\mathrm{NPQ_{corr}}$ is the NPQ correction for a profile at z_min (%), $\mathrm{NPQ_{max}}$ is the maximum NPQ correction for the fit (%), and $E_{kQ}(490)$ is the saturation irradiance for the fit (μW $\mathrm{cm^{-2}}$ $\mathrm{nm^{-1}}$). When the whole dataset is analysed (n = 5362) the relationship is not very strong ($\mathrm{NPQ_{max}} = 38.56\%$, $E_{kQ}(490) = 35.52\ \mu\mathrm{W \cdot cm^{-2} \cdot nm^{-1}}$). However when only the profiles that have a MLD that is 10m deeper than z_min are analysed ((MLD - z_min) > 10m; n = 2303), the relationship is considerably clearer ($\mathrm{NPQ_{max}} = 71.09\%$, $E_{kQ}(490) = 48.38\ \mu\mathrm{W \cdot cm^{-2} \cdot nm^{-1}}$). The primary reason for doing this is to focus the analysis on profiles that have enough depths resolved to obtain an accurate estimation of $\mathrm{NPQ_{corr}}$, and also to focus on mixed layers that span a significant range of irradiance.

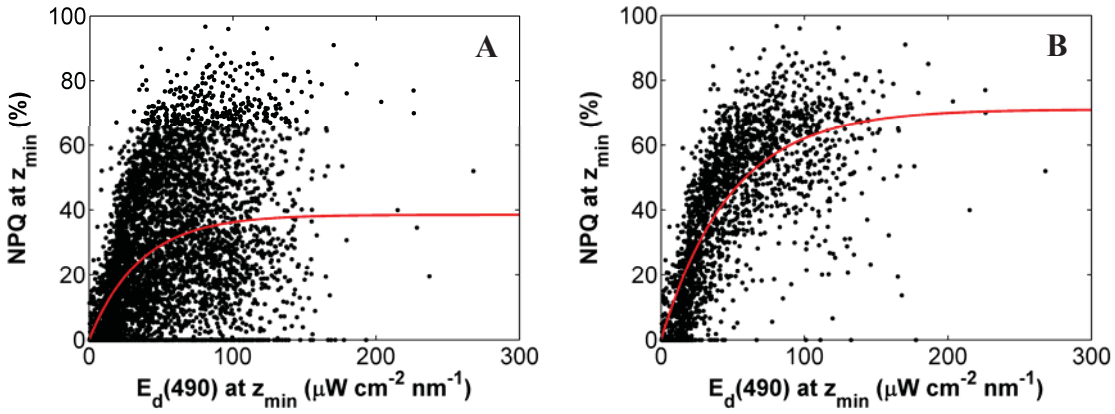

Figure 3.2. $\mathrm{NPQ_{corr}}$ plotted as a function of $E_\mathrm{d}(490, z_\mathrm{min})$ and fit to Equation 3.1. **(A):** Using the full dataset (n = 5362). **(B):** Using a subset of the dataset, consisting only of profiles where (MLD - z_min) > 10m (n = 2303). Notice that inclusion of profiles with shallow MLD weakens the relationship.

Analysis of individual missions reveals that the effect of MLD on the $\mathrm{NPQ_{corr}}$ vs. $E_\mathrm{d}(490, z_\mathrm{min})$ relationship is not consistent across seasons. The effect is more dramatic in certain months, especially during summer, where low estimates of $\mathrm{NPQ_{corr}}$ (despite high levels of $E_\mathrm{d}(490, z_\mathrm{min})$) can likely be attributed to the stratification of the water column, as evidenced by an extremely shallow MLD (Figure 3.3). This is in contrast to missions during the winter months, where there is a consistently deep MLD, and low estimates of $\mathrm{NPQ_{corr}}$ can likely be attributed to low levels of $E_\mathrm{d}(490, z_\mathrm{min})$ (Figure 3.4).

As mentioned in Section 2.3 this method can only be used to correct for NPQ in waters that are mixed at a rate sufficient to prevent the establishment of a gradient in phytoplankton biomass or chlorophyll (Cullen and Lewis 1988) – stratified water columns violate the assumptions of the method. This has important implications for the efficacy of the S08 NPQ correction for this dataset. It implies that, despite having $E_\mathrm{d}(490, z_\mathrm{min})$ values of sufficient magnitude to induce NPQ (as evidenced by profiles in lower-$\mathrm{NPQ_{corr}}$ bins being exposed to similar levels of $E_\mathrm{d}(490, z_\mathrm{min})$ as those profiles in higher bins), if the depth interval between z_min and the MLD is small the S08 method may underestimate the true magnitude of $\mathrm{NPQ_{corr}}$, or perhaps fail to detect it at all. This is also true if the MLD is shallow enough that NPQ is still occurring at that depth. An improper NPQ correction of the fluorescence data will propagate to improper $A(z)$ vs. $C(z)$ curves, and finally to an inaccurate *F*-factor estimate. Therefore it is important to recognize these limitations of the S08 NPQ correction.

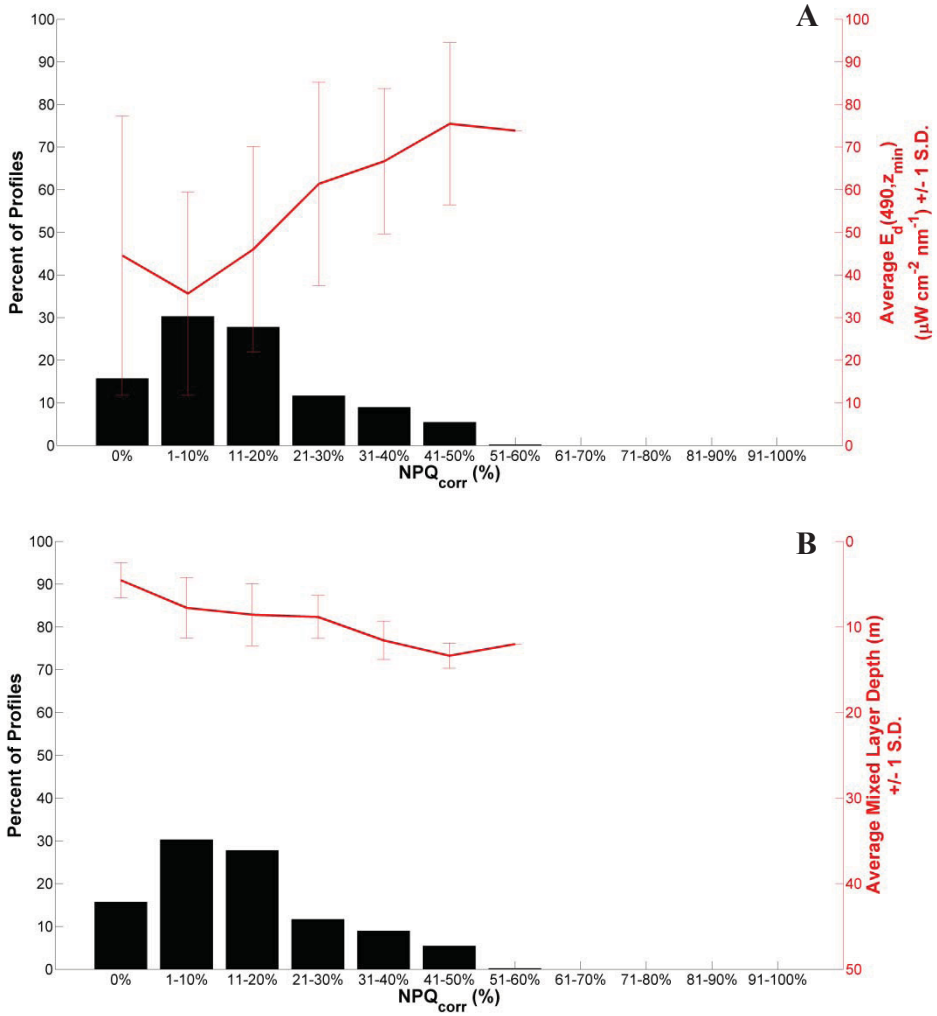

Figure 3.3. $\mathrm{NPQ_{corr}}$ (%) for 515 profiles during Mission #1 (2011-07-26). $\mathrm{NPQ_{corr}}$ was binned into 10% intervals and the percent of profiles in each interval, relative to the total number of mission profiles, was calculated (black bars). **(A)**: The corresponding $E_{\mathrm{d}}(490, z_{\mathrm{min}})$ $(\mu W \cdot \mathrm{cm}^{-2} \cdot \mathrm{nm}^{-1})$ for each $\mathrm{NPQ_{corr}}$ value was used to calculate the average per-bin $E_{\mathrm{d}}(490, z_{\mathrm{min}})$ ± 1 S.D. (red line). Notice that profiles with $\mathrm{NPQ_{corr}}$ less than 20% have approximately the same average $E_{\mathrm{d}}(490, z_{\mathrm{min}})$. **(B)**: The corresponding MLD (m) for each $\mathrm{NPQ_{corr}}$ value was used to calculate the average per-bin MLD ± 1 S.D. (red line). Notice that profiles with $\mathrm{NPQ_{corr}}$ less than 20% have very shallow MLD, suggesting an effect of MLD on the application of the S08 method during this mission, likely causing an underestimate of $\mathrm{NPQ_{corr}}$.

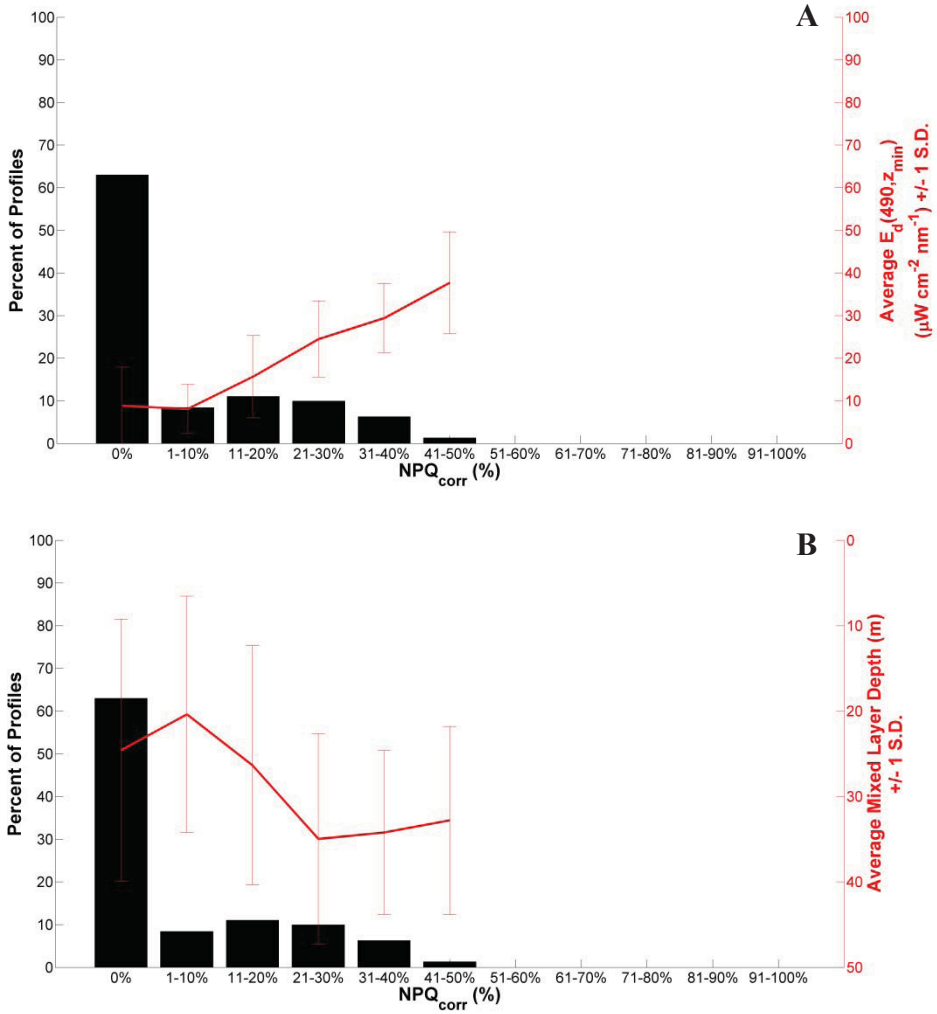

Figure 3.4. $\mathrm{NPQ_{corr}}$ (%) for 381 profiles during Mission #12 (2013-12-02). $\mathrm{NPQ_{corr}}$ was binned into 10% intervals and the percent of profiles in each interval, relative to the total number of mission profiles, was calculated (black bars). **(A)**: The corresponding $E_{\mathrm{d}}(490, z_{\mathrm{min}})$ ($\mu\mathrm{W} \cdot \mathrm{cm}^{-2} \cdot \mathrm{nm}^{-1}$) for each $\mathrm{NPQ_{corr}}$ value was used to calculate the average per-bin $E_{\mathrm{d}}(490, z_{\mathrm{min}})$ ± 1 S.D. (red line). Notice that $E_{\mathrm{d}}(490, z_{\mathrm{min}})$ increases as $\mathrm{NPQ_{corr}}$ increases, consistent with Figure 3.2. **(B)**: The corresponding MLD (m) for each $\mathrm{NPQ_{corr}}$ value was used to calculate the average per-bin MLD ± 1 S.D. (red line). Notice that profiles with $\mathrm{NPQ_{corr}}$ less than 20% have deeper MLD than the summer mission in Figure 3.3. This suggests that MLD is not a limiting factor in applying the S08 method to this mission, and that $\mathrm{NPQ_{corr}}$ should correlate more strongly with $E_{\mathrm{d}}(490, z_{\mathrm{min}})$ than during the summer missions.

3.2 Implementation of Xing *et al.* (2011) Methodology

Level 2 data were corrected for NPQ effects using the S08 methodology outlined in Section 2.3, then processed using the X11 methodology outlined in Section 2.4. Implementation of the X11 methodology provided unique *F*-factors on a per-profile basis (X11 $F(i)$) for each mission. Median $F(i)$ values, calculated on a per-transect basis, agreed well with the static *F*-factor determined by the fluorometer manufacturer, never deviating more than ± 20% (for full data see Table A.1 in Appendix A). If the per-transect median $F(i)$ is expressed as a percent difference from the manufacturer *F*-factor, the mean difference is 5.60 ± 7.35% S.D. for n = 24 transects. The mean IQR (IQR; difference between the 25th and 75th percentiles of the data) for the same 24 transects, normalised to their respective median $F(i)$, was 32.9%. This suggests strong general agreement between the X11 method and factory calibrations, despite fundamentally different approaches. However this does not address the variability in the X11 estimates on a per-profile basis within a mission, which is reflected in the full range of calculated $F(i)$, which ranged over a factor of 10. One cause of variability in $F(i)$ was inflated values in the nearshore region of some missions due to a confounding effect of CDOM, which will be investigated in more detail in Section 3.5. The other sources of variability are changes in the $fluor$ to $Chla$ relationship and the K_{bio} to $Chla$ relationship within the phytoplankton community, which will be discussed in more detail in Chapter 4.

Once the $F(i)$ for each mission were calculated they were plotted as a function of distance from shore to examine the data for any trends in the horizontal dimension (Figures 3.5 and 3.6). A linear slope was determined for each of two transects in a mission – the outgoing transect from the point of deployment to the point in the mission where the glider was furthest from shore, and the return transect from the point in the mission where the glider was furthest from shore to the point of its retrieval. It should be noted that for some transects a linear fit is inappropriate for determining a trend in $F(i)$ with distance from shore, due to the non-linear increase in $F(i)$ nearshore (qualitatively identified as n = 6 of 24 transects in Missions #6, #7, #8, and #12). A linear fit was nonetheless used in order to maintain comparability between missions. For regression information see Table A.2 in Appendix A, however interpret the results with caution.

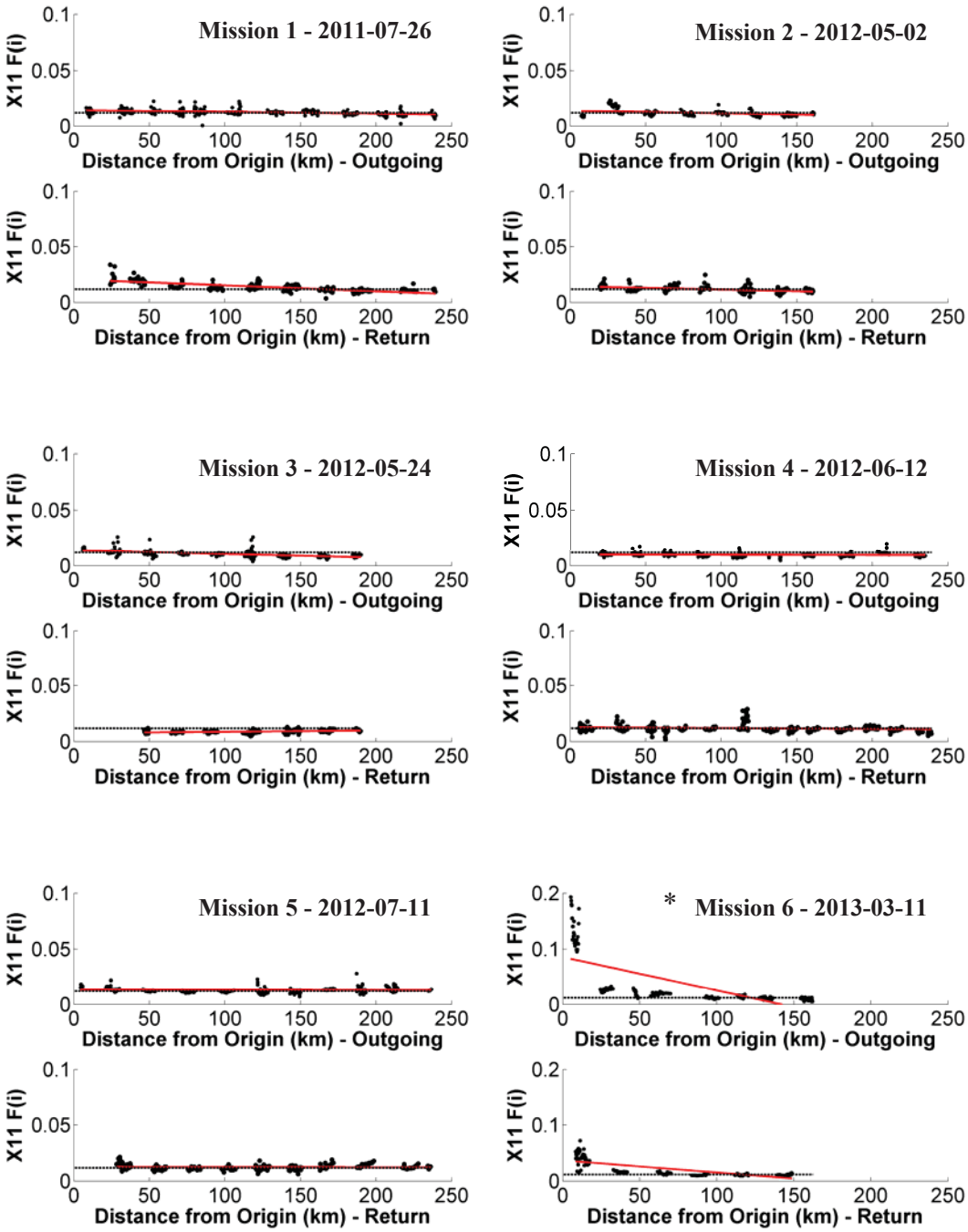

Figure 3.5. Outgoing and return transects of X11 $F(i)$ (mg Chla m^{-3} $count^{-1}$) plotted versus distance from shore for glider Missions #1 - 6. Slopes (red lines) indicate trends in X11 $F(i)$ with distance, and the manufacturer's *F*-factor (horizontal black line at 0.0117 mg Chla m^{-3} $count^{-1}$) provides a reference for X11 $F(i)$ variability. All transects showed a significant ($p < 0.05$) negative trend with distance except Mission 3 return transect (positive trend), and Missions 4 and 5 (no significant trend). Full regression information can be found in Table A.2 in Appendix A. Note that the y-axis of Mission 6 is on a different scale due to its high nearshore variability. Missions marked with a "*" should be interpreted with caution as they violate the assumptions of linear regression.

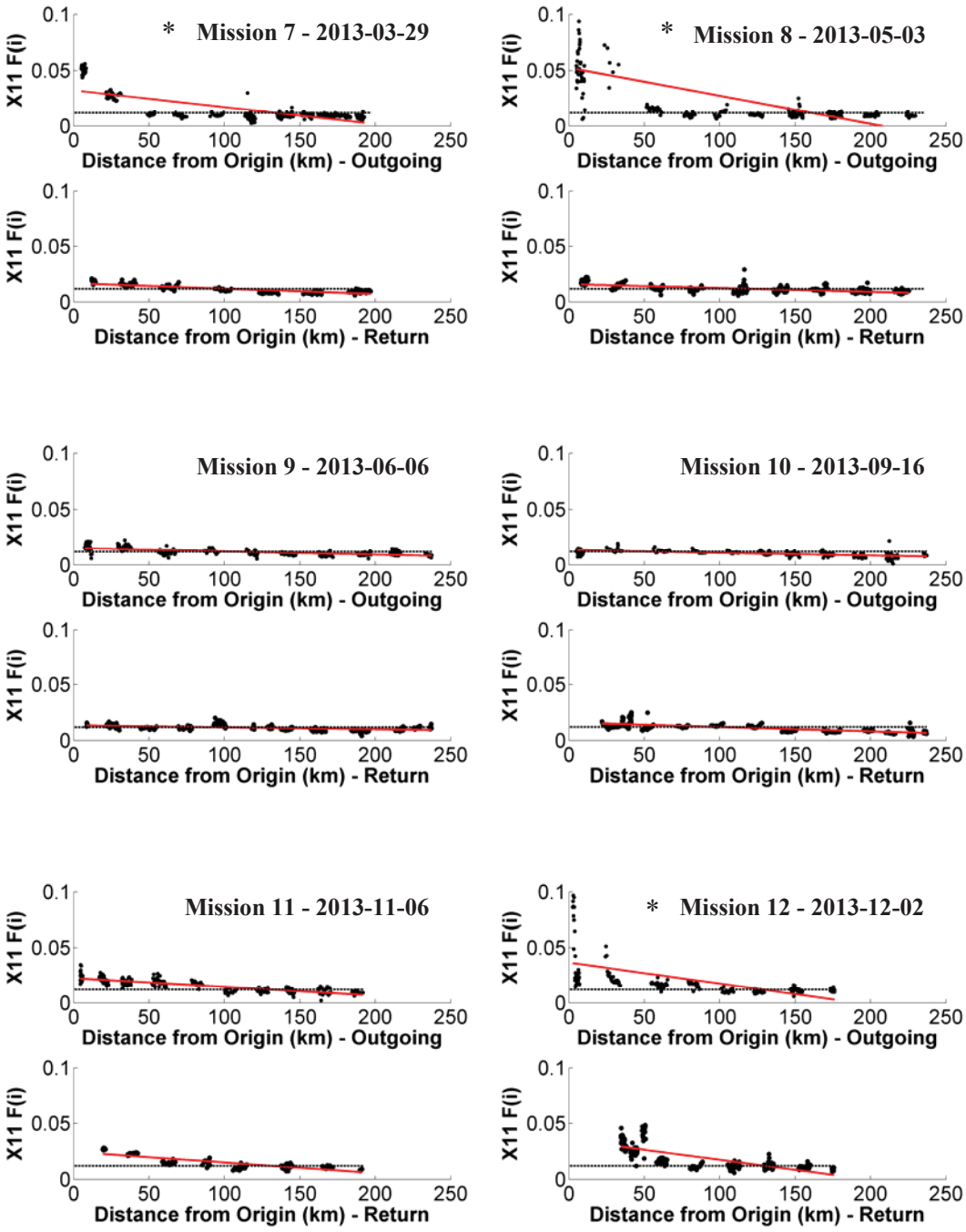

Figure 3.6. Outgoing and return transects of X11 $F(i)$ (mg Chla m^{-3} $count^{-1}$) plotted versus distance from shore for glider Missions #7 - 12. Slopes (red lines) indicate trends in X11 $F(i)$ with distance, and the manufacturer's F-factor (horizontal black line at 0.0117 mg Chla m^{-3} $count^{-1}$ for missions up to Mission 9, and 0.0121 mg Chla m^{-3} $count^{-1}$ for missions afterwards) provides a reference for X11 $F(i)$ variability. All transects showed a significant ($p < 0.05$) negative trend with distance. Full regression information can be found in Table A.2 in Appendix A. Missions marked with a "*" should be interpreted with caution as they violate the assumptions of linear regression.

Of the 24 transects, 19 had a negative slope with distance from shore that was significantly different than zero ($p < 0.05$; including the four non-linear transects mentioned above), 1 had a positive slope with distance from shore that was significantly different from zero ($p < 0.05$; Mission #3, return transect), and 4 had a slope that was not significantly different from zero ($p > 0.05$; both transects of both missions Mission #4 and Mission #5). These results would suggest that, generally, there is a weak trend of decreasing X11 $F(i)$ versus distance from shore. This is consistent with apparent fluorescence yield in the phytoplankton community increasing with increasing distance from shore, as the *F*-factor, expressed as $(\mathrm{mg\ Chla\ m^{-3}\ count^{-1}})$, is the inverse of fluorescence yield. However this trend might also reflect an onshore-offshore trend in how the underlying Morel model estimates $Chla$ from attenuation, with $Chla$ being subject to systematic overestimation nearshore. Further investigation of this trend with distance from shore is conducted in Section 3.5 with a focus on this latter issue.

In order to elucidate any seasonal trends in the average $F(i)$ and in the slope of $F(i)$ when plotted against distance from shore, the per-transect means and slopes were plotted as a function of time of year (Figure 3.7; Note: the "average" used in this context was the per-transect mean, as opposed to the per-transect median discussed at the beginning of Section 3.2 and in Table A.1). The per-transect slopes show a weak trend with season, with the steepest (most negative) slopes occurring during the beginning and ending months of the year and the shallowest (least negative) slopes occurring during the middle of the year. The per-transect means exhibit a similar trend, with inflated values in the winter months corresponding to the steeper slopes seen during the same period. This pattern shows that the more-steeply-sloped relationships in the winter/spring months are due to inflated near-shore $F(i)$ values (Figure 3.7), and not to a decrease in the off-shore $F(i)$ values (either condition could have resulted in steeper slopes). Reasons for this are explored in Section 3.5 and Chapter 4. It should be noted that these trends are driven by a small number of points, due to the low number of missions included in this analysis. Therefore the observations made here are only qualitative in nature, and a larger sample size is required to make more definitive claims about any quantitative seasonality in $F(i)$ patterns.

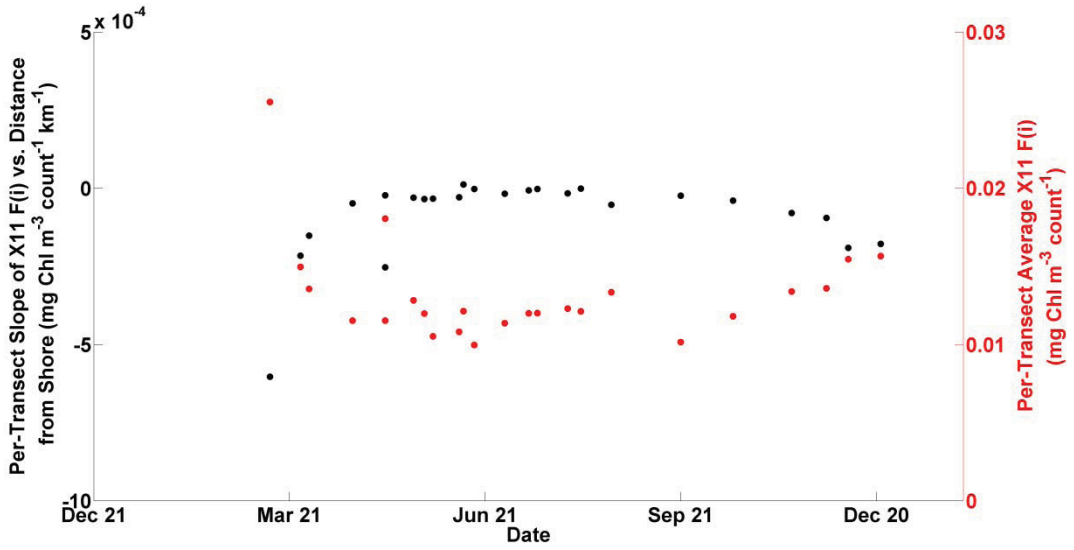

Figure 3.7. Per-transect slope values of the X11 $F(i)$ versus distance from shore relationship (black points) and per-transect mean X11 $F(i)$ values (red points) plotted as a function of time of year (n = 24). Note that the mission transects with more steeply negative slopes also have inflated average $F(i)$values. Also note that this effect is most pronounced during the winter/spring months, and is less pronounced in the summer/fall months.

3.3 Implementation of Modified Xing *et al.* (2011) Methodology

Results reported in Section 3.2 were obtained by applying the X11 method to data that were corrected for NPQ with the S08 methodology outlined in Section 2.5. In the following sections, a modified outlier correction is employed and depth-dependent *F*-factors are calculated.

3.3.1 Outlier Correction

Modifications were made to the X11 outlier correction procedure to correct for two main biases: 1.) The X11 method only removed outliers below the linear fit line, not above it, resulting in skewed $F(i)$ estimates during certain profiles, and 2.) The threshold used to define an outlier of $\frac{\left(\hat{A}(z)-A(z)\right)}{\hat{A}(z)} > 0.02$ was so stringent that it removed all natural curvature from the profile, forcing the $A(z)$ vs. $C(z)$ relationship to be linear with depth regardless of the initial shape of the profile. This eliminated potentially useful depth-

resolved information in the bio-optical relationships within the phytoplankton community, making it impossible to study any depth-dependent trends in those relationships. The outlier criteria were therefore changed to identify an outlier as any value of $A(z)$ outside of the 90% prediction interval for $\hat{A}(z)$ at a given value of $C(z)$, both above and below the fit line (Section 2.5.1). Additionally, non-linear fits were tested to determine whether they would provide better retention of depth-dependent information in the $A(z)$ vs. $C(z)$ relationship than the linear fit utilised by X11. The results of implementing these changes are outlined below.

Although there were no statistical tests done to quantify the effects of changing the outlier criteria (aside from a generalised comparison of model outputs – see Section 3.3.3), it is possible to identify a scenario where the modified method is an improvement over the original method. As outlined in Section 2.5, the original outlier detection method was designed to remove anomalous values of $A(z)$ below the slope line, caused by changes in $E_{\mathrm{d}}(490,0)$ which were presumably from passing cloud cover during otherwise sunny profiles. This removes the effect of variability in $E_{\mathrm{d}}(490,0)$ on the $A(z)$ vs. $C(z)$ relationship, meaning that any remaining variability in $A(z)$ vs. $C(z)$ can be attributed to changes in the $fluor$ to $Chla$ relationship, or to the $K_{\mathrm{d}}(490,0)$ to $Chla$ relationship. However the X11 method fails when there are anomalous values of $A(z)$ above the slope line, caused by changes in $E_{\mathrm{d}}(490,0)$ which would occur during sunny periods in an otherwise cloudy profile. The result of only removing outliers below the slope line during the iterative X11 process is an inaccurate $F(i)$ estimate any time the $A(z)$ vs. $C(z)$ data fluctuates above the slope line (Figure 3.8). By mirroring the outlier detection criterion both above and below the fit, this type of bias is avoided.

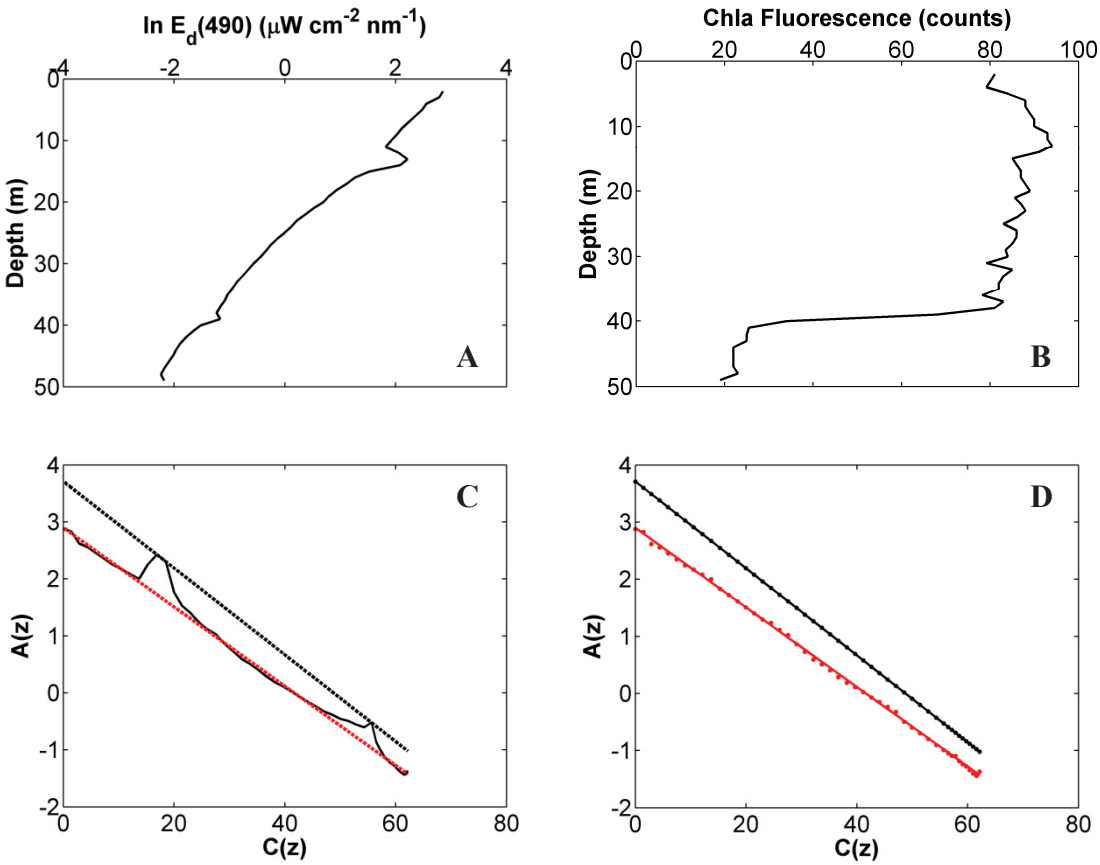

Figure 3.8. Glider profile from Mission #12 (2013-12-02) when the irradiance profile indicated two sunny patches during otherwise cloudy conditions. **(A)**: Depth profile of ln-transformed downwelling irradiance at 490 nm. Note the two spikes in $\ln E_d(490)$ at approximately z = 12m and z = 38m. **(B)**: Depth profile of NPQ-corrected chlorophyll *a* fluorescence, in raw counts. **(C)**: An $A(z)$ vs. $C(z)$ curve calculated using the data from 3.8.A and 3.8.B as inputs, with the final regression fit overlaid on the original profile data using the X11 outlier criteria (black dotted line) and the BC15 outlier criteria (red dotted line). Note the spikes in $A(z)$ at $C(12)$ and $C(38)$ that match those in 3.8.A. Also note that the X11 method identified the maximum values in the spikes as the uncontaminated values and all other points as outliers. **(D)**: The final, corrected $A(z)$ vs. $C(z)$ curve after the iterative outlier-removal method has completed and the missing data points have been interpolated from the final slope fit, using the X11 method (black line and data points; y = -0.0761x + 3.71) and the modified method (red line and data points; y = -0.0695 + 2.90). Note that due to the presence of the $C(12)$ and $C(38)$ spikes, the X11 method generated a steeper slope resulting in a larger $F(i)$ than the modified method (X11 $F(i)$ = 0.0194 mg Chla m^{-3} $count^{-1}$ vs. the modified $F(i)$ = 0.0169 mg Chla m^{-3} $count^{-1}$).

It is important to note that there is also a scenario in which the modified method is not a definitive improvement over the original method. Since the modified outlier criterion is based on the prediction interval for $\hat{A}(z)$ at a given value of $C(z)$, the acceptable range with which values of $A(z)$ can deviate from $\hat{A}(z)$ before being identified as outliers increases as the $A(z)$ vs. $C(z)$ relationship becomes more variable. Consequently, for profiles with considerable variability in the $A(z)$ vs. $C(z)$ relationship, the wider prediction intervals makes it less likely for the modified method to detect outliers, resulting in a noisier corrected profile (Figure 3.9). This is especially problematic if variability in the optical properties of the phytoplankton community with depth is occurring on the same temporal scale as any confounding signal, such as from a slowly passing cloud have a prolonged effect on values of $E_{\mathrm{d}}(490)$. In cases such as these, it is impossible to determine whether the X11 method or the modified method generates a final $F(i)$ estimate that is more representative of the true bio-optical conditions without comprehensive on-site validation.

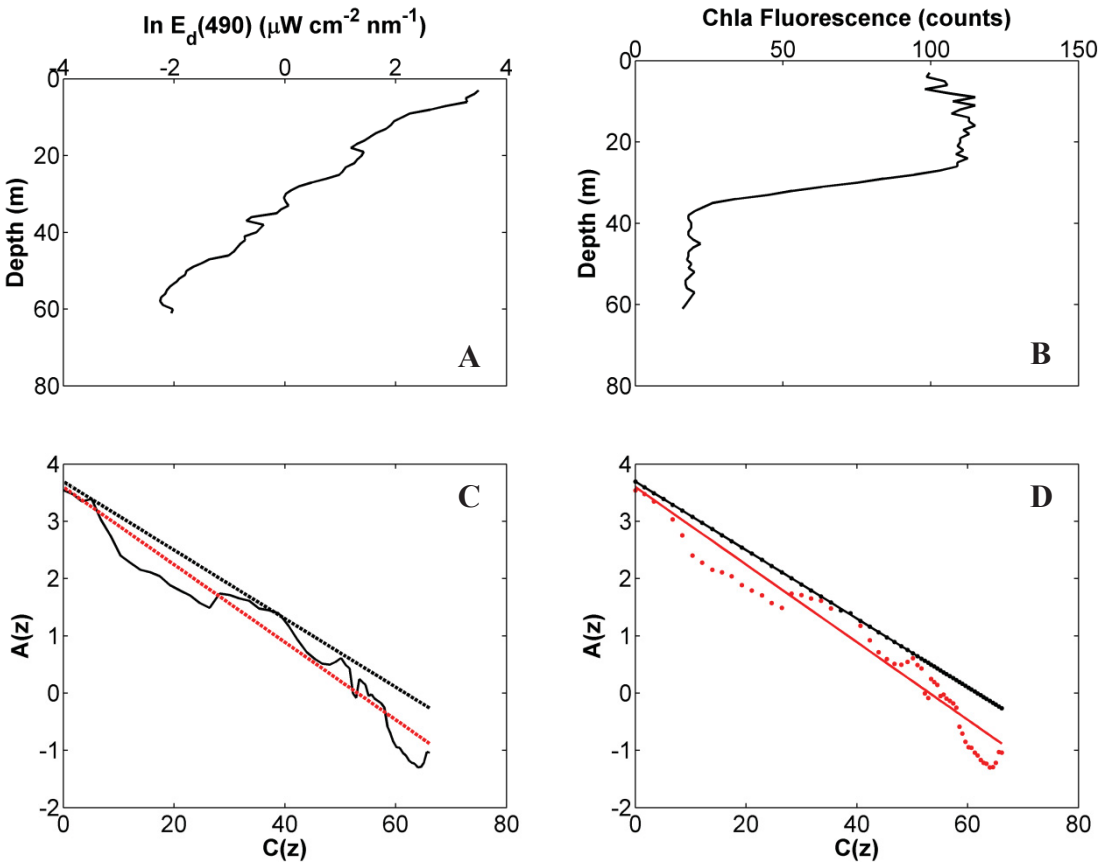

Figure 3.9 (Previous Page). Glider profile from Mission #12 (2013-12-02). **(A)**: Depth profile of ln-transformed downwelling irradiance at 490 nm. Note the large variability with depth that may be due to the effects of clouds. **(B)**: Depth profile of NPQ-corrected chlorophyll *a* fluorescence, in raw counts. **(C)**: An $A(z)$ vs. $C(z)$ curve calculated using the data from 3.9.A and 3.9.B as inputs, as described in Figure 3.8.C. **(D):** The final, corrected $A(z)$ vs. $C(z)$ curve after the iterative outlier-removal method has completed and the missing data points have been interpolated from the final slope fit, using the X11 method (black line and data points; y = -0.0598x + 3.69) and the modified method (red line and data points; y = -0.0678 + 3.60). Note that with the X11 method, all of the data points rigidly aligned with the linear fit. Also note that the modified method did not successfully identify any data points as outliers, leaving the large inherent variability of the profile unaltered. Without comprehensive on-site validation of the data, including a surface reference for $E_{\mathrm{d}}(490,0)$, it is difficult to determine which of the methods provided a more accurate representation of the bio-optical properties of the phytoplankton assemblage in this profile (X11 $F(i)$ = 0.0134 mg Chla m^{-3} count^{-1} vs. the modified $F(i)$ = 0.0162 mg Chla m^{-3} count^{-1}).

3.3.2 Retaining Depth-Dependent Information in the $A(z)$ vs. $C(z)$ Relationship

The validity of fitting a linear regression to the $A(z)$ vs. $C(z)$ profiles in this dataset was tested using a runs test, with the null hypothesis being that the residuals around the fit would be randomly distributed. If the residuals around the fit were randomly distributed it would imply that the linear fit was appropriate for the data. If the runs test failed because there were too few runs, it would mean that there was systematic deviation of the residuals around the fit and would imply that the fit may not be appropriate for the data. In the context of this data set, it would also imply that there was a systematic pattern in the $A(z)$ vs. $C(z)$ profile with depth. Of the profiles tested (n = 4283), 92.74% failed the runs test at a significance level of alpha = 0.05, rejecting the null hypothesis. Observing that many of the failures were associated with curvature in the $A(z)$ vs. $C(z)$ relationship, profiles were fitted with polynomial fits of 2nd through 5th order to determine a more appropriate fit for the relationship than a linear one (Table 3.1).

Table 3.1. Results of polynomial regressions of order 1 (linear) to 5 and of runs tests (MATLAB routine "runstest") at alpha = 0.05 on the $A(z)$ vs. $C(z)$ profiles in the data set (n = 5362). The column on the far right represents the total percentage of profiles that failed a runs test when fitted with each order of polynomial fit.

Order of Polynomial Fit	***Average per-profile Adjusted r^2***	***Average per-profile RMSE***	***Failed runs test percentage***
1	0.9894	0.0939 ± 0.0639	92.82
2	0.9936	0.0689 ± 0.0497	86.37
3	0.9960	0.0484 ± 0.0433	74.64
4	0.9966	0.0415 ± 0.0402	63.19
5	0.9972	0.0371 ± 0.0369	53.54

As the order of the polynomial fit increased the adjusted r^2 value also marginally increased. At the same time the measured *RMSE* decreased, as did the percentage of profiles that failed the runs test. Using no other metrics than these values, the results unsurprisingly suggest that the highest possible order of fit would be the "best" fit to use in order to maintain the depth-dependent variability of the original profile. However visual inspection of individual profiles over multiple missions revealed that this was not the case. For 4th and 5th order polynomials the fits were found to sometimes over-fit the data, neglecting to identify deviations that were consistent with cloud effects as being part of the unaffected profile – even though the removal of cloud-influenced points is the purpose of this step of the method (Figure 3.10.D and 3.10.E).

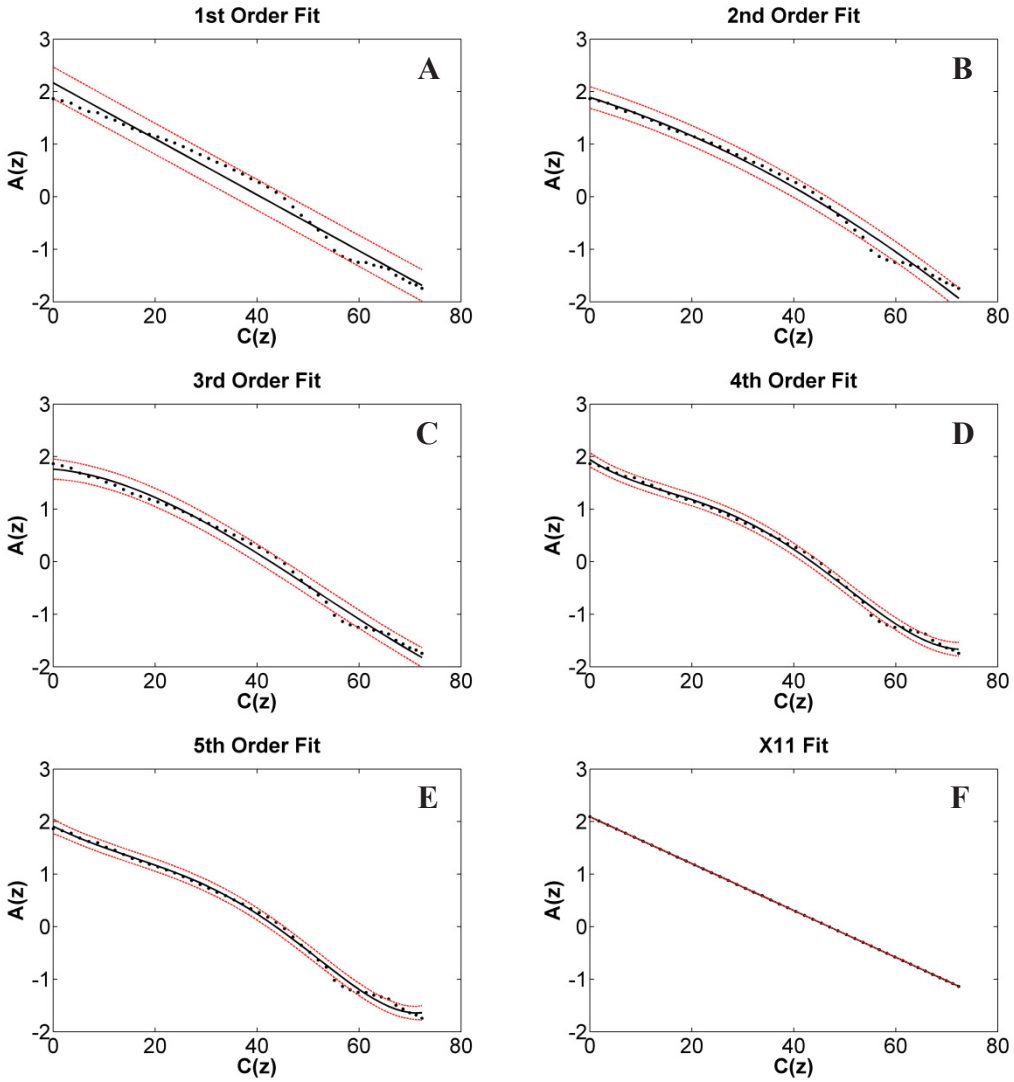

Figure 3.10. An $A(z)$ vs. $C(z)$ glider profile from Mission #12 (2013-12-02), including a deviation at approximately $C(50)$ consistent with a passing cloud. **(A - E)** *Initial* (before the iterative removal of outliers) polynomial fits of order one (linear) through five (black lines) along with the 90% prediction intervals (red dashes). **(F)** Final linear fit, calculated after the iterative removal of outliers using the original X11 method. Note that the initial linear fit (panel A) does not accurately track the shape of the profile with depth. Also note that the 4th and 5th order fits (panels D and E, respectively) incorporate the cloud-affected points where they should be excluded as outliers, which negates the purpose of this procedure. Finally note that while the original X11 method successfully eliminates the bump at $C(50)$ as an outlier, it also eliminates all variability with depth in the $A(z)$ vs. $C(z)$ relationship, prohibiting any investigation of depth-dependent trends.

The 3rd order polynomial fit, being the fit with the highest r^2, lowest *RMSE*, and lowest percentage of failed runs tests that was judged to not have a tendency to over-fit the data, was therefore determined to be the optimal choice of fit for the profiles in this dataset (with an acknowledgement that this last criterion is a subjective one). It was able to accurately fit both linear and non-linear profiles both with and without cloud-related variability in $E_{\mathrm{d}}(490,0)$ as well as, or better than, the linear approach taken by X11. In addition it was able to accurately retain the shape of any profiles that had curvature with depth, allowing for the analysis of any information contained in that curvature. It should be noted, however, that a 3rd-order polynomial fit has a maximum of two inflection points when used to fit a profile. Therefore if the shape of an $A(z)$ vs. $C(z)$ relationship contains more than two inflection points that are not caused by outliers, the 3rd order fit will not be sufficient to capture all of the variability with depth. The choice of a 3rd order fit is therefore not appropriate in all cases, and future work should investigate its applicability more closely. It will, however, serve in an operational sense for the work presented here.

3.3.3 Implementation of a Modified Full-profile *F*(i)

At this point in the analysis it is useful to quantify the differences made by the above modifications, relative to the $F(i)$ values calculated using the original X11 methodology, before making additional changes related to the investigation of depth-dependent trends described in the following section. To do this, a linear regression was fitted to the final $A(z)$ vs. $C(z)$ output that had been generated after identifying and correcting for outliers using 90% prediction intervals both above and below a 3rd order polynomial fit of the $A(z)$ vs. $C(z)$ relationship, as described above in Sections 3.3.1 and 3.3.2. This modified, full-profile, *F*-factor will be referred to as BC15 $F(i)$. When the two $F(i)$ estimates were plotted against each other (n = 5362; Figure 3.11), there was a correlation of r^2 = 0.9641 (y = 0.9949x – 0.0002, *RMSE* = 0.0025 $\mathrm{mg\ Chla\ m^{-3} \cdot count^{-1}}$, $p < 0.01$). This relationship was also quantified using the percent difference between the BC15 $F(i)$ and the X11 $F(i)$ of the same profile. When this per-profile percent-difference was averaged for the entire dataset, a value of 4.53% ± 20.08 was obtained (where BC15 $F(i)$ was on average 4.53% larger than X11 $F(i)$). This is consistent with what is known about the biases of the X11 method. Since their outlier-

detection criterion only detects outliers below the fit, there is a tendency for the iterative outlier-removal process to generate iteratively shallower X11 slopes, which translates into smaller $F(i)$ estimates (although this is not always the case, as the same condition is capable of generating steeper slopes and therefore larger $F(i)$ estimates).

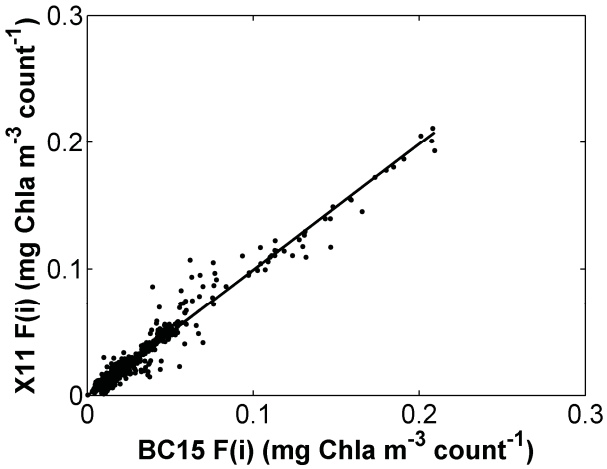

Figure 3.11. Linear regression between the X11 $F(i)$ and BC15 $F(i)$ for each profile in the dataset (n = 5362, y = 0.9949x – 0.0002, r^2 = 0.9641, *RMSE* = 0.0025 mg Chla $\mathrm{m}^{-3} \cdot \mathrm{count}^{-1}$, $p < 0.01$). When the percent difference between methods was compared for the entire data set, the BC15 $F(i)$ was 4.53% ± 20.08 larger than the X11 $F(i)$.

3.4 Depth-Resolved Patterns in the *A*(z) vs. *C*(z) Relationship

Once the $A(z)$ vs. $C(z)$ profiles were processed for outlier removal (Section 3.3) they were divided vertically into optical depths (ζ; Equation 2.4), and *F*-factors were generated for each optical depth as outlined in Section 2.6. These depth-resolved *F*-factors ($F(i,\zeta)$) were used to test the hypothesis that there is systematic variability in the underlying bio-optical relationships of the $A(z)$ vs. $C(z)$ relationship with depth, with the null hypothesis being that there is no systematic variability with depth and therefore there will be no consistent difference in the $F(i,\zeta)$ between optical depths. Recall that systematic changes in $F(i,\zeta)$ with optical depth would be caused by variability in either the relationship between $fluor$ and $Chla$ or between K_{bio} and $Chla$; the unique contributions of these two sources of variability cannot be separated using this method.

Boxplots representing per-optical depth $F(i,\zeta)$ as a percent difference from the X11 $F(i)$ of the same profile revealed a modest, though noticeable, trend with depth, with median variability being restricted to under 50% (n = 5362; Figure 3.12). Despite the

large variability in the outliers (where outliers are defined as being larger than [q3 + 1.5(q3 – q1)] or smaller than [q1 – 1.5(q3 – q1)], where q1 is the 25th percentile of the data and q3 is the 75th percentile of the data; this range should encompass approximately 99.3% of the data when the data are normally distributed), the shallowest and deepest optical depths exhibit larger relative *F*-factors than the middle optical depths. Using the "notch" function of the MATLAB "boxplot" routine (where notches, representing 95% confidence intervals around the median, are calculated as [$\text{Median} \pm 1.57\frac{(IQR)}{\sqrt{n}}$]), it is possible to approximate if medians are different from each other if their confidence intervals don't overlap. For all five optical depths, the median value of the $F(i,\zeta)$ was different from zero (meaning that the $F(i,\zeta)$ for that optical depth was different than the X11 $F(i)$ for that overall profile). In addition, the medians of each optical depth were different from each other. For optical depths 1 through 5, the percent difference of the median values of $F(i,\zeta)$ from the full-profile X11 $F(i)$ were 19.8%, 1.37%, -2.77%, 6.39% and 29.9%. From this it can be concluded that there is systematic variability in $F(i,\zeta)$ with optical depth, with a trend of larger $F(i,\zeta)$ at the shallowest and deepest optical depths, and that the null hypothesis can be rejected. This depth-dependent trend reflects changes in bio-optical relationships, which are affected by a combination of the $fluor$ to $Chla$ relationship and the K_{bio} to $Chla$ relationship. More specifically, low fluorescence per unit chlorophyll *a* and high attenuation per unit chlorophyll *a* both result in larger *F*-factors. The specifics of how this translates into the observed depth-dependent trend will be discussed in Chapter 4.

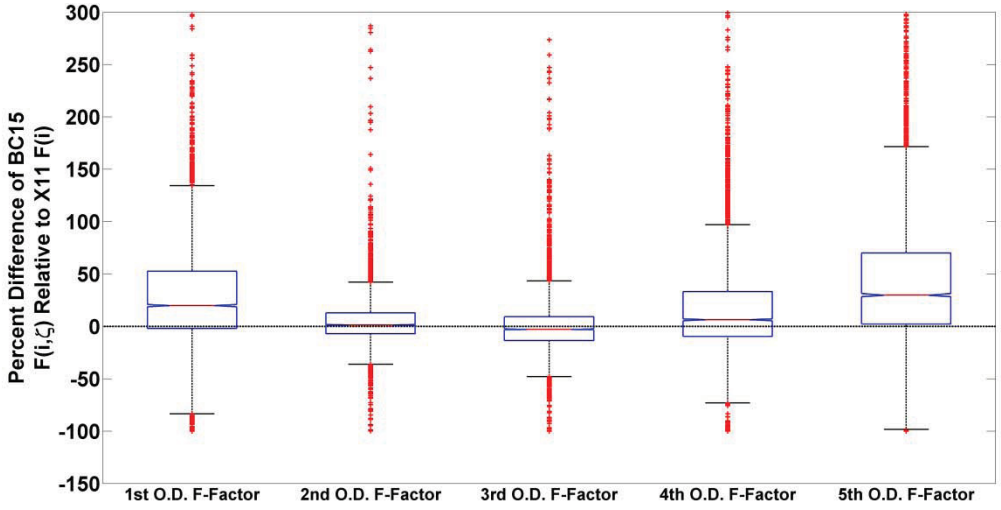

Figure 3.12. Boxplot showing the relative difference (in percent) between the *F*-factors at each optical depth ($F(i,\zeta)$) in a profile normalized to the X11 $F(i)$ for that profile (n = 5362). Median values for optical depths 1 through 5 were as follows: 19.8%, 1.37%, -2.77%, 6.39% and 29.9%. Note: The plot has been zoomed in for reasons of visual clarity, resulting in n = 56 outliers being above the displayed upper limit of this plot.

3.5 Investigating the Effects of CDOM on the Modified X11 Method

3.5.1 Influence on BC15 *F*(i) in the Horizontal Dimension

To examine the possible influences of CDOM, relative to $Chla$, on the estimation of the *F*-factor, a linear regression was conducted for each mission between the BC15 $F(i)$ and the $\mathrm{CDOM_{adj}}|_{z_{max}}^{z_{min}}{:}\,Chla|_{z_{max}}^{z_{min}}$ for each profile (see for example Figure 3.13.F, as well as Panel D on each page of the mission-specific figures in Section 3.7). This was done to test the hypothesis that BC15 $F(i)$ is affected by changes in the ratio of $\mathrm{CDOM_{adj}}|_{z_{max}}^{z_{min}}{:}\,Chla|_{z_{max}}^{z_{min}}$, with the null hypothesis being that there is no effect. This relationship was significant at $p < 0.01$ for all 12 missions, with r^2 values ranging from 0.06 to 0.90 (Table A.3 in Appendix A), thereby rejecting the null hypothesis. Regression results should be interpreted with caution for missions marked with an asterisk, as some underlying assumptions of regression were violated for those missions.

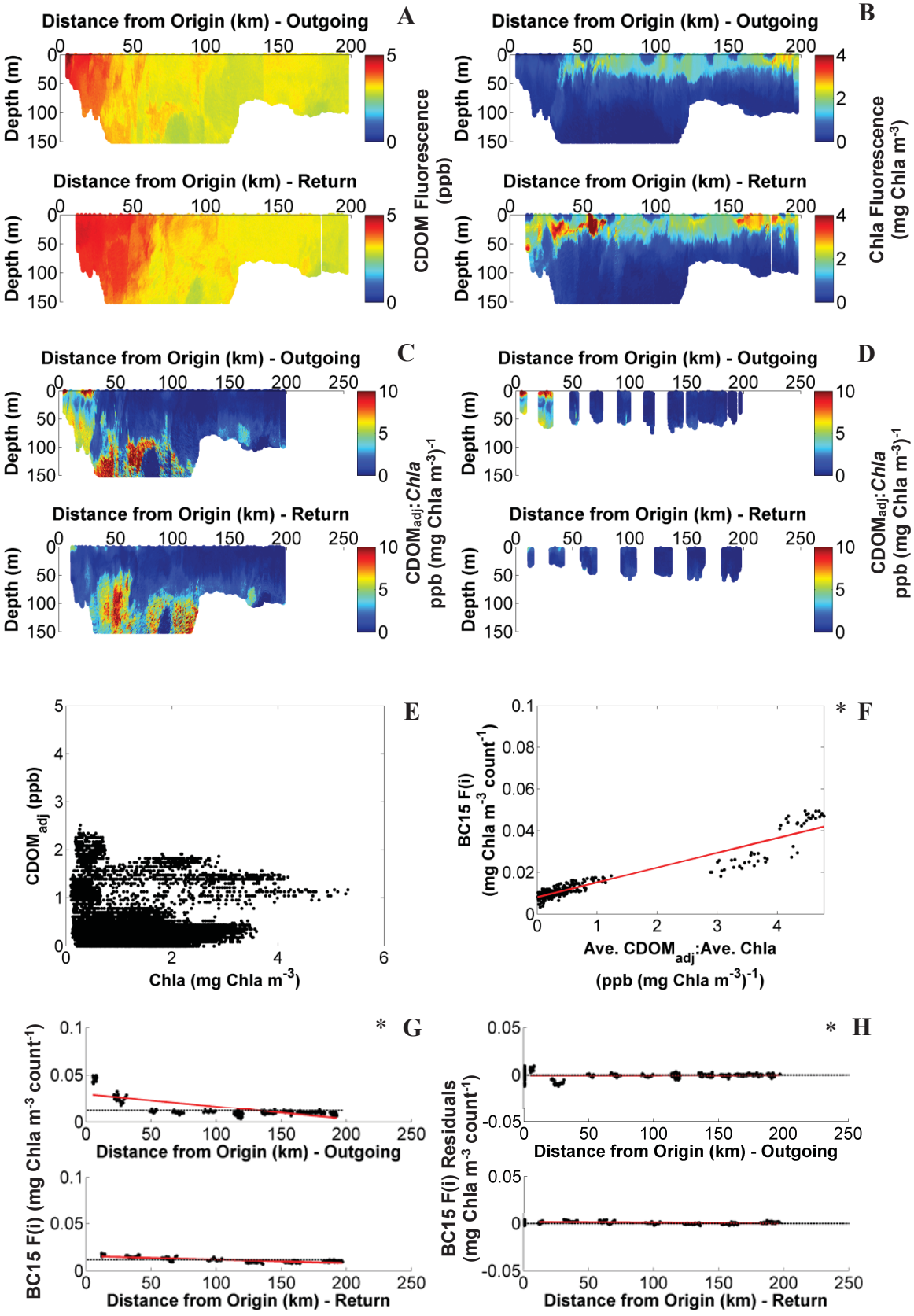
A
Distance from Origin (km) - Outgoing
Distance from Origin (km) - Return
Depth (m)
CDOM Fluorescence (ppb)
B
Chla Fluorescence (mg Chla m-3)
C
D
CDOMadj:Chla ppb (mg Chla m-3)-1
E
CDOMadj (ppb)
Chla (mg Chla m-3)
* F
BC15 F(i) (mg Chla m-3 count-1)
Ave. CDOMadj:Ave. Chla (ppb (mg Chla m-3)-1)
* G
BC15 F(i) (mg Chla m-3 count-1)
* H
BC15 F(i) Residuals (mg Chla m-3 count-1)

Figure 3.13 (Previous Page). Outgoing and return glider transects for Mission #7 (2013-03-29) plotted versus distance from shore. Plots with an asterisk should be interpreted with caution as some underlying assumptions of regression were violated. **(A)**: CDOM fluorescence (ppb). Note the high concentration nearshore for both transects. **(B)**: $Chla$ fluorescence (mg Chla m^{-3}). Note the high concentration nearshore only during the return transect. **(C)**: $CDOM_{adj}$:$Chla$ (ppb (mg Chla m^{-3})$^{-1}$). Note the high $CDOM_{adj}$:$Chla$ nearshore only in the outgoing transect. **(D)**: the same variable as 3.13.C, however only profiles containing Level 2 data are shown to demonstrate the sampling range of the method compared to the total glider track. **(E):** $CDOM_{adj}$ vs. $Chla$ data for the mission (n = 22,937). **(F)**: BC15 $F(i)$ (mg Chla m^{-3} $count^{-1}$) plotted against $\mathrm{CDOM_{adj}}|_{z_{max}}^{z_{min}}$: $Chla|_{z_{max}}^{z_{min}}$ (n = 526 profiles). For regression information see Table A.3 in Appendix A. **(G):** BC15 $F(i)$ vs. distance from shore. Note that the inflated $F(i)$ values nearshore in the outgoing transect correspond to the region of high $\mathrm{CDOM_{adj}}|_{z_{max}}^{z_{min}}$: $Chla|_{z_{max}}^{z_{min}}$ in 3.13.C (n = 526 profiles). **(H)**: The residuals of 3.13.F plotted as a function of distance from shore (n = 526 profiles). These residuals represent variability in $F(i)$ that cannot be attributed to the increasing contribution of CDOM, relative to $Chla$, on K_{bio}, as represented by $\mathrm{CDOM_{adj}}|_{z_{max}}^{z_{min}}$: $Chla|_{z_{max}}^{z_{min}}$. Note that the trend of decreasing $F(i)$ with distance in the outgoing transect of 3.13.G has been removed, suggesting that the trend was driven by high CDOM relative to $Chla$.

The residuals around the regression line of this relationship were then investigated for any patterns with distance from shore (Figures 3.14 and 3.15). It was determined that the previously observed trends in $F(i)$ with distance from shore were driven strongly by abnormally high $\mathrm{CDOM_{adj}}|_{z_{max}}^{z_{min}}$: $Chla|_{z_{max}}^{z_{min}}$ (the uncorrected BC15 $F(i)$ vs. distance from shore results mirrored those of the X11 $F(i)$ in both pattern and magnitude; see Table A.4 for BC15 $F(i)$ regression information, and Panel E on each page of the mission-specific figures in Section 3.7 for trends in BC15 $F(i)$ with distance from shore). Regression results should be interpreted with caution for missions marked with an asterisk, as some underlying assumptions of regression were violated for those missions. This can be observed in the differences between Figure 3.13.G and 3.13.H, where the inflated nearshore values of BC15 $F(i)$ that are present in the outgoing transect of Mission #7, before adjusting for the effect of $\mathrm{CDOM_{adj}}|_{z_{max}}^{z_{min}}$: $Chla|_{z_{max}}^{z_{min}}$, are no longer present in the plot of residuals as a function of distance from shore after adjusting for the effect of $\mathrm{CDOM_{adj}}|_{z_{max}}^{z_{min}}$: $Chla|_{z_{max}}^{z_{min}}$. If the trend displayed by the inflated near-shore values was not due to the contribution of $\mathrm{CDOM_{adj}}|_{z_{max}}^{z_{min}}$: $Chla|_{z_{max}}^{z_{min}}$ on the underlying bio-optical relationships, then plotting the residuals of the BC15 $F(i)$ vs.

$\mathrm{CDOM_{adj}}|_{z_{\max}}^{z_{\min}}$: $Chla|_{z_{\max}}^{z_{\min}}$ relationship would not have changed the distance from shore trend in BC15 $F(i)$. This is an important distinction to make; that this trend is due to the overwhelming optical influence of $\mathrm{CDOM_{adj}}|_{z_{\max}}^{z_{\min}}$: $Chla|_{z_{\max}}^{z_{\min}}$ on the underlying X11 equation nearshore in Case 2 waters, rather than being due to a change in the $fluor$ to $Chla$ or K_{bio} to $Chla$ relationships in the phytoplankton community.

The above process was applied to each mission in the data set, using the residuals of the BC15 $F(i)$ vs. $\mathrm{CDOM_{adj}}|_{z_{\max}}^{z_{\min}}$: $Chla|_{z_{\max}}^{z_{\min}}$ relationship to investigate variability in the portion of BC15 $F(i)$ vs. distance from shore that cannot be attributed to the increasing contribution of CDOM, relative to $Chla$, on the rate of attenuation of light in the water column. The trend of BC15 $F(i)$ residuals after the CDOM correction versus distance from shore, for each mission, can be seen in Figures 3.14 and 3.15. Of the 24 transects, 11 had a slope that was not significantly different from zero at alpha = 0.05, compared to just 4 BC15 $F(i)$ transects before the CDOM correction was made. Of the remaining transects, 7 had a negative slope with distance from shore that was significantly different than zero at alpha = 0.05 compared to 20 pre-correction BC15 $F(i)$transects, and 6 had a positive slope with distance from shore that was significantly different from zero at alpha = 0.05 compared to zero pre-correction BC15 $F(i)$transects. The most notable result is that of the 6 BC15 $F(i)$ transects over 4 missions that exhibited a non-linear increase in $F(i)$ nearshore (n = 6 of 24 transects in Missions #6, 7, 8, and 12), all transects had a corrected slope vs. distance from shore that was at least an order of magnitude smaller than the pre-corrected slope, and 2 of the transects (outgoing transects for Missions #7 and 8) were no longer significantly different than zero at alpha = 0.05. The unsuccessfully-corrected Mission #6 (2013-03-11) can be traced to a poorly defined slope in the BC15 $F(i)$ vs. $\mathrm{CDOM_{adj}}|_{z_{\max}}^{z_{\min}}$: $Chla|_{z_{\max}}^{z_{\min}}$ regression, which resulted in highly variable residuals. This can be viewed in the mission-summary plots for this mission found at the end of the Chapter 3, in Section 3.7. For regression information on the BC15 $F(i)$ versus distance from shore and for the BC15 $F(i)$ residuals versus distance from shore, see Tables A.4 and A.5 respectively in Appendix A. Results for missions marked with an asterisk should be interpreted with caution as some underlying assumptions of regression were violated.

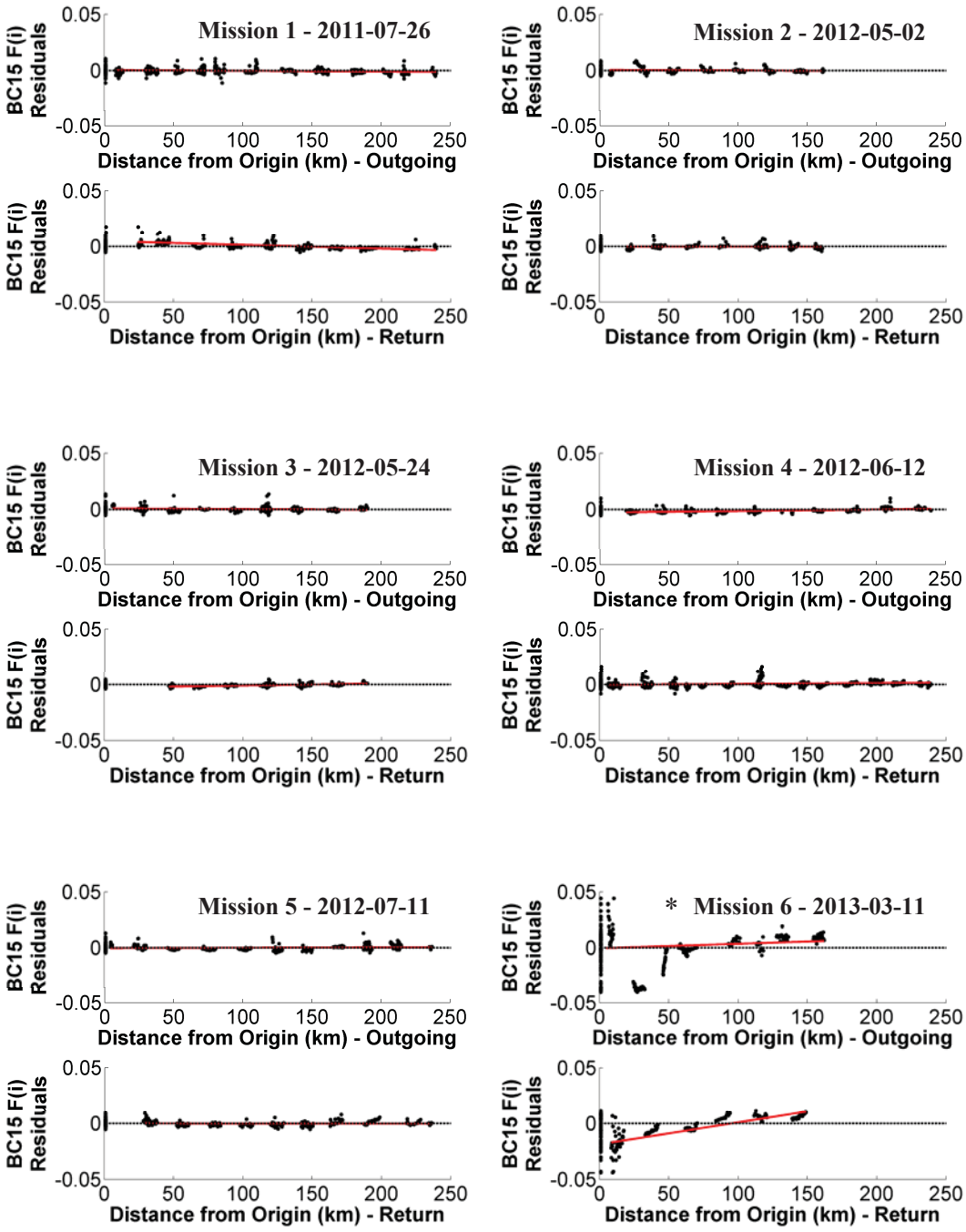

Figure 3.14. Outgoing and return transects of BC15 $F(i)$ residuals (mg Chla m^{-3} $count^{-1}$) from the BC15 $F(i)$ vs. $CDOM_{adj}|_{z_{max}}^{z_{min}}$: $Chla|_{z_{max}}^{z_{min}}$ relationship, plotted versus distance from shore for glider Missions #1 - 6. Slopes (red lines) indicate trends in BC15 $F(i)$ residuals with distance, and the horizontal black line at 0 mg Chla m^{-3} $count^{-1}$ provides a reference for BC15 $F(i)$ residual variability. With the exception of Mission #6, transects show only minor, or insignificant, trends with distance from shore. Full regression information can be found in Table A.4 in Appendix A, however the results for missions marked with a "*" should be interpreted with caution.

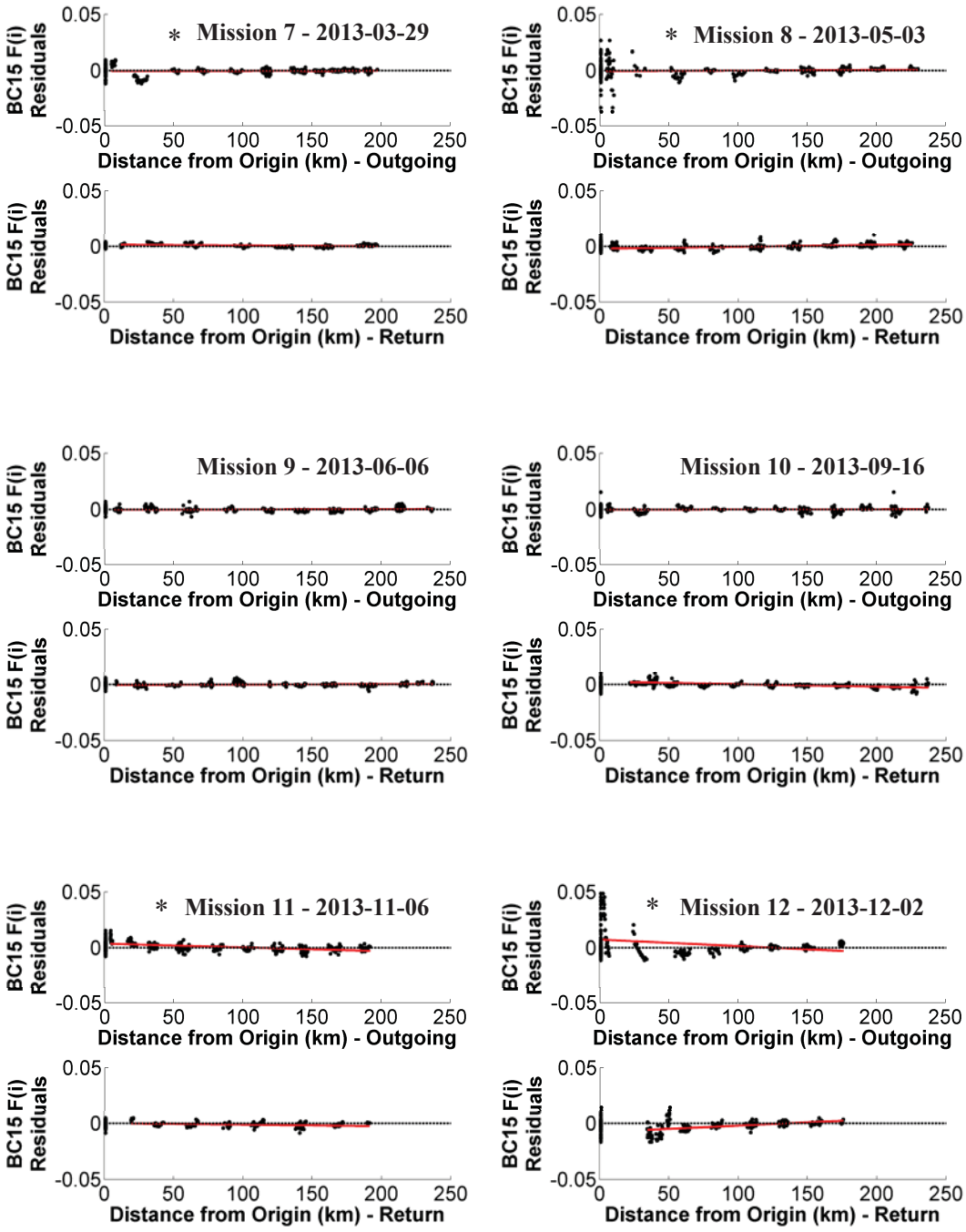

Figure 3.15. Outgoing and return transects of BC15 $F(i)$ residuals (mg Chla m^{-3} $count^{-1}$) from the BC15 $F(i)$ vs. $\mathrm{CDOM_{adj}}|_{z_{max}}^{z_{min}}$:$Chla|_{z_{max}}^{z_{min}}$ relationship, plotted versus distance from shore for glider Missions #7 - 12. Slopes (red lines) indicate trends in BC15 $F(i)$ residuals with distance, and the horizontal black line at 0 mg Chla m^{-3} $count^{-1}$ provides a reference for BC15 $F(i)$ residual variability. With the exception of Mission #12, transects show only minor or insignificant trends with distance from shore. Full regression information can be found in Table A.4 in Appendix A, however the results for missions marked with a "*" should be interpreted with caution.

3.5.2 Influence on BC15 *F*(i,ζ) in the Vertical Dimension

To look for consistent influences of $\mathrm{CDOM_{adj}}{:}\,Chla$ on BC15 $F(i,\zeta)$ in the vertical dimension, a linear regression was conducted between the BC15 $F(i,\zeta)$ and the $\mathrm{CDOM_{adj}}{:}\,Chla$ for each data point in a mission (in contrast to finding a single residual per profile, as was described in the previous section). The residuals around the slope of this relationship were then investigated for any systematic patterns with depth by visualising the data using a boxplot (n = 54,138, Figure 3.16). The per-optical depth patterns exhibited by the residuals of the BC15 $F(i,\zeta)$ vs. $\mathrm{CDOM_{adj}}{:}\,Chla$ relationship are similar to those of the original data (see Figure 3.12), although with slightly smaller deviations in the median values and with larger variability in the outliers. These median values, for optical depths 1 through 5, were as follows, expressed as $\mathrm{mg\ Chla\ m^{-3}\ count^{-1}}$: 0.0013, -0.0005, -0.0015, -0.0011, and -0.0006. Expressed as a percent-difference from the manufacturer's *F*-factor of 0.0117 $\mathrm{mg\ Chla\ m^{-3}\ count^{-1}}$ (in order to provide some context for the magnitude of these residual values) these median per-optical depth *F*-factor residuals, for optical depths 1 through 5, are as follows: 11.5%, -3.98%, -12.8%, -9.80%, and -5.15%. Generally, removing the effects of $\mathrm{CDOM_{adj}}{:}\,Chla$ on BC15 $F(i,\zeta)$ did not change the observable patterns with depth (compare the above percent-differences with those calculated in Section 3.4). There is a weak trend with optical depth, with the most-negative residuals found at the middle optical depths and less negative residuals found at the shallowest- and deepest optical depths. For all five optical depths, none of the 95% confidence intervals around the median value of the BC15 $F(i,\zeta)$ residuals for that optical depth overlapped. However, one difference of note when comparing these results to the original BC15 $F(i,\zeta)$ trends in Figure 3.12, is that the distribution of residuals in the 5th optical depth is more similar to the middle optical depths than the shallowest optical depth. This would imply that there was an effect of $\mathrm{CDOM_{adj}}{:}\,Chla$ within this optical depth that did not occur in the shallower optical depths.

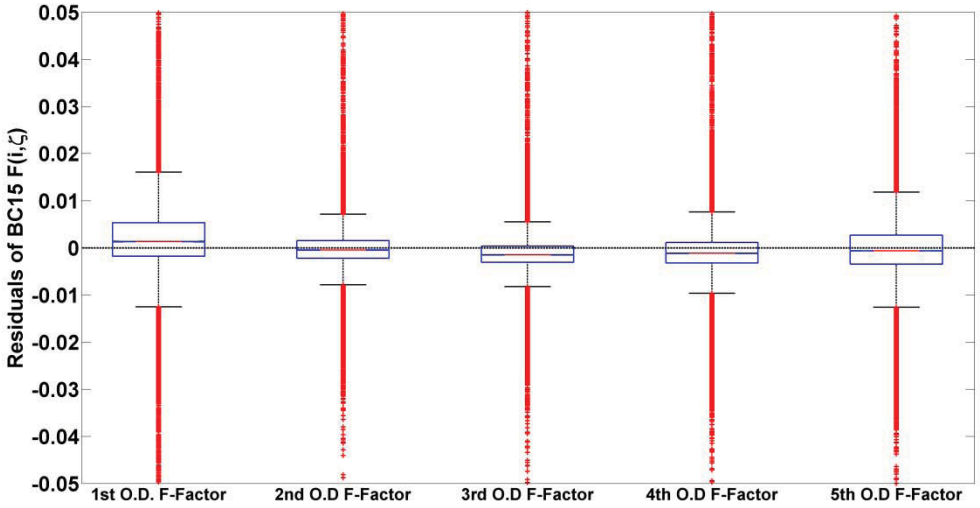

Figure 3.16. Boxplot of the residuals from the BC15 $F(i,\zeta)$ (mg Chla m^{-3} $count^{-1}$) versus $CDOM_{adj}$: $Chla$ (ppb · (mg Chla m^{-3})$^{-1}$) relationship, with the data divided by optical depth (n = 54,138). The median values for optical depths 1 through 5 are as follows, expressed as mg Chla m^{-3} $count^{-1}$: 0.0013, -0.0005, -0.0015, -0.0011, and -0.0006. Note the weak trend with depth, where residuals at the shallowest and deepest optical depths are more positive than the residuals at the middle optical depths. For the sake of visualisation, the plot has been zoomed in to better display the central trend of the data (not displayed are n = 868 outliers outside of the -0.05 to +0.05 limits).

The residuals in these two analyses represent variability in the BC15 F-factors that cannot be attributed to the increasing contribution of CDOM, relative to $Chla$, on the rate of attenuation of light in the water column. They can be used to test the hypothesis that the effect of independently varying CDOM concentration, relative to $Chla$, on the F-factor overwhelms the effects of changes in $fluor$ to $Chla$ or K_{bio} to $Chla$ on the F-factor. From the above observations, it can be concluded that the influence of $CDOM_{adj}|_{z_{max}}^{z_{min}}$: $Chla|_{z_{max}}^{z_{min}}$ was the primary contributor to the observed trends in BC15 $F(i)$ vs. distance from shore, completely overwhelming any influence of the $fluor$ to $Chla$ relationship or the K_{bio} to $Chla$ relationship that may have existed. For the observed trends with depth, $CDOM_{adj}$: $Chla$ was a contributor, but did not overwhelm the contributions of $fluor$ to $Chla$ or the K_{bio} to $Chla$, as the same trends were observable both before and after the process of isolating the residuals. It did however have a minor effect on the distribution of the data in the deepest (5^{th}) optical depth. These trends will be discussed in more detail in Chapter 4.

It is important to note that although the inferred influence of $\mathrm{CDOM_{adj}}$: $Chla$ on the BC15 *F*-factors can be visualised, qualitatively showing its effects, the process as presented here cannot be used as a quantitative correction for inflated *F*-factors. As can be seen in Figures 3.14 through 3.16, *F*-factor residuals can vary by more than ± 0.05 mg Chl m^{-3} $count^{-1}$. Assuming an initial *F*-factor on the order of 0.0117 mg Chl m^{-3} $count^{-1}$ (the value of the fluorometer manufacturer *F*-factor for the majority of the missions), a correction of -0.05 (mg Chl m^{-3} $count^{-1}$) would result in a negative conversion factor, which is nonsensical.

3.6 Comparison of Chlorophyll *a* Estimates from Different *F*-factors

Water samples were collected at the beginning and end of glider deployments, whenever conditions permitted it, for direct laboratory determination of extracted $Chla$ to be used for comparison with $Chla$ estimates from $fluor$ using four different *F*-factors: the manufacturer's static *F*-factor, X11's per-profile $F(i)$, BC15's per-profile $F(i)$, and BC15's depth-resolved $F(i,\zeta)$. By comparing these $Chla$ estimates to the laboratory-determined $Chla$, it is possible to test whether the X11 or BC15 *F*-factors are an improvement over the static manufacturer's *F*-factor, with the null hypothesis that there is no improvement. An example profile for one of these comparisons can be seen in Figure 3.17. Notice that using the two full-profile $F(i)$s generate $Chla$ estimates closer to the extracted values than does the manufacturer *F*-factor. Also notice that while the BC15 $F(i,\zeta)$ Chla estimate in the first optical layer (where an optical depth, ζ, is approximately 10 m for this profile) is further from the extracted $Chla$ than any of the other estimates, it is very close to the extracted $Chla$ for the second optical layer. No conclusion can be drawn about the deeper optical layers, as there are no water samples with which to validate the estimates. This example profile highlights the potential for the full-profile methods to increase accuracy over the static manufacturer *F*-factor, while also highlighting the potential for the depth-resolved approach to introduce artificial noise between optical layers.

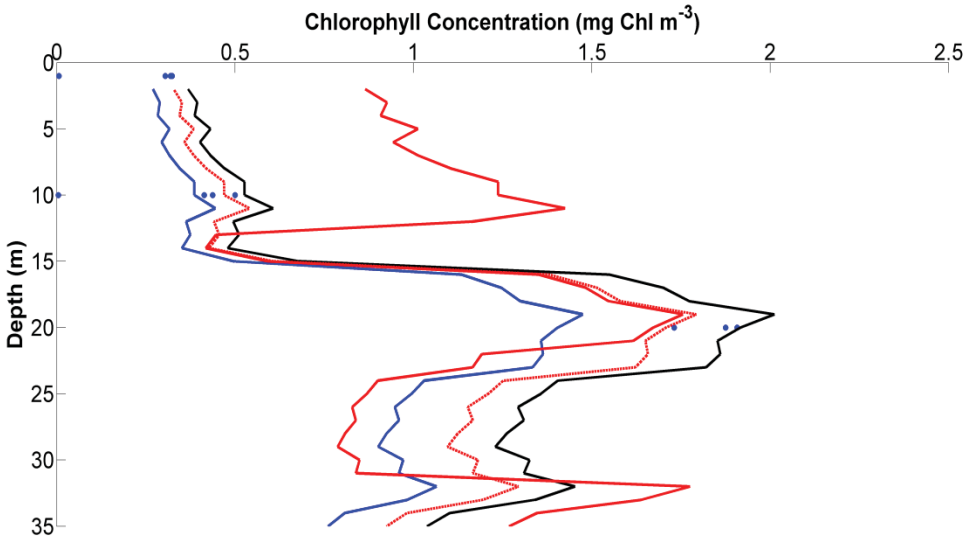

Figure 3.17. An example profile from Mission #3 (2012-05-24) comparing laboratory-determined extracted $Chla$ (mg Chla m^{-3}) from water samples (blue dots at 1 m, 10 m and 20 m; each depth done in triplicate) to $Chla$ from raw fluorescence counts estimated using various F-factors (mg Chla m^{-3} $count^{-1}$): the manufacturer's F-factor (blue line; F = 0.0117), $Chla$ from raw fluorescence counts using the X11 $F(i)$ (black line; $F(i)$ = 0.0160), $Chla$ from BC15 $F(i)$ (red dashed line; $F(i)$ = 0.0142) and $Chla$ from raw fluorescence counts using the BC15 $F(i,\zeta)$ (red line; $F(i,1)$ = 0.0375; $F(i,2)$ = 0.0139; $F(i,3)$ = 0.0102; $F(i,4)$ = 0.0195). Water samples were taken 6 hours before the glider profile was made.

When all of the available data is considered (n = 39), the $Chla$ estimates using the manufacturer's F-factor varied from extracted $Chla$ values by an average of 77.01% ± 54.05%. When using X11 $F(i)$, $Chla$ estimates varied from extracted $Chla$ values by an average of 199.17% ± 280.79%. When using BC15 $F(i)$, $Chla$ estimates varied from extracted $Chla$ values by an average of 144.12% ± 117.67%. When using BC15 $F(i,\zeta)$, $Chla$ estimates varied from extracted $Chla$ values by an average of 236.46% ± 342.44%. A full list of the data, expressed as percent-difference between the extracted $Chla$ value and the $Chla$ value estimated using the four different F-factors, can be seen in Table A.6, in Appendix A. These results suggest that the full-profile F-factors introduce more variability into the estimation of $Chla$ than the manufacturer's value does, and that the depth-resolved $F(i,\zeta)$ introduces even more variability, likely in the form of vertical structure in the estimated $Chla$ profiles that is almost certainly artefactual.

A more direct comparison can be made when extracted $Chla$ is plotted versus the $Chla$ estimates using the four different *F*-factors (Figure 3.18; n = 39). This reveals that the correlation between extracted $Chla$ and estimated $Chla$ from any of the methods is very weak. The BC15 $F(i,\zeta)$ generates an r^2 = 0.04. The BC15 $F(i)$ generates an r^2 = 0.18. The X11 $F(i)$ generates an r^2 = 0.05. Even the manufacturer's *F*-factor – which is unaffected by the attenuation-related problems of the two other methods, and should have a stronger correlation – only has an r^2 of 0.25. It is also worth noting that the X11 and BC15 *F*-factors generally over-estimate the extracted $Chla$ value (compared to a 1:1 relationship with extracted $Chla$), likely due to the effects of increased attenuation from a near-shore increase in $\mathrm{CDOM_{adj}}$:$Chla$. These results should be interpreted with caution as some underlying assumptions of regression were violated.

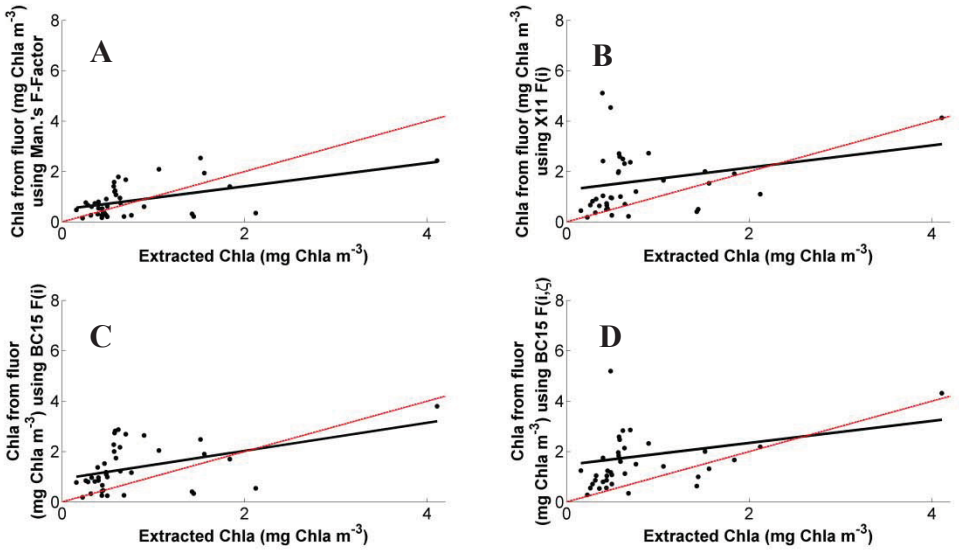

Figure 3.18. The relationship between extracted $Chla$ (mg Chla m^{-3}) determined from the laboratory analysis of water samples, and $Chla$ estimated from *in situ* fluorescence counts using each of four *F*-factors (n = 39). Included are a linear regression fit (black line) and a 1:1 line for reference (red line). **(A)**: Manufacturer's *F*-factor, r^2 = 0.25. **(B)**: X11 $F(i)$, r^2 = 0.05. **(C)**: BC15 $F(i)$, r^2 = 0.18. **(D)**: BC15 $F(i,\zeta)$, r^2 = 0.04. Note that the X11 and BC15 *F*-factors do not improve the $Chla$ estimate over the manufacturer's *F*-factor for this data. These results should be interpreted with caution as some underlying assumptions of regression were violated.

From the above results, it can be concluded that the X11 and BC15 *F*-factors do not improve the estimation of $Chla$ compared to the manufacturer's static *F*-factor *for these water samples.* The manufacturer's *F*-factor results in a lower average percent-deviation from the extracted $Chla$ values and it shows a higher correlation with those same extracted $Chla$ values. It should be noted, however, that the low correlation between extracted and estimated $Chla$, even when using the manufacturer's *F*-factor, suggests that these water samples may not be appropriate for definitively assessing the quality of the X11 and BC15 $Chla$ estimates. This topic is discussed in more detail in Chapter 4.

3.7 Mission Summary Figures

In order to provide some context for the preceding results, six key variables for summarising each glider mission are plotted here. These six figures are as follows: **A.)** Transects of $Chla$ fluorescence, estimated using the manufacturer's *F*-factor ($\mathrm{mg\ Chla\ m^{-3}}$). **B.)** Transects of CDOM (ppb). **C.)** Transects of the $\mathrm{CDOM_{adj}}$: $Chla$ ratio ($\mathrm{ppb\ (mg\ Chla\ m^{-3})^{-1}}$). **D.)** Full-mission data for BC15 $F(i)$ ($\mathrm{mg\ Chla\ m^{-3}count^{-1}}$) vs. $\mathrm{CDOM_{adj}}|_{z_{\max}}^{z_{\min}}$: $Chla|_{z_{\max}}^{z_{\min}}$ ($\mathrm{ppb\ (mg\ Chla\ m^{-3})^{-1}}$). Note the dynamic x-axis scale between missions, and the larger y-axis limit for Mission #6 (2013-03-11). **E.)** Transects of BC15 $F(i)$. Note the larger y-axis limit for Mission #6 (2013-03-11). **F.)** Transects of BC15 $F(i)$ residuals ($\mathrm{mg\ Chla\ m^{-3}count^{-1}}$) from around the BC15 $F(i)$ vs. $\mathrm{CDOM_{adj}}|_{z_{\max}}^{z_{\min}}$: $Chla|_{z_{\max}}^{z_{\min}}$ relationship. Results for figures D, E, and F that are marked with an asterisk should be interpreted with caution, as some underlying assumptions of regression were violated for those missions.

Mission #1 – 2011-07-26

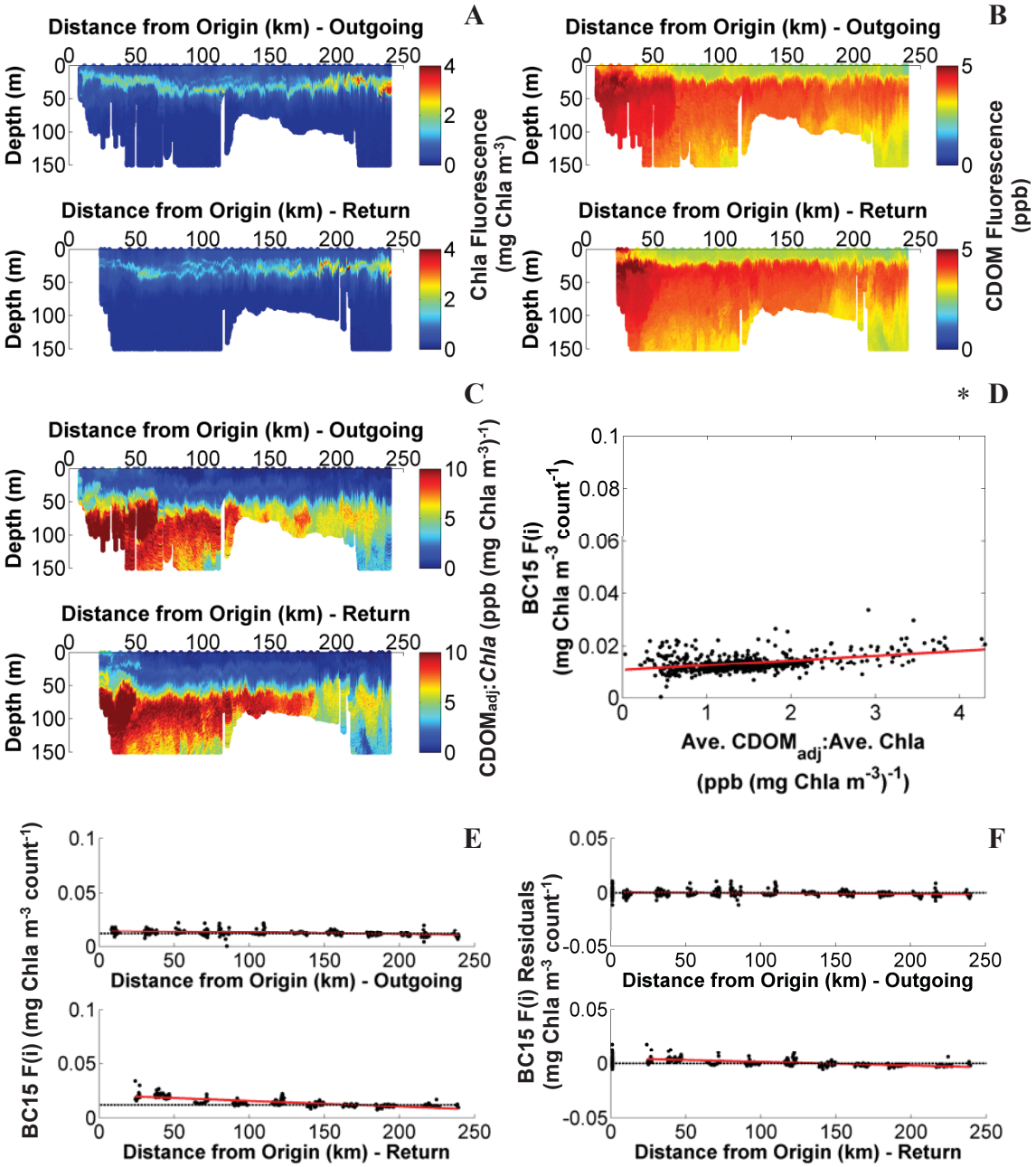

Mission #2 – 2012-05-02

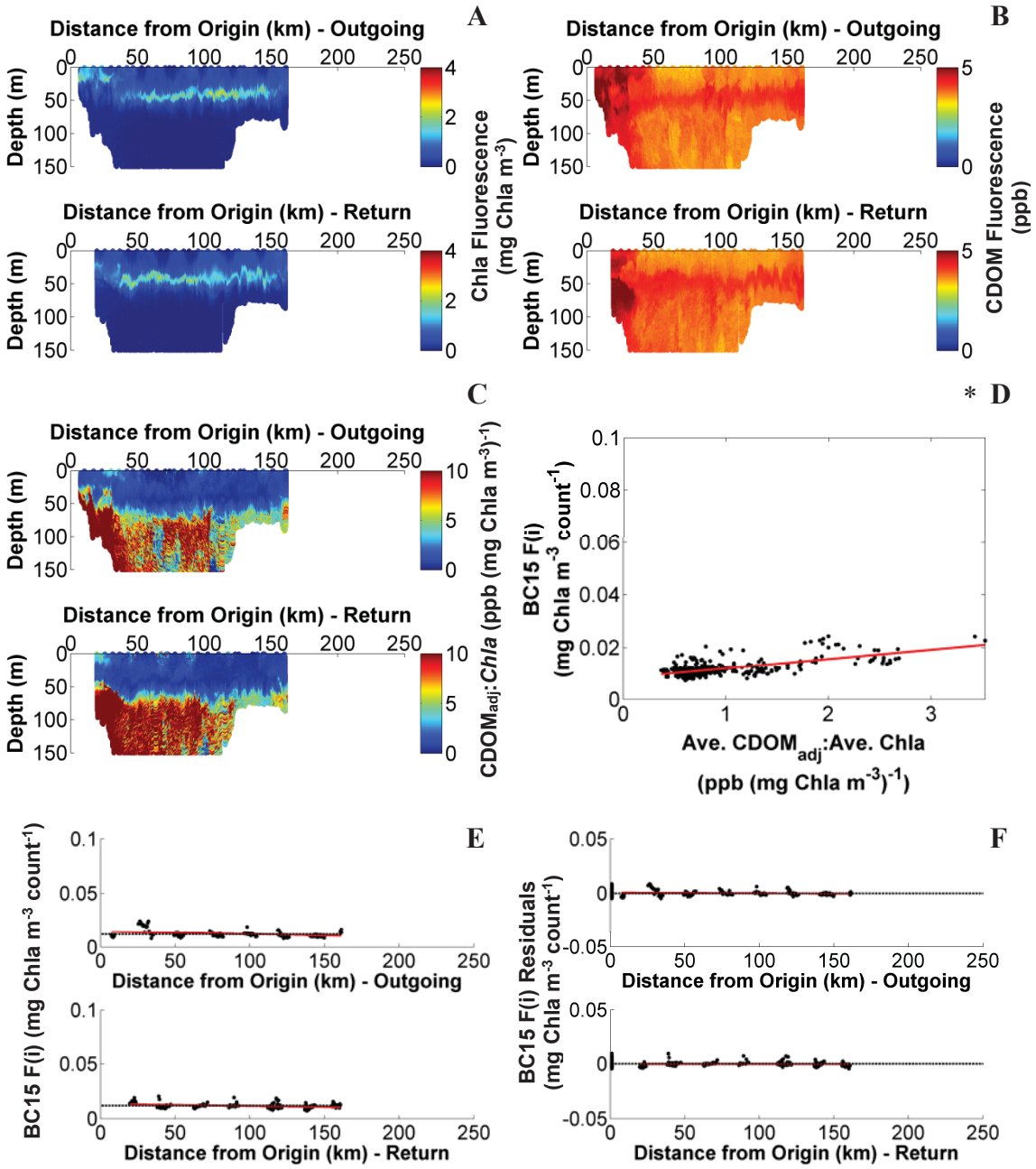

Mission #3 – 2012-05-24

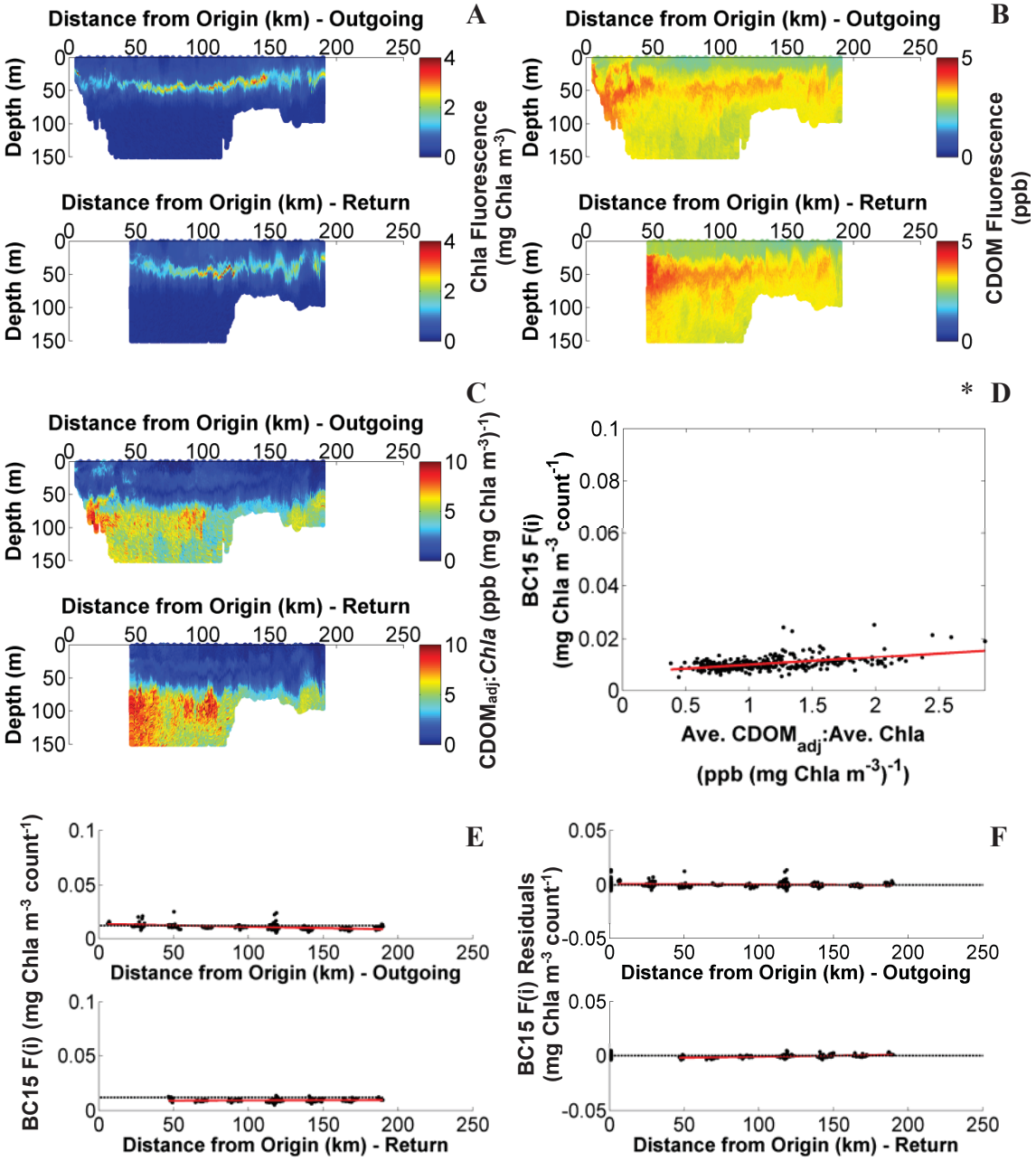

Mission #4 – 2012-06-12

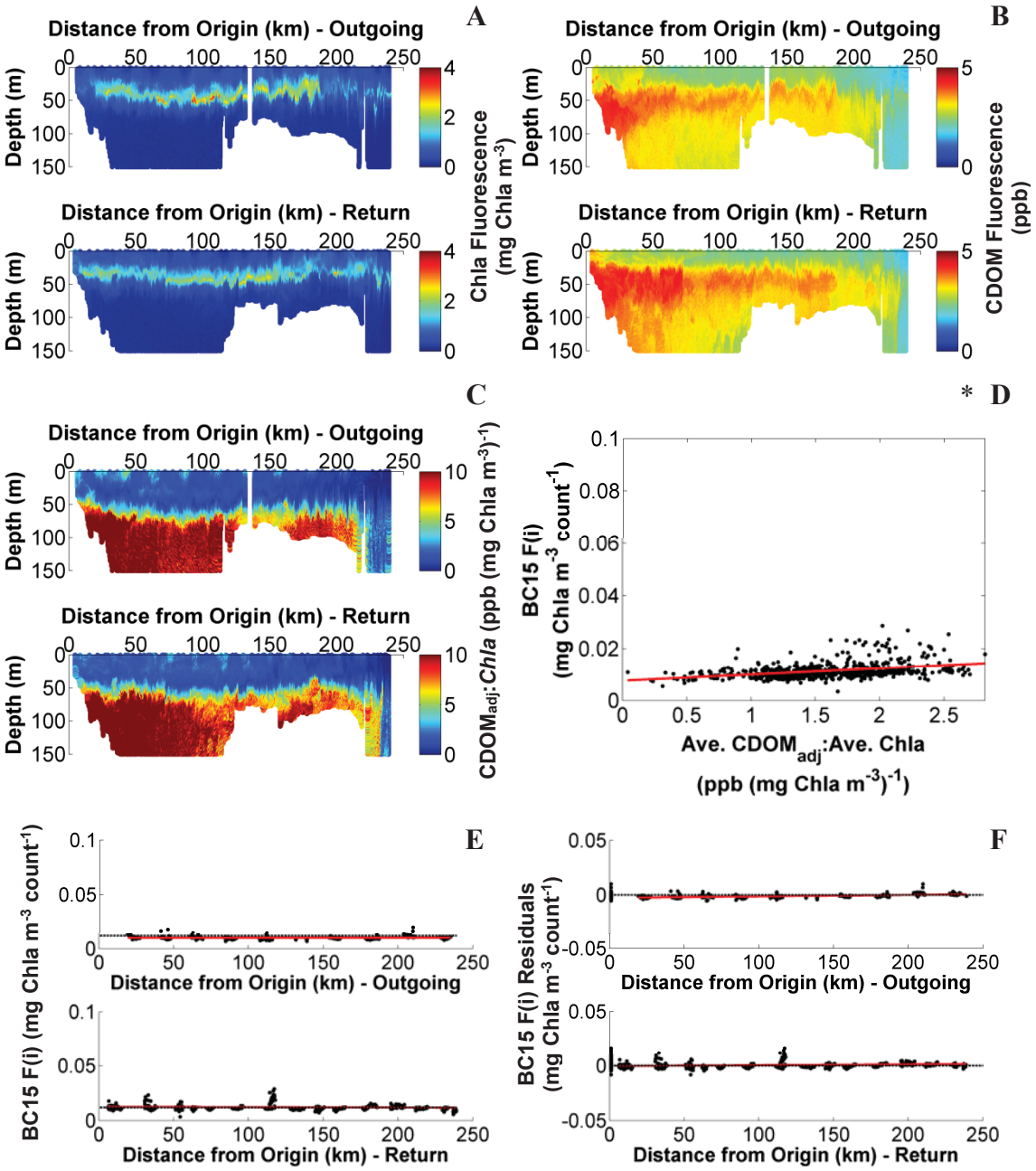

Mission #5 – 2012-07-11

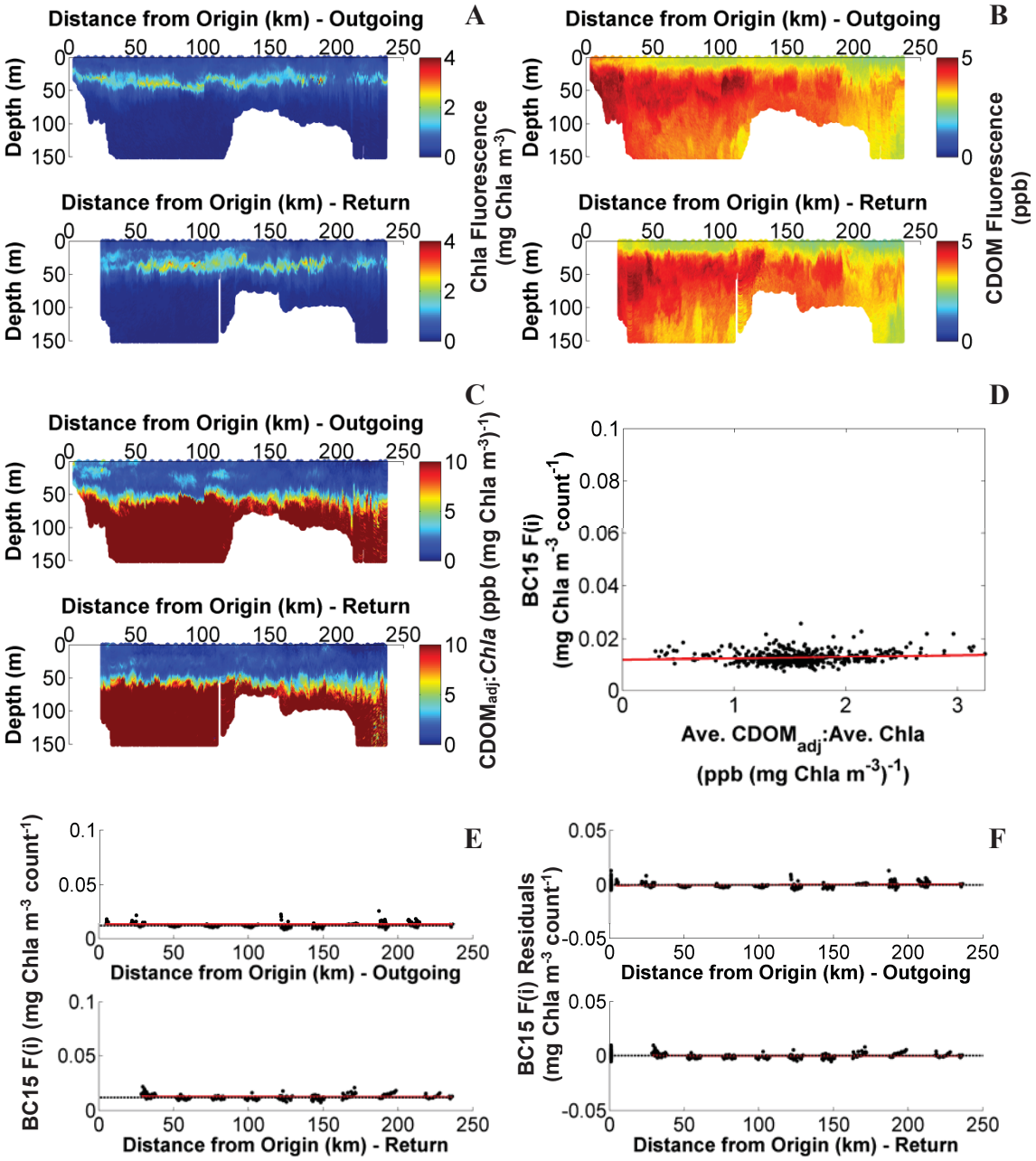

Mission #6 – 2013-03-11

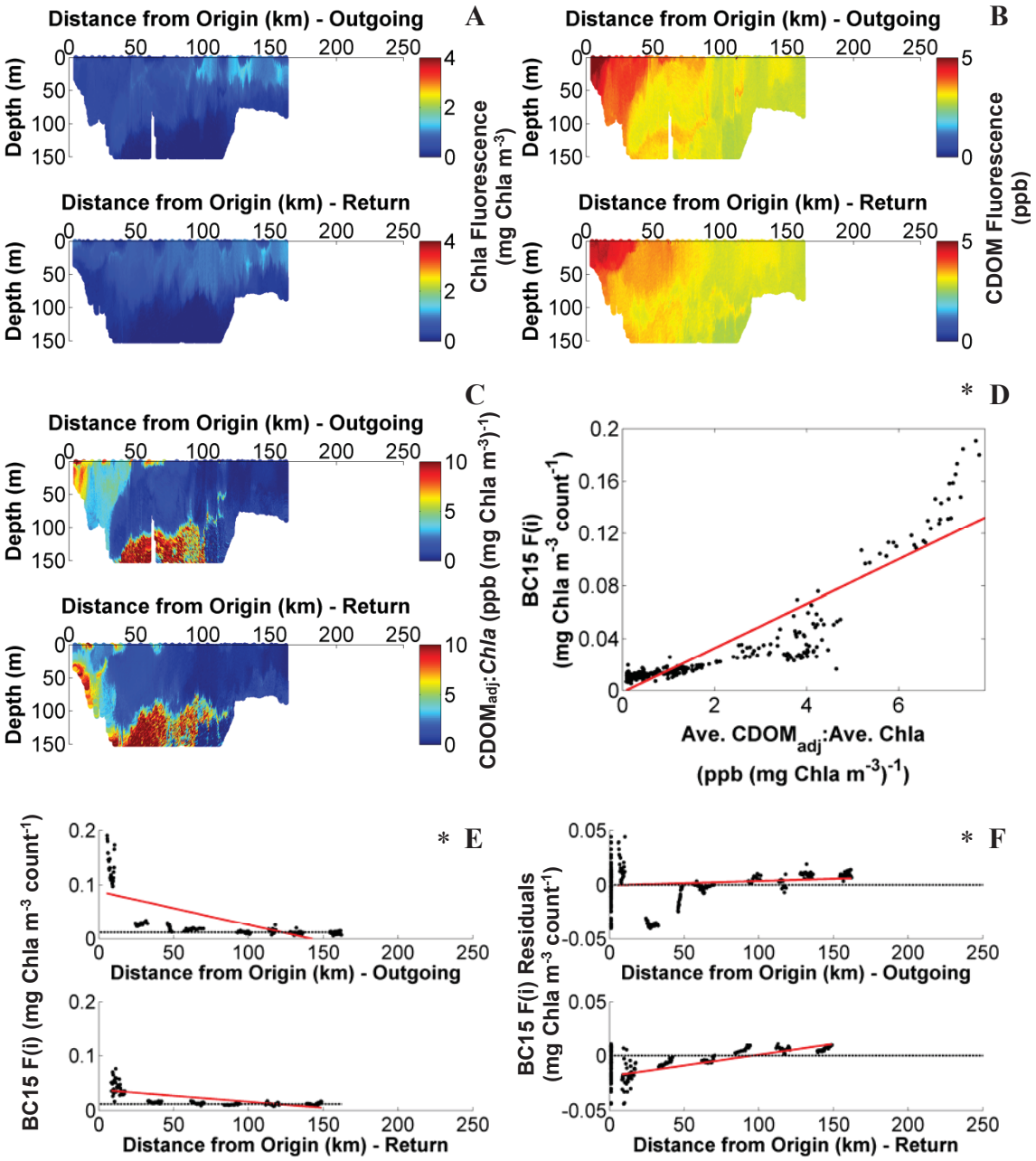

Mission #7 – 2013-03-29

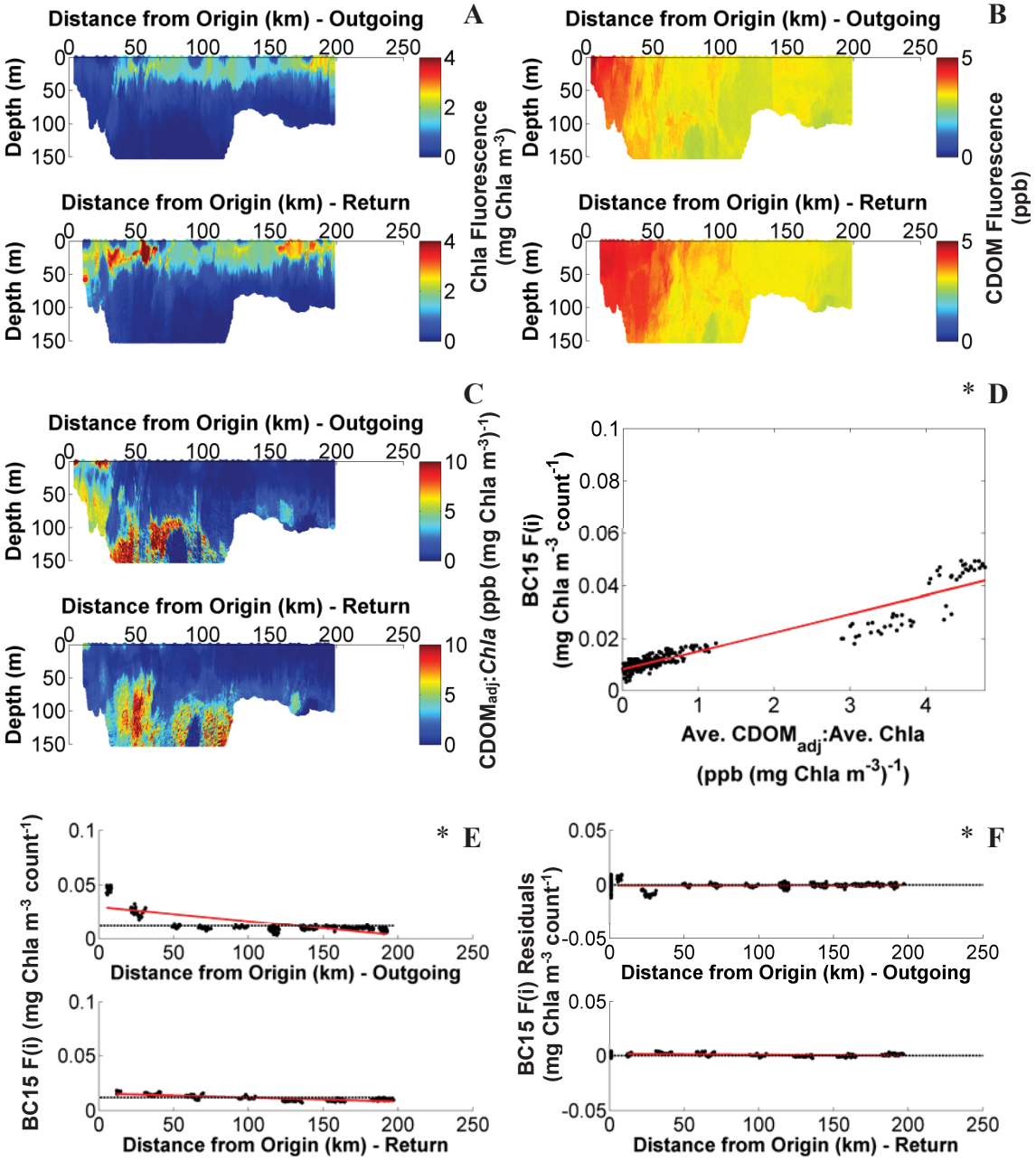

Mission #8 – 2013-05-03

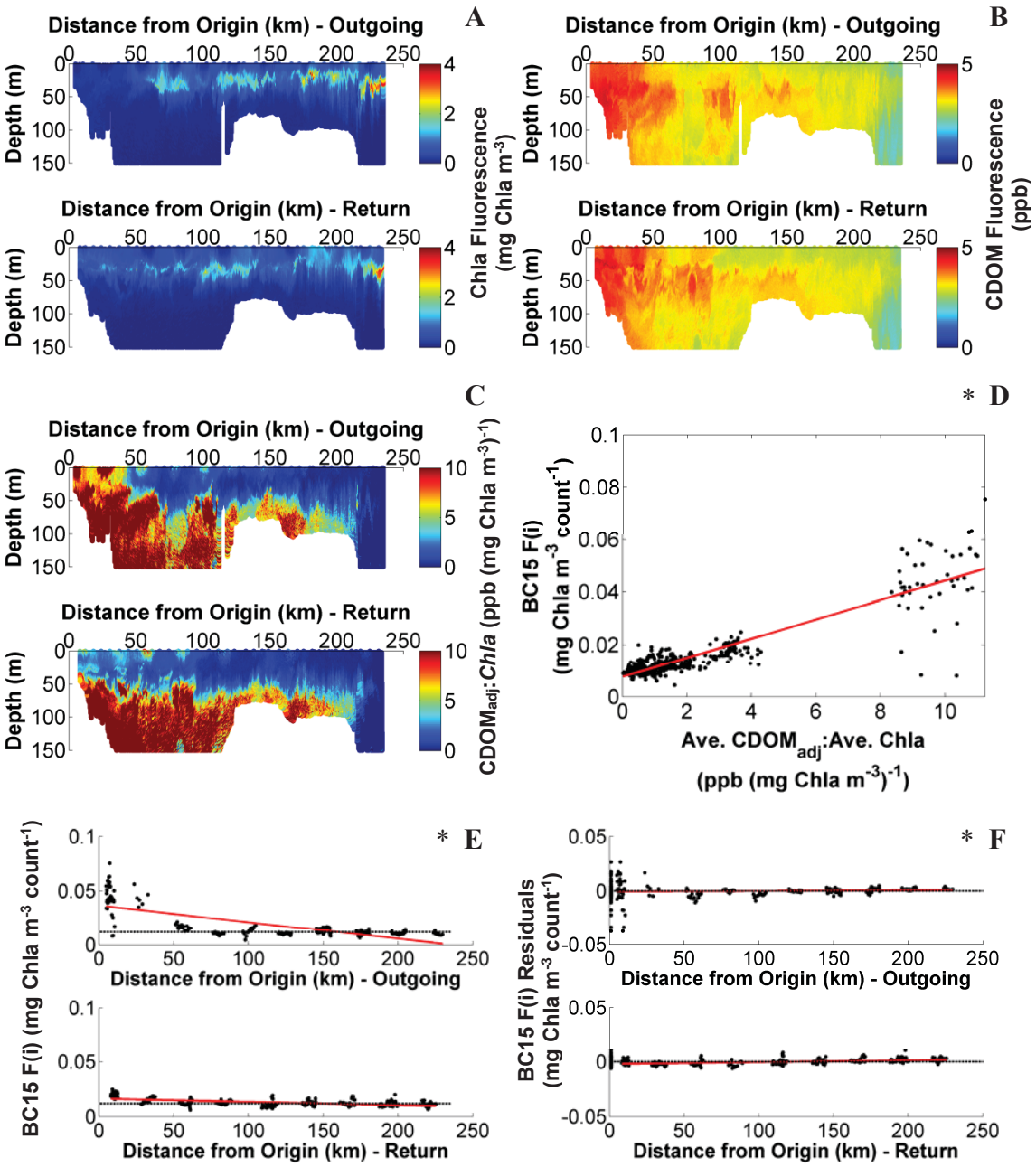

Mission #9 – 2013-06-06

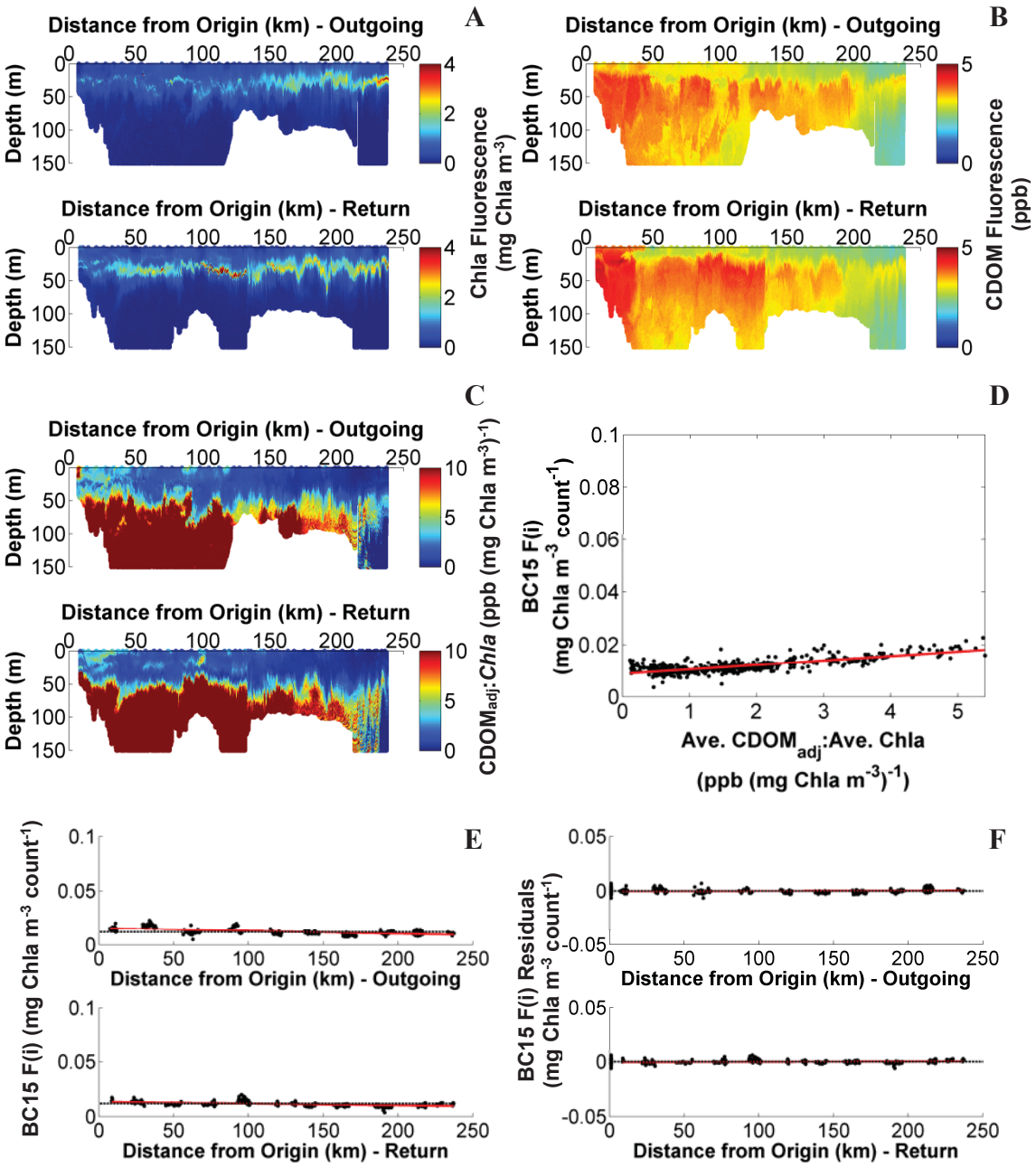

Mission #10 – 2013-09-16

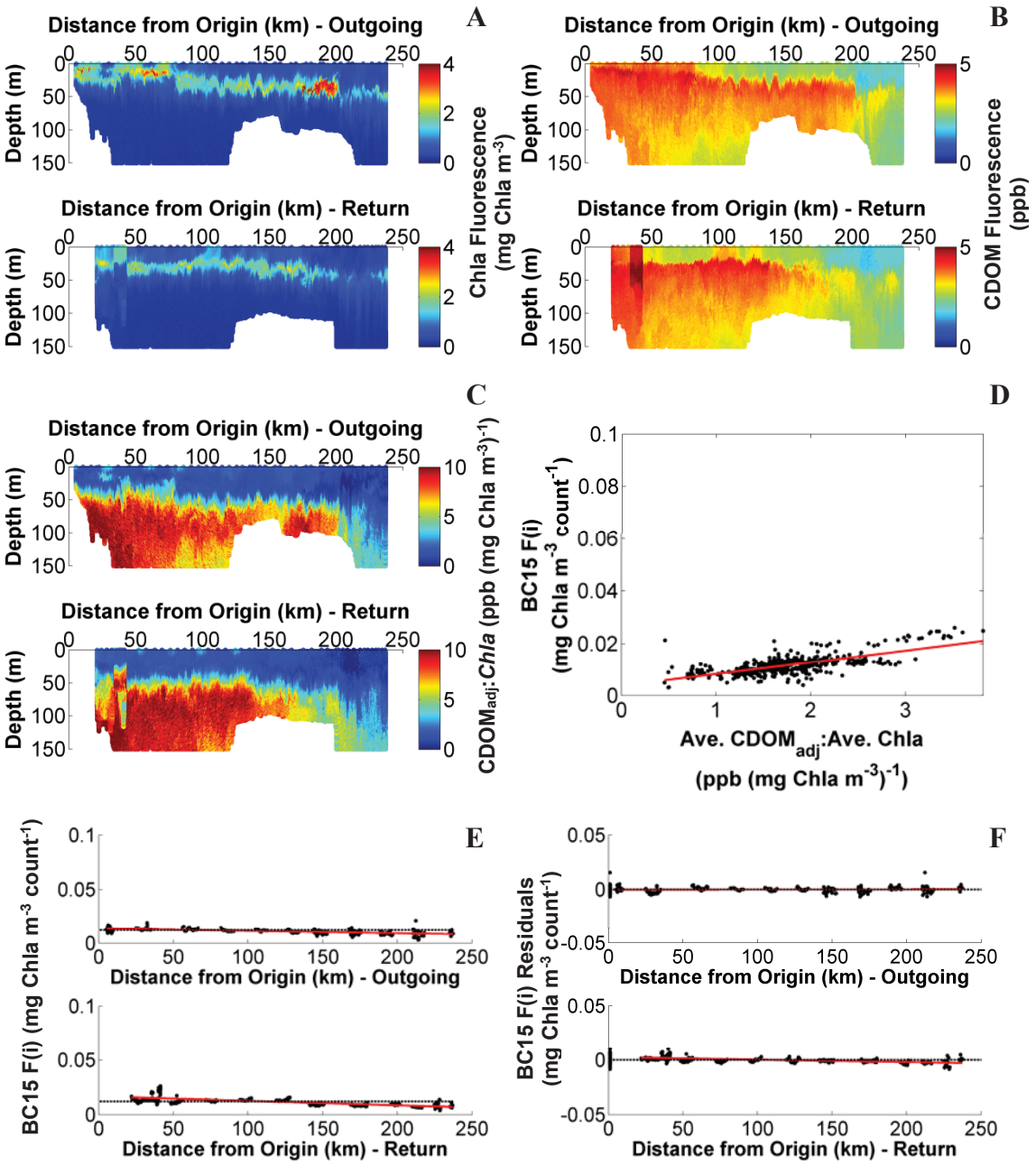

Mission #11 – 2013-11-06

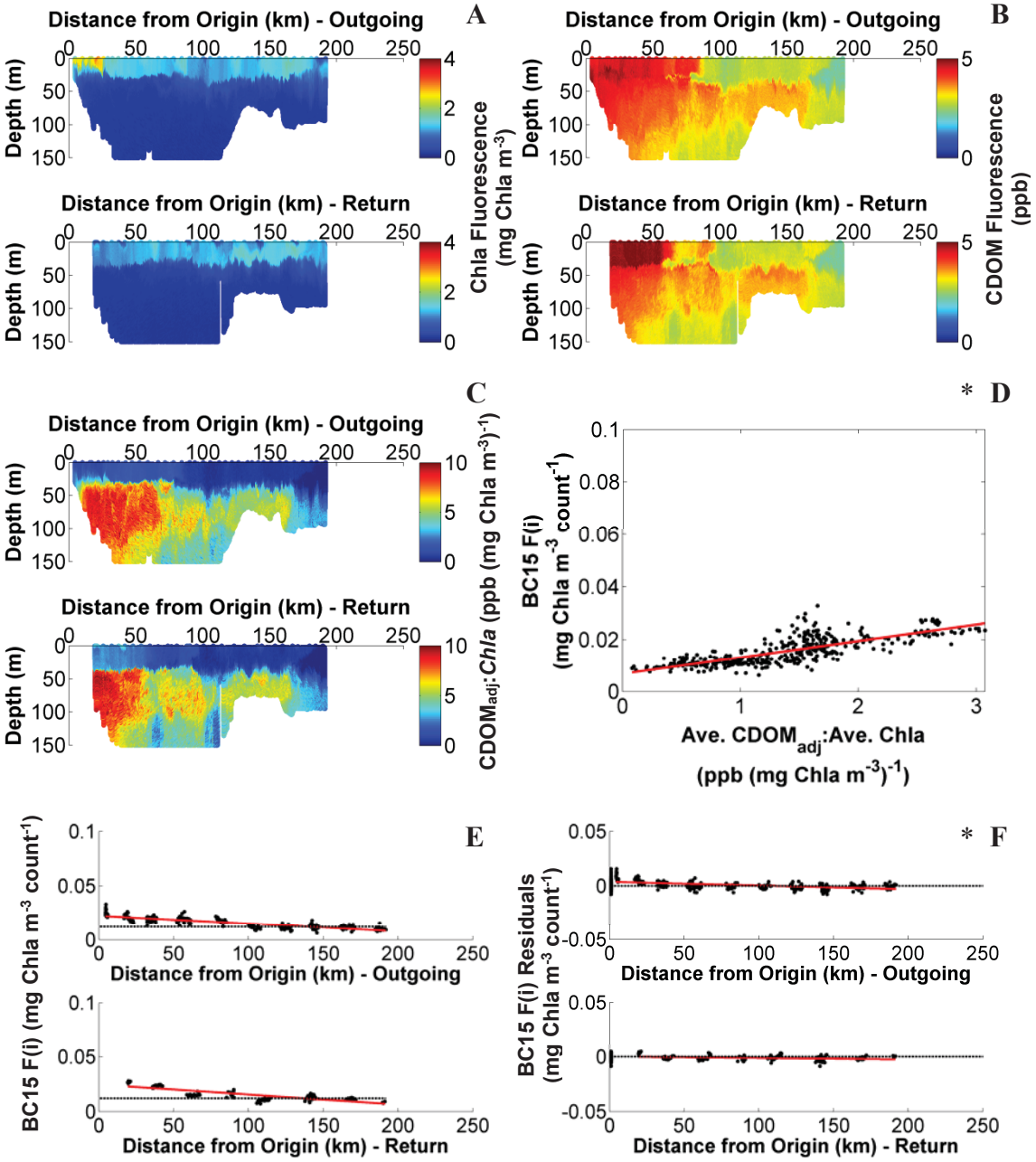

Mission #12 – 2013-12-02

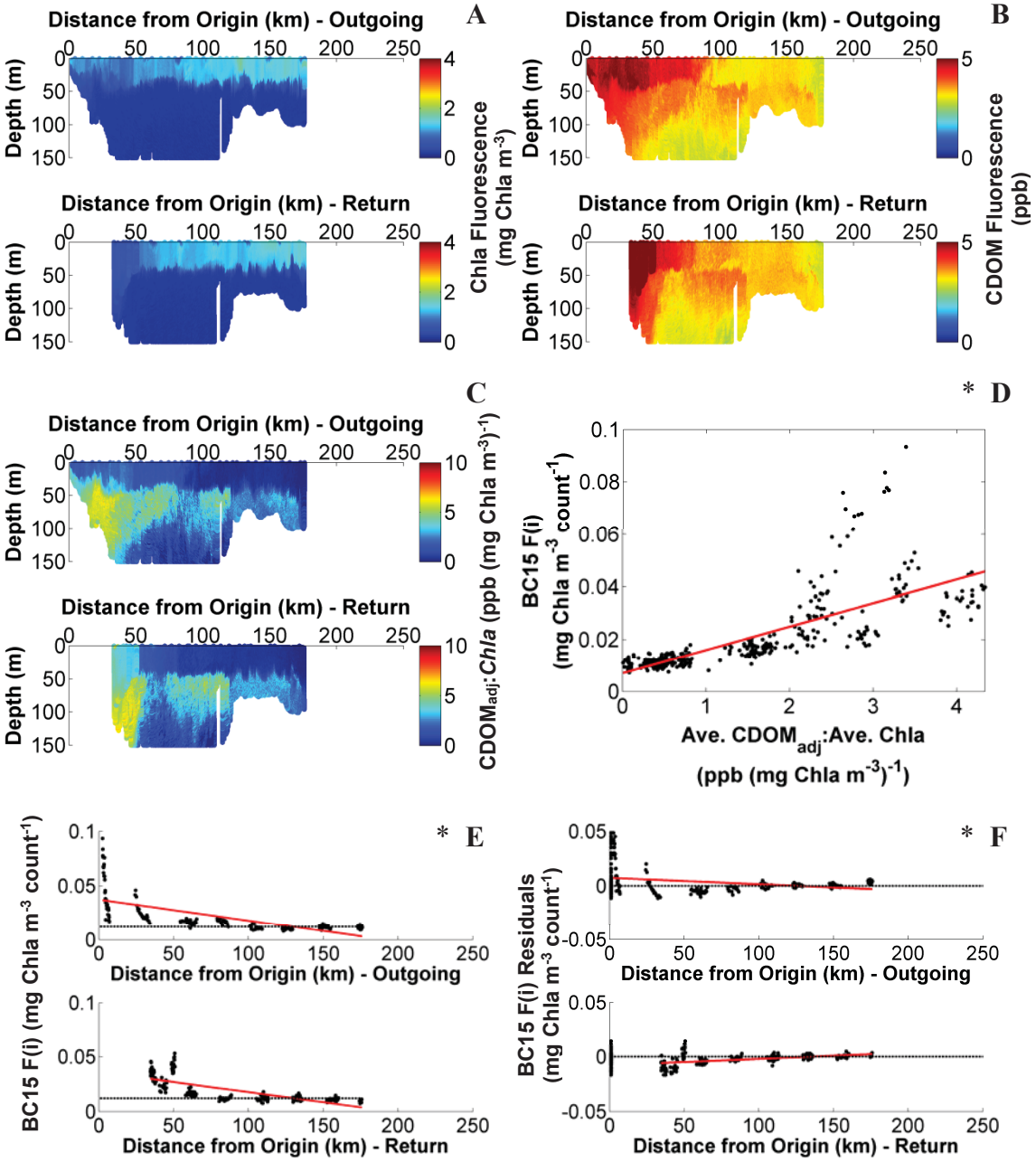

CHAPTER 4 DISCUSSION

Quantifying a variable conversion factor between $fluor$ and $Chla$ can be difficult because of the taxonomic differences between groups of phytoplankton, and the ability of individual phytoplankton to acclimate to fluctuations in their environment on the scale of minutes to days (Cullen and Lewis 1988). The effects of this, from changes in intracellular pigment concentration, cell size, and internal pigment packaging, all of which affect the chlorophyll *a*-specific absorption coefficient of the cell (Sosik 1996; Ciotti et al. 1999; Finkel 2001), to differences in the fluorescence yield characteristics of the cell (Kiefer 1973b; Cleveland and Perry 1987; Huot and Babin 2010), are significant enough that any meaningful attempts to relate $fluor$ to $Chla$ must, by necessity, attempt to accommodate these factors whenever possible. The X11 method, and the BC15 modifications to it, implicitly accommodates these taxonomic and physiological changes in both the $fluor$ to $Chla$ and the K_{bio} to $Chla$ relationships through the dynamic *F*-factor. Without delving into specific changes in the photophysiology of the phytoplankton community, X11 acknowledged that the patterns in $F(i)$ they observed during their study (which, due to the depth-integrated nature of the method could only explicitly investigate trends in the horizontal dimension) were attributable to a combination of taxonomy and physiology, in addition to methodological error (Xing et al. 2011). The change in taxonomic composition is particularly relevant, as species-type (or more specifically, pigment composition) drives more than 70% of the variability in fluorometer calibration using monospecific cultures, as reflected in the conversion factor for $fluor$ to $Chla$ (Proctor and Roesler 2010). A taxonomic change is such a strong driver of variability because it inherently changes all of the other aforementioned properties that affect the $fluor$ to $Chla$ and the K_{bio} to $Chla$ relationships.

Through the analyses described in Chapter 3, it was possible to test multiple hypotheses relating to the presence of significant trends in the calculated *F*-factors, and whether the results could be attributed to changes in the bio-optical relationships of the phytoplankton community. The implications of those results are discussed in the following sections. Additionally, there were influences on the *F*-factors that were not related to variability in the bio-optical properties of the phytoplankton, and errors

inherent to the methodologies incorporated into this study that have yet to be discussed, which will be explored in the following sections as well.

4.1 Implementation of the X11 and BC15 *F*(i)

4.1.1 Implementation of X11 *F*(i) Relative to Static *F*-factor

In the nearest X11 sample site (North Atlantic Ocean, in the Iceland Basin) to the region used in this study (North Atlantic Ocean, Scotian Shelf), X11 calculated $F(i)$ that varied over a range of 20% to 90% of the manufacturer's *F*-factor over a period of 10 months. The median per-transect X11 $F(i)$s in this study varied relative to the static manufacturer *F*-factors over a range of approximately -20% to +5% (Table A.1) – a range of the same order of magnitude. When looking at all measured $F(i)$ values in place of per-transect medians, the data in this study did vary over a much larger range during some missions (the largest X11 $F(i)$ obtained was approximately 0.2 mg Chl m^{-3} $count^{-1}$ during Mission #6, approximately 20x larger than the manufacturer *F*-factor). However as determined in Chapter 3, extreme variability in values of X11 $F(i)$ can typically be attributed to the confounding effects of non-covarying CDOM in the $\mathrm{CDOM_{adj}}$: $Chla$ relationship, which affects the accuracy of the $Chla$ estimate from the underlying Morel relationship. As the X11 dataset only consisted of Case 1 waters this was not an issue that needed to be addressed by X11, unlike this study which consisted of both Case 1 and Case 2 waters.

The similarity between the median per-transect X11 $F(i)$ values and the manufacturer's supplied *F*-factor, even when the effects of independently-varying CDOM are still affecting the $F(i)$ estimates, is worth emphasising. For the data set analysed in this thesis the manufacturer's *F*-factor can be said to provide a sufficiently accurate *F*-factor estimate without complicating the analysis with the assumptions and influences of the multi-parameter X11 approach.

4.1.2 Implementation of BC15 *F*(i) Relative to X11 *F*(i)

The BC15 $F(i)$ procedure included modifications that addressed two potential sources of error in the X11 method. The first was unidirectional outlier removal, where

the X11 method would only remove outliers below the iteratively-fitted linear regression line for the $A(z)$ vs. $C(z)$ relationship, resulting in underestimates of $F(i)$. This was resolved by making the outlier-identification process bidirectional, so that it could identify outliers both above and below the regression line (Section 3.3.1). The second was an overly stringent outlier removal criterion that eliminated all depth-depended variability in the $A(z)$ vs. $C(z)$ profile and forced the final corrected profile to be strictly linear with depth. This was resolved through a combination of loosening the criterion for identifying an outlier to those data points outside the 90% prediction interval of $\hat{A}(z)$ at a given value of $C(z)$, and by fitting the $A(z)$ vs. $C(z)$ relationship with a cubic fit in place of the linear fit (Section 3.3.2).

Taken as a dataset-wide average, the per-profile percent-difference between the two estimates was 4.53% ± 20.08% (where BC15 $F(i)$ was on average 4.53% larger than X11 $F(i)$). Since the X11 outlier-detection criterion only detects outliers below the fit, there is a tendency for the iterative outlier-removal process to generate iteratively shallower X11 slopes, which translates into smaller $F(i)$ estimates (although this is not always the case). The above result is therefore consistent with what would be expected based on the observed bias of the unidirectional X11 outlier method.

The important observation to make about the BC15 $F(i)$ versus X11 $F(i)$ comparison is that there was no discernible difference between the two estimates on a dataset-wide level, with linear regression revealing a nearly 1:1 relationship and a y-intercept of near zero (Section 3.3.3 and Figure 3.11). This indicates that, aside from the change in outlier-detection criteria which corrects for a specific case (isolated increases in $E_{\mathrm{d}}(\lambda, 0)$ during otherwise cloudy profiles) the assumption of linearity with depth of the X11 method is satisfactory.

One issue that will need to be resolved through future research will be determining which of the $F(i)$ estimates is closer to the concentration of chlorophyll *a in situ*. Without comprehensive water samples for validation, it is not possible to determine if the changes in $F(i)$ from the BC15 methodology increased or decreased the accuracy of the estimate compared to the X11 methodology – only that the estimate is different.

4.2 Trends in the X11 and BC15 *F*-factors

4.2.1 Horizontal Trends in X11 *F*(i) and BC15 *F*(i)

Accounting for the effects of $\mathrm{CDOM}_{\mathrm{adj}}|_{z_{\max}}^{z_{\min}}$: $Chla|_{z_{\max}}^{z_{\min}}$ on BC15 $F(i)$ revealed that there was little or no spatial pattern with distance in the residual variability of the *F*-factor. Of the 24 transects, 11 had a relationship with distance from shore that was not significantly different from zero (Table A.5 in Appendix A) and the remaining transects (with the exception of Mission #6, 2013-03-11, which was poorly corrected for the effects of $\mathrm{CDOM}_{\mathrm{adj}}|_{z_{\max}}^{z_{\min}}$: $Chla|_{z_{\max}}^{z_{\min}}$) displayed only weak trends with distance from shore. This led to a rejection of the hypothesis that spatially coherent changes in *F*-factor were due to changes in the bio-optical relationship between $fluor$ and $Chla$, or between K_{bio} and $Chla$.

There is, however, some evidence that a nearshore to offshore trend in the *F*-factor of a shelf region is possible. Nearshore to offshore trends of increasing fluorescence yield have been observed and associated with decreasing nutrient availability over the same distance (Kiefer 1973a). Changes in the taxonomic composition of the phytoplankton community with distance from shore can also occur, affecting, among other optically-relevant factors, the ratio of pigment concentration to total phytoplankton biomass (Buck et al. 1996). Since smaller-celled phytoplankton are thought to have a competitive advantage in low nutrient conditions due to their higher affinity for nutrients (Agawin et al. 2000), it is conceivable to have a scenario where smaller phytoplankton species in oligotrophic waters offshore are present with different optical characteristics than larger phytoplankton species in eutrophic waters nearshore. It is therefore reasonable to assume that patterns in X11 $F(i)$ and BC15 $F(i)$ would correlate with changes in nutrient regime and its associated taxonomic groupings from nearshore to offshore, if such a trend were to exist. The fact that half of the missions in this dataset still exhibit a non-zero trend with distance suggests that it is possible that trends in $F(i)$ with distance from shore do exist, but that the coarseness of the CDOM correction utilised in this study may have overshadowed any observable patterns. More sensitive analyses of trends with distance may be an interesting avenue of future research.

Another factor that may affect trends in $F(i)$ with distance from shore is the Scotian Current, which flows in a southwestern direction in the nearshore region of the Scotian Shelf, bringing fresher (less saline) water down from the Gulf of St. Lawrence and the Labrador Current (Han et al. 1997). This is significant, as CDOM concentration can be inversely related to salinity in surface waters, in part due to the contribution of continental inputs (Ferrari and Dowell 1998; Foden et al. 2008). The analyses conducted in this study showed that the missions with steeper slopes in *F*-factor versus distance were caused by an increase in the ratio of $\mathrm{CDOM_{adj}}|_{z_{\max}}^{z_{\min}}:Chla|_{z_{\max}}^{z_{\min}}$ in the nearshore data and that these missions occurred during the winter and early spring months (Figure 3.7 in Section 3.2). The Scotian Current also experiences a seasonal cycle, with transport being highest in the winter and spring (up to ~0.9 Sv), and lower in the summer and fall (down to ~0.3 Sv; Han et al. 1997; Hannah et al. 2001). Additional literature research would need to be done to discover seasonal variation in the width of the Scotian Current as it crosses the Halifax Line, to determine if this width correlates well with the width of the region where *F*-factors are affected by anomalously high $\mathrm{CDOM_{adj}}|_{z_{\max}}^{z_{\min}}:Chla|_{z_{\max}}^{z_{\min}}$. It would also be necessary to determine the CDOM characteristics of the current over the year, to determine whether the periods of increased current flow correlated with an increase in CDOM concentration.

4.2.2 Vertical Trends in BC15 *F*(i,ζ)

X11 note that the influences that require a dynamic *F*-factor in the horizontal dimension, such as changes in the taxonomy and photophysiology of the phytoplankton assemblage, are also applicable in the vertical dimension (Xing et al. 2011). This idea is supported by the rejection of the hypothesis by this study that there is no variability with depth in the $A(z)$ vs. $C(z)$ relationship, determined through analysis of the validity of a linear fit to that relationship (Section 3.3) and the investigation of systematic variation around the fit with depth. This trend with depth was still present after correcting for variability in $E_{\mathrm{d}}(490,0)$ through the removal of outliers, as well as after removing the effects of $\mathrm{CDOM_{adj}}$:$Chla$ from the determination of BC15 $F(i,\zeta)$. This strongly suggests that the observed pattern in *F*-factor with depth is a result of variability in either the

$fluor$ to $Chla$ or the $K_{\mathrm{bio}}(490)$ to $Chla$ relationships (since it is not possible to distinguish between the influences of the two relationships without more discerning analyses). The observed trend indicates that phytoplankton in the shallowest and deepest optical depths have some combination of low fluorescence per unit chlorophyll *a* and high attenuation per unit chlorophyll *a*, resulting in larger *F*-factors for those regions.

When the percent-differences were compared between depth-resolved $F(i,\zeta)$ and the corresponding per-profile X11 $F(i)$ over the dataset (Section 3.4, Figure 3.12), a spatially consistent pattern is suggested, with depth-dependent variation of median values between approximately -3% and +30% depending on optical depth (n = 5,362). This trend with depth was still visible in the $F(i,\zeta)$ residuals after removing the effects of $\mathrm{CDOM_{adj}}$:$Chla$ on the relationship (Section 3.5, Figure 3.16), with median $F(i,\zeta)$ fluctuating between approximately -13% and +12% (n = 54,138; note that this estimate was derived by taking the median per-optical-depth value and dividing it by the manufacturer's *F*-factor value for the corresponding mission, in order to provide a standard to which the percent deviations of the residuals could be compared. This method of estimation is only used to provide a context for the scale of variability expressed in the residuals of $F(i,\zeta)$). These are noticeable changes with depth, but not very large given the magnitude of other sources of variability in the $fluor$ to $Chla$ relationship. The limited variability in median $F(i,\zeta)$ with depth is supported by the results of X11, who note that their depth-integrated model is able to account for 76% of the variability (r^2 = 0.76, n = 156) between coincident measurements of $Chla$ using HPLC analysis and $Chla$ estimated from an *in situ* fluorometer using their $F(i)$ at 490 nm. It could therefore be concluded that an assumption of linearity with depth would explain enough of the variability in the *F*-factor relationship that a consideration of the depth-dependent effects is unnecessary to obtain a sufficiently accurate estimate of $Chla$.

One change of note between the pre- and post-CDOM adjusted *F*-factor data is the drop in median $F(i,\zeta)$ in the 5$^{\mathrm{th}}$ optical depth, relative to the medians of the other optical depths. This would suggest that, while the overall trend with depth was retained after removing the effects of $\mathrm{CDOM_{adj}}$:$Chla$ on $F(i,\zeta)$, there was a small effect of $\mathrm{CDOM_{adj}}$:$Chla$ within the 5$^{\mathrm{th}}$ optical depth. Closer examination of per-mission transects of $\mathrm{CDOM_{adj}}$:$Chla$ reveal that in some missions, the waters of the 5$^{\mathrm{th}}$ optical depth

contained high values of CDOM$_{adj}$:*Chla* (Figure 4.1). This scenario resulted in artificially high *F*-factors followed by lower *F*-factor residuals after the CDOM$_{adj}$:*Chla* adjustment, just like the high CDOM$_{adj}$:*Chla* waters nearshore.

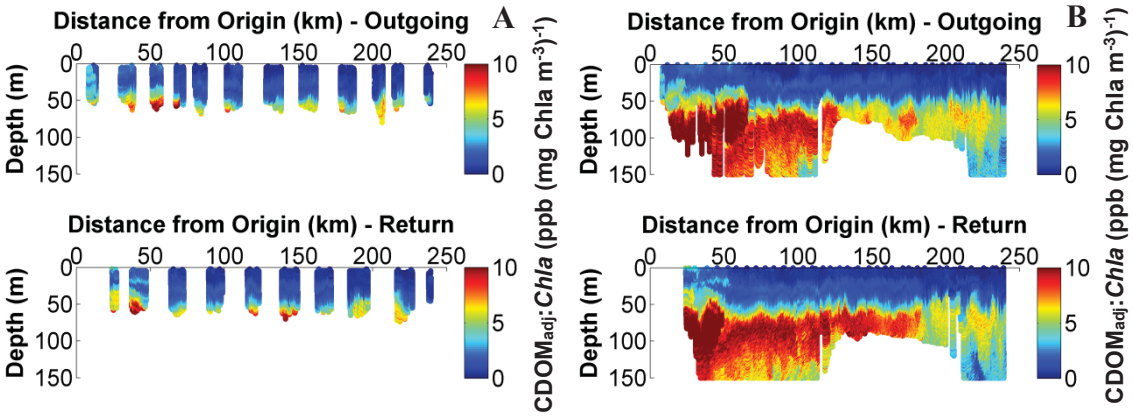

Figure 4.1. Outgoing and return glider transects for Mission #1 (2011-07-26). **(A):** CDOM$_{adj}$:*Chla* (ppb (mg Chla m^{-3})$^{-1}$) versus distance from shore. Only profiles containing Level 2 data are shown to demonstrate the sampling range of the method compared to the total glider track. Note that the bottom of most profiles contain water with high CDOM$_{adj}$:*Chla*. **(B)**: the same variables and transects as 4.1.A, except displaying all of the available glider data for context, not just Level 2 profiles. Note that the high CDOM$_{adj}$:*Chla* regions in the deep water column are extensive. This would suggest that in order to obtain accurate $F(i,\zeta)$ estimates with depth, the profiles should not include the fifth optical depth as was done for this analysis.

Although useful general trends with depth were determined, the magnitude of the variability around the median values cannot be ignored. Variability with depth, whether before or after the removal of CDOM$_{adj}$:*Chla* effects, is on the order of several hundred percent for depth-dependent estimates in individual profiles. This implies that there are many profiles in which the general trends with depth from Figures 3.12 and 3.16 are not applicable, and the blanket application of a per-depth $F(i,\zeta)$ based on these median values would result in errors in the *Chla* estimate larger than if no correction with depth had been attempted at all. This makes a correction of this nature impractical. This is evident in the example glider profile in Figure 3.17 demonstrating a matchup between estimated and extracted *Chla*, where the estimates using $F(i,\zeta)$ introduced large variability in estimated *Chla* that was likely artefactual, causing inconsistencies with depth. Despite this, there is reason to expect variability in the *F*-factor relationship with

depth, and it is possible that the magnitude of variability in the *median* $F(i,\zeta)$ is representative of real variability in the bio-optical properties of the phytoplankton community. The ratio of $Chla$ to carbon (mg Chl m^{-3} g^{-1}) can vary by a factor of 10 with depth, as community composition changes and as phytoplankton up- and downregulate $Chla$ in order to compensate for changing light and nutrient regimes (cf. Cullen 1982 and references contained therein). This is in addition to changes in intracellular pigment concentration (Ciotti et al. 1999) and the influence of light and nutrients on the fluorescence yield properties of the plankton (Kiefer 1973a; b; Huot and Babin 2010). Chlorophyll *a*-specific absorption is also known to vary in the vertical dimension (Sosik 1996). The combination of these physiological changes involving both the $fluor$ to $Chla$ relationship as well as the K_{bio} to $Chla$ relationship, would change the bulk optical properties of the phytoplankton community at different depths and would be reflected in variability in the BC15 $F(i,\zeta)$ estimates. Considering the scale of these influences, a difference of approximately 50% in $F(i,\zeta)$ between optical depths is not unrealistic.

To summarise, despite the overall trend in the median $F(i,\zeta)$ with optical depth, the magnitude of variation in the outliers makes a quantitative application of a dynamic $F(i,\zeta)$ with depth impractical. Additionally, without comprehensive coincident water samples to validate the accuracy of the per-optical depth $F(i,\zeta)$, it cannot be determined whether these variations are true representations of changes in the phytoplankton assemblage or whether they are artefacts of the methodology. It can only definitively be stated that there is a qualitative trend with optical depth, with larger $F(i,\zeta)$ in the first and (potentially) fifth optical depths of the water column. It will have to be the focus of future work to investigate these trends more thoroughly, and to determine whether a quantitative relationship can be determined in such a way as to allow for the reliable implementation of a variable $F(i,\zeta)$. Additionally, an assumption of linearity with depth such as that made by X11 could explain enough of the variability in the *F*-factor relationship that a consideration of the depth-dependent effects is unnecessary to obtain an accurate estimate of $Chla$ on a per-profile basis.

4.3 Comparison of *Chla* Estimates from Fluorescence using the Manufacturer, X11, and BC15 *F*-factors

Comparisons presented in Section 3.6 suggested that the X11 and BC15 *F*-factors do not improve the estimation of $Chla$ compared to the manufacturer's static *F*-factor for the water samples obtained for validation. However there are several factors which would suggest that the water samples used may not be appropriate for definitively assessing the quality of the X11 and BC15 $Chla$ estimates. This is due to a combination of the small number of available samples (n = 39 samples over 14 sampling days), the fact that each profile only had 1-3 depths available for matchup (generally the entire depth of the profile was not represented by the depths sampled, nor were all of the major structural features of the $Chla$ profile), the fact that the water samples were not always obtained coincident to the glider profile (samples occurred between 0 and 23 hours after the last glider profile, depending on the logistics of retrieval), and, for the X11 and BC15 values, the increased variability in the *F*-factor estimate caused by $CDOM_{adj}$:$Chla$ due to the nearshore nature of the sampling regime. In order to obtain a more robust relationship more samples would need to be taken at a larger number of depths and times. Additionally, in order to make a direct comparison and determine whether the BC15 *F*-factors were an improvement over the X11 $F(i)$ and the manufacturer's *F*-factor, a set of water samples exclusively from Case 1 waters would need to be compiled so that the methods could be applied in the environmental context they were intended for: waters that are optically dominated by the concentration of phytoplankton.

A 2010 study by Proctor and Roesler that investigated the relationship between the $fluor$ to $Chla$ conversion factor and the variables of taxonomy, growth irradiance, and growth phase, found a similar level of variability when comparing extracted $Chla$ to $Chla$ estimated from fluorescence using the static manufacturer *F*-factor of a similar WET Labs fluorometer without any site-specific calibration (a correlation of r^2 = 0.24 between extracted $Chla$ and $Chla$ estimated from fluorescence, n = 8; compared to the relationship determined using the water samples in this study with a correlation of r^2 = 0.25, n = 39). Their solution was to determine separate *F*-factor calibrations for different phytoplankton species and growth conditions, and apply the appropriate *F*-factor based

on the dominant taxa present in a study site. Their criterion for selecting the appropriate *F*-factor was based on taxa, because they determined that 71% of the variability between *F*-factors could be attributed to species. Once the *F*-factor that properly accounted for the local phytoplankton assemblage was applied to the *fluor* data in place of the static manufacturer *F*-factor, the correlation between extracted $Chla$ and $Chla$ estimated from fluorescence increased from $r^2 = 0.24$ to $r^2 = 0.96$ ($n = 8$). In fact, in order to properly adjust the *F*-factors on a per-species basis to obtain such a high correlation, their study, which investigated the species-specific response of 34 species of phytoplankton, discovered a 10-fold difference in the between-species *F*-factors necessary to obtain the final $Chla$ estimates when using a 470 nm excitation WET Labs fluorometer (similar to the fluorometer used in this study). Since the scaling factor for the WET Labs fluorometer used in this study was determined using a laboratory monoculture of phytoplankton of the diatom species *Thalassiosira weissflogii*, a similar correction is likely required to obtain accurate *in situ Chla* estimates assuming that the species composition in the study area changes with time (note: the magnitude of this change will depend on the specific species compositions and will not necessary be as large as 10-fold). The automation of this process, to provide an on-site conversion factor capable of accounting for variability in the bio-optical properties of the phytoplankton community, is the core application of the X11 method and the BC15 modifications to it. Based on the results of Proctor and Roesler (2010), this is obviously a necessary objective to attain.

4.4 The Effect of CDOM on the Underlying Morel (1988) Model

Estimates of $K_{\mathrm{bio}}(\lambda)$ from the equations underlying the X11 method attribute all changes in the attenuation of light in the water column to changes in concentration of chlorophyll *a* and covarying substances (Morel 1988). This assumption applies to Case 1 waters where variability in the optical properties of the water column are dominated by phytoplankton and its covariates. However attempting to quantify changes in $K_{\mathrm{bio}}(\lambda)$ with a single parameter (*Chla* in this case) when there are multiple and non-covarying contributors to the optical signal (i.e., in Case 2 waters) means that the method is particularly susceptible to error from non-planktonic sources. More specifically, increased attenuation from these non-planktonic contributors will be interpreted by the

model as increased $Chla$ relative to the $fluor$ signal, resulting in a larger F-factor calculation. This is not to say that the model does not implicitly include some optical contribution from non-planktonic particles. Rather, the model has variation around its calculated coefficient values, as it is a statistical average of empirical data of the $K_{\mathrm{bio}}(\lambda)$ response to changes in phytoplankton concentration as estimated by $Chla$, and these values implicitly include a contribution from CDOM and any other substances that covary with the phytoplankton abundance. Error is introduced when these non-planktonic particles and substances contribute in a different proportion than is implicitly included in the Morel model. The attenuating effects of non-planktonic substances (namely CDOM) and their effects on model estimates is acknowledged both by Morel and by X11 (Morel 1988; Xing et al. 2011), however neither directly propose a solution other than to identify data points that are from Case 2 waters and remove them (Morel 1988) or to suggest that investigating the discrepancy in model estimates when using $K_{\mathrm{bio}}(412)$ compared to $K_{\mathrm{bio}}(490)$ could reveal potential CDOM influences (Xing et al. 2011). It was the isolation of this error in the underlying Morel model, caused by the optical contribution of non-covarying CDOM concentration, that was the reason for investigating the patterns in $\mathrm{CDOM}_{\mathrm{adj}}$:$Chla$ and attempting to remove their influence (Section 3.4).

Recall that the methods employed in this study were only able to identify regions of anomalous CDOM contribution to the calculation of the F-factor. Although the goal was to determine a quantitative relationship that allowed for a meaningful correction of BC15 F-factors affected by anomalous $\mathrm{CDOM}_{\mathrm{adj}}$:$Chla$, the magnitude of the residual variability around the BC15 F-factor versus $\mathrm{CDOM}_{\mathrm{adj}}$:$Chla$ relationship made this kind of correction prohibitive (although much more so on a per-data-point basis than on a per-profile basis). A different approach will have to be taken to remove the attenuating effects of contributors that don't covary with the phytoplankton concentration if this method is to be successfully implement into glider transects on the Scotian Shelf, or any other study area that contains Case 2 waters.

The most obvious solution to this problem would be to incorporate an additional term into Equation 1.9 (the Morel equation that estimates $K_{\mathrm{bio}}(\lambda)$ as a function of $Chla$ and scaling coefficients), so that $K_{\mathrm{bio}}(\lambda)$ is not expressed solely as a function of $Chla$. Morel (1988) states that their choice to define the model using only a $Chla$ term was

driven by the fact that $Chla$ was "often the only available index with which can be used to quantify the biogenic content". With advances in the miniaturisation and deployability of autonomous optical sensors there is no reason why simultaneous measurements of multiple parameters should not be incorporated wherever possible. This is not a novel idea, and other researchers were investigating this approach even previous to Morel's work (Smith and Baker 1978; Baker and Smith 1982). The Smith and Baker work included a third term, $K_{\mathrm{D}}(\lambda)$, used to represent attenuation from dissolved organic material that doesn't covary with chlorophyll *a*. Even more relevant to the current work is the approach taken by Xing et al. (2012) to correct for the effects of CDOM on the estimate of $K_{\mathrm{d}}(\lambda)$. They isolated that part of absorption which is attributable to yellow substance from the total magnitude and variability of $K_{\mathrm{d}}(\lambda)$, generating a multi-parameter equation for estimating $K_{\mathrm{d}}(\lambda)$ from $Chla$ and CDOM absorption (estimated from CDOM fluorescence). Despite the applicability of the Xing et al. (2012) approach to the CDOM problem encountered in this work, it was not incorporated directly into this thesis because, in order to obtain a calibrated CDOM fluorescence estimate, the method involves an identical approach for the simultaneous processing of fluorescence and irradiance profiles found in X11. As a consequence, it incorporates the same assumptions that were directly under investigation in this thesis. It did not seem appropriate to investigate the assumptions and limitations of the X11 method using the Xing et al. (2012) method under these conditions. If an approach analogous to the X11 method is to be implemented in a context that involves optically complex waters, however, alternatives such as the Baker and Smith (1982) coefficients or the Xing et al. (2012) approach should be investigated as potential solutions.

Another potential solution would be to identify and remove profiles that are in Case 2 waters, then determine a metric with which to interpolate or extrapolate an *F*-factor for the missing profiles. The difficulty here is determining an objective criterion for delineating between Case 1 vs. Case 2 waters. The classification of ocean waters into Case 1 and Case 2 began with Morel and Prieur (1977), whose observations led to the designation of Case 1 waters as those whose optical properties are determined primarily by phytoplankton and their covariates, and Case 2 waters as those whose optical properties are significantly influenced by other constituents that do not covary with

phytoplankton (Mobley et al. 2004). The criterion used by Morel and Prieur (1977) for the Case 1 versus Case 2 division was based on the ratio of chlorophyll *a* concentration (mg Chla m^{-3}) to the scattering coefficient (m^{-1}). They noted, however, that there is no sharp division between the two classifications; rather, it is more of a continuum. This criterion of an "anomalously high scattering coefficient" was what Morel used a decade later to identify and exclude samples taken in Case 2 waters when calculating the empirical relationship that currently underlies the X11 method (Morel 1988). It may be possible to successfully classify Case 1 versus Case 2 waters on the Scotian Shelf in a similar fashion. Regardless, future work will have to be done along the lines suggested above to determine a quantitative correction for the influence of $\mathrm{CDOM_{adj}}$: $Chla$ on *F*-factors for this method before it can reliably be applied in Case 2 waters. Until such a time as this can be accomplished, the manufacturer's static *F*-factor is the more reliable option.

4.5 Additional Sources of Error Inherent to the Dataset and Method

The shallowest point reached by the glider per profile, z_{min}, averaged over the dataset of n = 5362 profiles was 2.30 ± 0.80m. This introduced error into the calculation of any parameters that required a surface reference value, with two examples of particular relevance – first, the lack of a surface reference for $E_{\mathrm{d}}(490)$ and $fluor$ having a potential effect on the full-profile $\overline{K}_{\mathrm{d}}(490)$ estimate and the shape of the $A(z)$ vs. $C(z)$ relationship. Second, the lack of surface references for $b_{\mathrm{bp}}(660)$ and density affecting estimates of the mixed layer depth and estimates of the magnitude of non-photochemical quenching. In addition to these sources of error, the effects of variability in the light field of the water column unrelated to the physiological state of the phytoplankton, as well as variability in measurements caused by the sensor itself, also need to be considered.

The missing surface data in $E_{\mathrm{d}}(490)$ is a relatively simple case. Unless light in the missing several metres is attenuated differently from the current depth-averaged estimate of $\overline{K}_{\mathrm{d}}(490)$, the $E_{\mathrm{d}}(490)$ can be reconstructed through extrapolation to the surface with confidence. It should be acknowledged however that any unaccounted-for variability in

the optical properties over the missing depth intervals may have had an effect on full-profile $\overline{K}_{\mathrm{d}}(490)$ estimates, which in turn would have altered the estimates of optical depths used to delineate vertical layers of the water column in this study. Additionally, changes in $E_{\mathrm{d}}(490, z)$ or $fluor$ that deviated from the current depth-average over the missing interval would alter the shape of the $A(z)$ vs. $C(z)$ relationship over that same interval (namely the first optical depth). Aside from the above speculation, it is impossible to determine whether the missing data had any effect on $\overline{K}_{\mathrm{d}}(490)$ estimates or on the shape of the $A(z)$ vs. $C(z)$ relationship for this dataset without having real values for the missing depth range.

It is hard to quantify the effect of the lack of surface references for $b_{\mathrm{bp}}(660)$ and density on estimates of MLD and NPQ, however the qualitative effect on both can be intuitively determined. Our criteria for the MLD involved a fixed delta-difference in both density (0.125 kg m^{-3}) and $b_{\mathrm{bp}}(660)$ (2.5 x 10^{-4} m^{-1}). In a scenario where the mixed layer was uniformly mixed down to the MLD the missing portion of the surface data would have no effect as it would align with the depth-averaged values. In a scenario where the density or $b_{\mathrm{bp}}(660)$ decreased towards the surface, which would be most typical under stratified conditions, the delta-difference threshold would be reached at a shallower depth than what was calculated during this analysis. It can therefore be concluded that any error in the MLD estimates should be systematic overestimates of the true MLD depth. The implications of this carry through to estimates of NPQ. If a profile's estimate of MLD was deeper than the true MLD, then the $RFB(z_{MLD})$ (ratio of $fluor$ to $b_{\mathrm{bp}}(660)$ at the MLD used to correct for NPQ in the shallower depths) could be from phytoplankton that are not acclimated to the same environmental conditions as phytoplankton in shallower waters, and therefore could have different photo-adaptive states (Cullen and Lewis 1988). This would potentially provide an inappropriate $RFB(z_{MLD})$ relative to the phytoplankton in the mixed layer. Additionally, values for the magnitude of the NPQ effect for each profile (see Figure 3.1 in Section 3.1) were made by calculating the difference between the $fluor$ values at $z_{\min}$ before and after the NPQ correction (Equation 2.7). In profiles where $z_{\min}$ does not equal 0 m, the missing data is obviously from a layer shallower than $z_{\min}$. It can therefore be concluded that any phytoplankton in the missing layer are experiencing greater levels of $E_{\mathrm{d}}(490, z)$ than what was recorded at $z_{\min}$. Based on the

relationship that NPQ increases with increasing $E_{\mathrm{d}}(490, z)$ (see Figure 3.2 in Section 3.1), it can therefore be assumed that any phytoplankton present in that layer would be experiencing higher levels NPQ. It can therefore be concluded that any error in our estimates of NPQ would be systematic underestimates of the full degree of NPQ experienced by phytoplankton just below the surface in a given profile.

Variability in the light field of the water column that is unrelated to the physiological state of the phytoplankton is another source of error in the optical calculations made during this thesis. This has already been addressed in one respect in earlier chapters as it pertains to transient sunny and cloudy periods during an $A(z)$ vs. $C(z)$ profile affecting values of $E_{\mathrm{d}}(490,0)$. However an additional case of this would be fluctuations in the near-surface light field due to the focusing/diverging effect of surface waves (Zaneveld et al. 2001). Even in calm conditions, surface waves cause "bright" and "dark" patterns in the underlying water column as the wave patterns either amplify or interfere with each other. The noise in measurements of $E_{\mathrm{d}}(490, z)$ from this phenomenon can result in profiles with an irradiance maximum at several meters depth (rather than at the surface; Zaneveld et al. 2001). This is likely the cause of the abnormally low $A(z)$ data points near the surface of some profiles that had to be removed during Level 2 processing (Section 2.2.2), and might even be a source of variability in $F(i, \zeta)$ estimates if the effect was dramatic enough to alter the shape of the $A(z)$ vs. $C(z)$ profile over that interval.

Variability in the readings of the sensors themselves is another source of potential error, and one that was not explicitly examined in this thesis. Electronic instrumentation, including optical instrumentation, is often sensitive to changes in temperature and pressure (Roesler and Boss 2008), which can be detected by tracking changes in the background/dark counts of an instrument during calibration (Proctor and Roesler 2010). The fluorometers in this study rely on an LED (Light Emitting Diode) light source, which is known to have variable output and stability over the lifetime of the bulb (Moe et al. 2005), which influences the estimate of $Chla$ from $fluor$ as it violates the assumption of a constant light source (see Section 1.3.1). Biofouling, the growth of organic material on a sensor over the course of a deployment, can also cause a gradual drifting in an optical signal, requiring cleaning, preventative measures, or post-deployment processing to

correct for any bias caused by the growth (Davis et al. 1997; Lehaitre et al. 2008; Roesler and Boss 2008), although signs of biofouling were not observed on the gliders used in this study. Another issue pertains to measurements of $E_{\mathrm{d}}(\lambda, z)$ and it arises when the physical orientation of the sensor is considered. Due to the cosine effect, where $E_{\mathrm{d}}(\lambda, z)$ measured on a flat plane decreases as a function of the cosine of the average angle of incoming light (Mobley 1994; Berwald et al. 1995; Kirk 2011), any tilting of the sensor could result in fluctuations in the measured values of $E_{\mathrm{d}}(490, z)$. This can be further complicated by changes in sea state causing large volumes of bubbles and other optically-complex surface conditions causing changes in $E_{\mathrm{d}}(\lambda, 0)$ (Roesler and Boss 2008). All of the above conditions could have affected the bio-optical measurements used in this thesis, contributing to noise and variability in the instrument signals, however their effects were not explicitly quantified.

4.6 *F*-factor Implementation Recommendations

One of the main objectives of this thesis was to provide a recommendation to the Ocean Tracking Network for the implementation of a dynamic $fluor$-to-$Chla$ conversion factor capable of accounting for taxonomic and physiological changes in the phytoplankton assemblage for use with autonomous glider platforms operating on the Scotian Shelf in the absence of traditional validation methods. Given the results of the analyses presented in this thesis, the following suggestions are presented for the future use of the X11-based calibration methodology, both in the context of Slocum Gliders on the Scotian shelf as well as more generally wherever the X11 methodology may be implemented:

1. In any Case 1 waters where the X11 methodology would routinely be applied (for example with ARGO buoys, the platform for which the method was originally developed), the BC15 $F(i)$ modifications to the method suggested in this thesis pertaining to the bi-directional outlier correction utilising the 90% prediction interval should be incorporated. Although the error are relatively small, the biases introduced by the overly strict, unidirectional X11 outlier criteria should, and can, be rectified.

2. The use of a cubic fit to retain depth-dependent variability in the $A(z)$ vs. $C(z)$ relationship should be evaluated on a per-dataset basis and not blindly incorporated. The cubic fit was chosen for this dataset based on the study's objectives, but there is no assurance that this trend is universal. Additionally, the X11 assumption of a uniform *F*-factor with depth has been supported by the findings in this thesis. The results showed that variability in the median *F*-factor with depth did not exceed ±12%, implying that depth-dependent variability can potentially be ignored without severely compromising the overall accuracy of the $Chla$ estimate and therefore the use of a cubic fit to retain depth-dependent information may be unnecessary.
3. Due to the large variability that arises when applying *F*-factors on a per-optical depth basis (on the order of several hundred percent) it is not recommended that a per-optical depth *F*-factor be implemented in the method's current form. This issue could potentially be revisited in future research if refinements are made to the underlying bio-optical models.
4. There were difficulties in applying the modified X11 method when specifically considering gliders operating on the Scotian Shelf. Since the gliders dive at a rate that can generate multiple profiles per hour (in contrast to a single profile every ~10 days as in the X11 study), applying a per-profile *F*-factor could cause artificial between-profile discontinuities due to the high frequency with which the *F*-factor would change. Without a more comprehensive *in situ* validation regime in place the degree to which this is a problem could not be discerned in this work, but the decorrelation scale of the *F*-factor with distance from shore is something that should be investigated before the X11 method is implemented on a sampling platform that conducts profiles as frequently as a Slocum glider. Additionally the glider traverses through both Case 1 and Case 2 waters, and in its current form the method for removing the influence of $\mathrm{CDOM_{adj}}$: $Chla$ on the *F*-factor is not refined enough to provide reliable post-correction *F*-factor values. The optical relationships relating $fluor$ to $Chla$ were overwhelmed by the non-covarying CDOM component, and future work will have to be done to determine a quantitative correction for the influence of $\mathrm{CDOM_{adj}}$: $Chla$ on *F*-

factors before this method can reliably be applied to transects that contain Case 2 waters. A per-profile correction may eventually be possible once the $CDOM_{adj}$:$Chla$ relationship has been accounted for, however a more thorough investigation is required than was conducted here, with a considerably more robust coincident water sample regime in order to validate the on-site measurements, before that correction should be trusted.

There are many avenues of future research mentioned above with the potential to resolve the complicated relationships revealed in the body of this thesis, and it should be emphasised that some of the aforementioned difficulties could be resolved with relatively minor alterations to the methodology. However given the sum of the uncertainties outlined above, as they pertain to the implementation of a per-profile *F*-factor, it is not recommended that the X11 method, *in its current form*, be implemented for use with OTN gliders on the Scotian Shelf. Until such a time as these uncertainties can be more thoroughly investigated, the manufacturer's static *F*-factor is the most reliable option for the automated conversion of $fluor$ to $Chla$ for Slocum gliders operating on the Scotian Shelf.

CHAPTER 5 CONCLUSION

The overall objective of this thesis was to investigate an optics-based approach for estimating chlorophyll *a* concentration using ocean gliders. This was accomplished through the application and modification of an established bio-optical method for increasing the accuracy of optics-based estimates of $Chla$ by complementing chlorophyll *a* fluorescence measurements with measurements of downwelling irradiance via the diffuse attenuation coefficient, applied on a per-sampling-profile basis (Xing et al. 2011; X11). This method generated $fluor$-to-$Chla$ conversion factors (*F*-factors) capable of accounting for taxonomic and physiological changes in the phytoplankton assemblage in the absence of traditional validation methods. Modifications were made in order to correct for biases in the original method, allowing for a more robust treatment of outliers within the relationship as well as for the retention, and subsequent analysis, of depth-resolved information in the *F*-factor relationship. Trends in *F*-factor versus distance from shore, and versus depth, were explored for 12 glider transects conducted over a period of 3 years. The underlying causes of the trends were investigated and their influences on the calculation of the *F*-factor analysed.

Several issues were identified and addressed with modifications to the method. First, the fluorescence data were corrected for NPQ effects to prevent inaccuracies in the $A(z)$ vs. $C(z)$ relationship using a different methodology than what was used by X11. By utilising the methodology of Sackmann et al. (2008), the effects of NPQ could be scaled to particle abundance (as a proxy for phytoplankton abundance) through the incorporation of particulate backscattering measurements. This analysis determined a significant relationship between NPQ and $E_{\mathrm{d}}(490)$ at z_{min}, with NPQ corrections of up to 90% in some profiles. A limitation to the correction was determined, where shallow mixed layer depths could result in underestimates of the NPQ effect. Second, the criteria for detecting and removing outliers from $A(z)$ vs. $C(z)$ profiles was modified, allowing for a more robust determination of outliers from the general trend as well as allowing for the retention, and subsequent analysis, of depth-dependent information in the profile. This was accomplished by replacing the linear fit used by X11 to detect outliers with a cubic fit, by increasing the amount of variability around the fit tolerated by the outlier-

removal method by using the 90% prediction intervals around the fit, and finally by changing the uni-directional outlier limitation of the X11 method to a bi-directional one that was applicable on both sides of the fit.

Horizontal patterns in the *F*-factor across the Scotian Shelf, typically of a negative slope with distance from shore, were predominantly influenced by concentrations of CDOM varying independently of concentrations of $Chla$ in near-shore regions of the study area. The *F*-factor was consistently overestimated when $CDOM_{adj}$:$Chla$ was high. When this relationship was accounted for, through the investigation of the residual *F*-factors around the *F*-factor versus $CDOM_{adj}$:$Chla$ relationship, the horizontal trend with distance was removed. However the residuals around the corrected relationship were of a sufficient magnitude to prevent a profile-by-profile quantitative correction for the *F*-factor when in CDOM-influenced Case 2 waters.

Vertical trends in the *F*-factor, delineated by optical depth in the water column with larger *F*-factors in the shallowest and deepest portions of the euphotic zone of the upper water column, were predominantly influenced by some combination of the $fluor$ to $Chla$ relationship and the K_{bio} to $Chla$ relationship – it is not possible to separate the individual influences of these two relationships with this method. Adjusting for the effect of $CDOM_{adj}$:$Chla$ on the depth-resolved *F*-factors did not eliminate the trend with optical depth, although it did have a small influence on the lowest (5^{th}) optical depth due to high deep-water CDOM concentrations relative to *fluor*. Despite the qualitative trend observable in the depth-resolved *F*-factors, which can be useful as a diagnostic tool for general changes in the bio-optical properties of the phytoplankton community with depth, the magnitude of the variability around the central trend made a depth-resolved application of *F*-factors within a profile impractical.

As a final recommendation, the X11 method, even with the modifications presented in this thesis, should not be implemented on Slocum gliders operating on the Scotian Shelf. There is potential for the method if a more rigorous investigation of the variability underlying the *F*-factor relationship can be conducted, assuming that any investigation has a program in place to obtain similarly rigorous *in situ* validation of the data. Until such a time as these relationships can be more thoroughly investigated, however, the

manufacturer's static F-factor is the most reliable option for the automated conversion of $fluor$ to $Chla$ for Slocum gliders operating on the Scotian Shelf.

APPENDIX A DATA TABLES

Table A.1. Per-transect median $F(i)$ values calculated using the X11 method, as well as associated interquartile ranges (IQR). The manufacturer's *F*-factor was 0.0117 mg Chla $m^{-3}count^{-1}$ for missions through to 2013-06-06, and 0.0121 for the remainder. The percent difference between the two *F*-factor estimates is listed. Note that the X11 method provides median values similar to the manufacturer's calibration (± 20%).

Mission Date	*Direction*	*Profile Count (n)*	*Median Per-Leg X11 F(i)*	*IQR*	*Percent Difference*
Mission #1	Out	325	0.0121	0.0031	3.41
(2011-07-26)	In	190	0.0123	0.0038	4.75
Missions #2	Out	161	0.0110	0.0031	-6.21
(2012-05-02)	In	166	0.0118	0.0034	0.53
Mission #3	Out	220	0.0101	0.0029	-13.49
(2012-05-24)	In	135	0.0113	0.0035	-3.38
Mission #4	Out	228	0.0097	0.0023	-17.23
(2012-06-12)	In	410	0.0111	0.0020	-4.79
Mission #5	Out	241	0.0117	0.0029	-0.35
(2012-07-11)	In	249	0.0117	0.0023	0.36
Mission #6	Out	200	0.0118	0.0077	1.12
(2013-03-11)	In	138	0.0117	0.0036	0.15
Mission #7	Out	349	0.0096	0.0023	-18.11
(2013-03-29)	In	177	0.0113	0.0037	-3.76
Mission #8	Out	218	0.0100	0.0034	-14.79
(2013-05-03)	In	226	0.0114	0.0031	-2.39
Mission #9	Out	243	0.0100	0.0025	-14.96
(2013-06-06)	In	264	0.0113	0.0025	-3.39
Mission #10	Out	223	0.0100	0.0026	-17.65
(2013-09-16)	In	247	0.0116	0.0035	-4.19
Mission #11	Out	229	0.0110	0.0082	-9.26
(2013-11-06)	In	145	0.0122	0.0036	1.06
Mission #12	Out	187	0.0104	0.0059	-13.66
(2013-12-02)	In	194	0.0123	0.0063	1.74

Table A.2. Linear regression results for X11 $F(i)$ plotted as a function of distance from shore. One slope was calculated for each of two transects for the mission. All regressions were significant at $p < 0.05$ except for Missions 2012-06-12 and 2012-07-11. Transects marked with an asterisk had non-linear trends with distance and should be interpreted with caution as they violate underlying assumptions of linear regression.

Mission Date	***Direction***	***Profile Count (n)***	***Slope ± 95% CI (mg Chla m^{-3} $count^{-1}$ km^{-1})***	***Y-int. ± 95% CI (mg Chla m^{-3} $count^{-1}$)***	***r^2***
Mission #1	Out	325	$-1.61 \times 10^{-5} \pm 3.94 \times 10^{-6}$	0.0144 ± 0.0005	0.1659
(2011-07-26)	In	190	$-5.26 \times 10^{-5} \pm 7.02 \times 10^{-6}$	0.0207 ± 0.0010	0.5372
Missions #2	Out	161	$-2.24 \times 10^{-5} \pm 9.49 \times 10^{-6}$	0.0137 ± 0.0010	0.1206
(2012-05-02)	In	166	$-3.00 \times 10^{-5} \pm 8.85 \times 10^{-6}$	0.0147 ± 0.0010	0.2141
Mission #3	Out	220	$-3.29 \times 10^{-5} \pm 6.90 \times 10^{-6}$	0.0138 ± 0.0008	0.2881
(2012-05-24)	In	135	$1.21 \times 10^{-5} \pm 5.66 \times 10^{-6}$	0.0076 ± 0.0008	0.1183
Mission #4	Out	228	$-2.10 \times 10^{-6} \pm 3.81 \times 10^{-6}$	0.0100 ± 0.0005	0.0052
(2012-06-12)	In	410	$-6.71 \times 10^{-6} \pm 7.92 \times 10^{-6}$	0.0128 ± 0.0011	0.0067
Mission #5	Out	241	$-2.18 \times 10^{-6} \pm 4.92 \times 10^{-6}$	0.0131 ± 0.0007	0.0032
(2012-07-11)	In	249	$-9.52 \times 10^{-7} \pm 4.26 \times 10^{-6}$	0.0126 ± 0.0006	0.0008
Mission #6	*Out	200	$-6.03 \times 10^{-4} \pm 9.19 \times 10^{-5}$	0.0855 ± 0.0090	0.4581
(2013-03-11)	*In	138	$-2.16 \times 10^{-4} \pm 3.08 \times 10^{-5}$	0.0370 ± 0.0028	0.5849
Mission #7	*Out	349	$-1.52 \times 10^{-4} \pm 1.43 \times 10^{-5}$	0.0321 ± 0.0019	0.5548
(2013-03-29)	In	177	$-4.80 \times 10^{-5} \pm 4.91 \times 10^{-6}$	0.0169 ± 0.0007	0.6796
Mission #8	*Out	218	$-2.53 \times 10^{-4} \pm 9.26 \times 10^{-5}$	0.0525 ± 0.0125	0.1182
(2013-05-03)	In	226	$-3.45 \times 10^{-5} \pm 5.69 \times 10^{-6}$	0.0161 ± 0.0008	0.3895
Mission #9	Out	243	$-2.88 \times 10^{-5} \pm 4.33 \times 10^{-6}$	0.0151 ± 0.0006	0.4170
(2013-06-06)	In	264	$-1.73 \times 10^{-5} \pm 3.70 \times 10^{-6}$	0.0135 ± 0.0005	0.2442
Mission #10	Out	223	$-2.37 \times 10^{-5} \pm 4.01 \times 10^{-6}$	0.0132 ± 0.0005	0.3800
(2013-09-16)	In	247	$-3.92 \times 10^{-5} \pm 5.25 \times 10^{-6}$	0.0161 ± 0.0007	0.4693
Mission #11	Out	229	$-7.89 \times 10^{-5} \pm 6.71 \times 10^{-6}$	0.0223 ± 0.0007	0.7035
(2013-11-06)	In	145	$-9.45 \times 10^{-5} \pm 9.60 \times 10^{-6}$	0.0245 ± 0.0011	0.7258
Mission #12	*Out	187	$-1.90 \times 10^{-4} \pm 4.07 \times 10^{-5}$	0.0364 ± 0.0041	0.3152
(2013-12-02)	*In	194	$-1.78 \times 10^{-4} \pm 2.26 \times 10^{-5}$	0.0354 ± 0.0024	0.5559

Table A.3. Linear regression results for the BC15 $F(i)$ vs. $\mathrm{CDOM}_{\mathrm{adj}}|_{z_{\max}}^{z_{\min}} : Chla|_{z_{\max}}^{z_{\min}}$ relationship. For the regression equation, slopes have units of $(\mathrm{mg\ Chla\ m^{-3}})^2 \cdot (\mathrm{count} \cdot \mathrm{ppb})$ and y-intercepts have units of $\mathrm{mg\ Chl\ m^{-3}\ count^{-1}}$. Results with an asterisk should be interpreted with caution as some underlying assumptions of regression were violated.

Mission Date	*Profiles (n)*	*Regression Equation*	r^2	*p*
Mission #1 (2011-07-26)	*515	y = 0.0019x + 0.0106	0.17	*
Missions #2 (2012-05-02)	*327	y = 0.0036x + 0.0084	0.43	*
Mission #3 (2012-05-24)	*355	y = 0.0030x + 0.0069	0.26	*
Mission #4 (2012-06-12)	*638	y = 0.0024x + 0.0076	0.06	*
Mission #5 (2012-07-11)	490	y = 0.0006x + 0.0117	0.02	< 0.01
Mission #6 (2013-03-11)	*338	y = 0.0169x – 0.0013	0.79	*
Mission #7 (2013-03-29)	*526	y = 0.0071x + 0.0081	0.90	*
Mission #8 (2013-05-03)	*441	y = 0.0037x + 0.0077	0.82	*
Mission #9 (2013-06-06)	507	y = 0.0017x + 0.0089	0.60	< 0.01
Mission #10 (2013-09-16)	470	y = 0.0045x + 0.0038	0.50	< 0.01
Mission #11 (2013-11-06)	*374	y = 0.0063x + 0.0069	0.60	*
Mission #12 (2013-12-02)	*381	y = 0.0089x + 0.0071	0.57	*

Table A.4. Linear regression results, including slopes (mg Chl m^{-3} $count^{-1}$ km^{-1}) and y-intercepts (mg Chl m^{-3} $count^{-1}$) of the BC15 $F(i)$ versus distance from shore relationship. Transects marked with † had slopes that were not significantly different from zero at alpha = 0.05 (n = 4 transects). Transects marked with an asterisk should be interpreted with caution as they violate underlying assumptions of linear regression.

Mission Date	***Direction***	***Profiles (n)***	***BC15 $F(i)$ vs. Distance***	***r^2***	***p***
Mission #1	Out	325	$y = -1.56x10^{-5}x + 0.0146$	0.15	< 0.01
(2011-07-26)	In	190	$y = -5.20x10^{-5}x + 0.0209$	0.56	< 0.01
Missions #2	Out	161	$y = -2.50x10^{-5}x + 0.0146$	0.11	< 0.01
(2012-05-02)	In	166	$y = -1.75x10^{-5}x + 0.0134$	0.11	< 0.01
Mission #3	Out	220	$y = -2.49x10^{-5}x + 0.0133$	0.22	< 0.01
(2012-05-24)	†In	135	$y = 3.55x10^{-6}x + 0.0090$	0.01	0.22
Mission #4	†Out	228	$y = 7.90x10^{-7}x + 0.0098$	0.00	0.67
(2012-06-12)	In	410	$y = -4.73x10^{-6}x + 0.0126$	0.01	0.04
Mission #5	†Out	241	$y = -7.75x10^{-7}x + 0.0130$	0.00	0.75
(2012-07-11)	†In	249	$y = -2.01x10^{-6}x + 0.0129$	0.00	0.33
Mission #6	*Out	200	$y = -6.20x10^{-4}x + 0.0877$	0.45	*
(2013-03-11)	*In	138	$y = -2.20x10^{-4}x + 0.0380$	0.54	*
Mission #7	*Out	349	$y = -1.30x10^{-4}x + 0.0297$	0.56	*
(2013-03-29)	In	177	$y = -3.62x10^{-5}x + 0.0156$	0.65	< 0.01
Mission #8	*Out	218	$y = -1.50x10^{-4}x + 0.0366$	0.55	*
(2013-05-03)	In	226	$y = -2.91x10^{-5}x + 0.0163$	0.30	< 0.01
Mission #9	Out	243	$y = -2.57x10^{-5}x + 0.0154$	0.39	< 0.01
(2013-06-06)	In	264	$y = -1.62x10^{-5}x + 0.0136$	0.25	< 0.01
Mission #10	Out	223	$y = -2.16x10^{-5}x + 0.0134$	0.38	< 0.01
(2013-09-16)	In	247	$y = -4.07x10^{-5}x + 0.0167$	0.44	< 0.01
Mission #11	Out	229	$y = -7.33x10^{-5}x + 0.0224$	0.73	< 0.01
(2013-11-06)	In	145	$y = -9.17x10^{-5}x + 0.0247$	0.72	< 0.01
Mission #12	*Out	187	$y = -1.90x10^{-4}x + 0.0373$	0.47	*
(2013-12-02)	*In	194	$y = -1.80x10^{-4}x + 0.0360$	0.56	*

Table A.5. Linear regression results, including slopes (mg Chl m^{-3} $count^{-1}$ km^{-1}) and y-intercepts (mg Chl m^{-3} $count^{-1}$) of the BC15 $F(i)$ residual values versus distance from shore relationship (residuals from BC15 $F(i)$ vs. $\mathrm{CDOM_{adj}}|_{z_{max}}^{z_{min}}$: $Chla|_{z_{max}}^{z_{min}}$ relationship). Transects marked with † had slopes that were not significantly different from zero at alpha = 0.05 (n = 11 transects). Removing the influence of $\mathrm{CDOM_{adj}}|_{z_{max}}^{z_{min}}$: $Chla|_{z_{max}}^{z_{min}}$ on BC15 $F(i)$ caused a reduction of at least an order of magnitude of the trend versus distance for these missions. Results with an asterisk should be interpreted with caution as some underlying assumptions of regression were violated.

Mission Date	***Direction***	***Profiles (n)***	***BC15 $F(i)$ Residuals vs. Distance***	***r^2***	***p***
Mission #1	Out	325	$y = -6.40\times10^{-6}x + 0.0004$	0.02	0.01
(2011-07-26)	In	190	$y = -3.34\times10^{-5}x + 0.0048$	0.34	< 0.01
Missions #2	†Out	161	$y = -4.72\times10^{-6}x + 0.0005$	0.01	0.24
(2012-05-02)	†In	166	$y = -8.74\times10^{-7}x - 0.0000$	0.00	0.81
Mission #3	†Out	220	$y = -5.67\times10^{-6}x + 0.0008$	0.02	0.06
(2012-05-24)	In	135	$y = 1.85\times10^{-5}x - 0.0028$	0.23	< 0.01
Mission #4	Out	228	$y = 1.34\times10^{-5}x - 0.0027$	0.22	< 0.01
(2012-06-12)	†In	410	$y = 7.04\times10^{-6}x - 0.0002$	0.01	0.07
Mission #5	†Out	241	$y = 3.35\times10^{-6}x - 0.0003$	0.01	0.17
(2012-07-11)	†In	249	$y = -8.21\times10^{-7}x + 0.0000$	0.00	0.69
Mission #6	*†Out	200	$y = 4.10\times10^{-5}x - 0.0006$	0.01	*
(2013-03-11)	*In	138	$y = 1.96\times10^{-4}x - 0.0187$	0.64	*
Mission #7	*†Out	349	$y = 1.97\times10^{-6}x - 0.0006$	0.00	*
(2013-03-29)	In	177	$y = -7.97\times10^{-6}x + 0.0016$	0.12	< 0.01
Mission #8	*†Out	218	$y = 5.23\times10^{-6}x - 0.0006$	0.00	*
(2013-05-03)	In	226	$y = 1.69\times10^{-5}x - 0.0020$	0.20	< 0.01
Mission #9	†Out	243	$y = 2.34\times10^{-6}x - 0.0003$	0.01	0.15
(2013-06-06)	In	264	$y = 2.83\times10^{-6}x - 0.0004$	0.02	0.04
Mission #10	†Out	223	$y = 8.54\times10^{-7}x - 0.0002$	0.00	0.71
(2013-09-16)	In	247	$y = -2.22\times10^{-5}x + 0.0025$	0.33	< 0.01
Mission #11	*Out	229	$y = -3.41\times10^{-5}x + 0.0037$	0.30	*
(2013-11-06)	In	145	$y = -1.38\times10^{-5}x + 0.0003$	0.09	< 0.01
Mission #12	*Out	187	$y = -5.87\times10^{-5}x + 0.0074$	0.09	*
(2013-12-02)	*In	194	$y = 5.82\times10^{-5}x - 0.0079$	0.25	*

Table A.6. Water samples collected with glider deployments (n = 39 samples, over 14 different days), used to determine $Chla$ at depth ("*Chla Extracted*"; mg Chla m^{-3}). At each depth sampled a $Chla$ estimate was generated using each of four F-factors – the manufacturer's, X11 $F(i)$, BC15 $F(i)$ and BC15 $F(i,\zeta)$. The accuracy of these estimates was expressed as a percent-difference from the average $Chla$ Extracted value.

Mission Date	*Depth*	*Chla Extracted*	*Man. F. % Diff.*	*X11 F(i) % Diff.*	*BC15 F(i) % Diff.*	*BC15 F(i,ζ) % Diff.*
2012-05-02	1	1.56	24.6	-1.6	21.8	-15.5
	10	1.06	96.9	55.5	92.5	33.5
	20	1.52	67.4	32.3	63.7	32.0
2012-05-24	1	0.32	-14.5	16.6	3.9	173.9
	10	0.45	-14.3	17.0	4.2	174.8
	20	1.84	-23.6	4.3	-7.1	-9.0
2012-06-12	1	0.26	195.8	157.7	225.1	113.9
	10	0.36	106.3	79.7	126.8	49.2
2012-07-11	1	1.43	-77.4	-71.4	-71.3	-55.5
	10	0.44	19.5	51.6	51.9	135.5
	20	0.57	176.4	250.8	251.6	221.2
2013-03-11	1	0.48	-43.4	839.6	145.9	975.8
	10	0.47	-24.7	1123.1	227.3	1171.6
	30	0.39	-19.3	1207.3	250.5	1670.2
2013-03-25	1	0.76	-64.6	58.9	53.9	97.5
	10	0.90	-32.3	203.8	194.1	158.9
2013-03-29	1	0.44	-61.6	69.3	-40.0	97.9
	20	0.40	37.6	506.3	114.9	339.0
2013-04-18	1	1.44	-85.0	-64.9	-76.5	-30.5
	10	2.12	-83.5	-47.8	-74.2	3.4
	30	4.11	-40.8	0.7	-7.5	5.1
2013-05-21	1	0.44	-38.2	14.2	-1.6	29.4
	10	0.50	26.3	92.2	101.1	117.8
	30	0.32	87.5	180.6	198.6	224.5
2013-06-06	1	0.68	-67.2	-66.0	-60.5	-49.2
	10	0.23	-30.3	-15.8	-15.9	26.1
	30	0.29	133.9	189.8	181.9	150.0
2013-06-27	1	0.49	87.9	98.8	126.5	143.0
	20	0.40	101.2	161.0	142.5	102.2
	40	0.50	-57.6	-46.4	-48.9	43.5
2013-09-16	1	0.64	19.2	10.8	91.7	76.6
	10	0.59	83.1	70.2	194.4	171.2
	30	0.16	207.6	185.9	394.5	694.9
2013-10-10	1	0.57	150.1	246.4	302.1	246.7
	10	0.62	190.0	304.9	366.1	359.2
	20	0.70	140.2	239.9	286.1	309.3
2013-11-22	1	0.58	113.2	347.0	384.7	326.0
	5	0.58	109.4	372.4	376.1	350.3
	30	0.63	50.7	265.1	242.7	237.9

BIBLIOGRAPHY

Adir, N., H. Zer, S. Shochat, and I. Ohad. 2003. Photoinhibition – a historical perspective. Photosynth. Res. **76**: 343–370.

Agawin, N. S. R., C. M. Duarte, and S. Agusti. 2000. Nutrient and temperature control of the contribution of picoplankton to phytoplankton biomass and production. Limnol. Oceanogr. **45**: 591–600.

Ahn, Y.-H., A. Bricaud, and A. Morel. 1992. Light backscattering efficiency and related properties of some phytoplankters. Deep. Res. **39**: 1835–1855.

Babin, M., A. Morel, H. Claustre, A. Bricaud, Z. Kolber, and P. G. Falkowski. 1996a. Nitrogen- and irradiance-dependent variations of the maximum quantum yield of carbon fixation in eutrophic, mesotrophic and oligotrophic marine systems. Deep. Res. I **43**: 1241–1272.

Babin, M., A. Morel, and B. Gentili. 1996b. Remote sensing of sea surface Sun-induced chlorophyll fluorescence: consequences of natural variations in the optical characteristics of phytoplankton and the quantum yield of chlorophyll a fluorescence. Int. J. Remote Sens. **17**: 2417–2448.

Baker, K. S., and R. C. Smith. 1982. Bio-optical classification and model of natural waters. 2. Limnol. Oceanogr. **27**: 500–509.

Banse, K. 1977. Determining the carbon-to-chlorophyll ratio of natural phytoplankton. Mar. Biol. **41**: 199–212.

Banse, K. 2004. Should we continue to use the 1% light depth convention for estimating the compensation depth of phytoplankton for another 70 years? Limnol. Oceanogr. Bull. **13**: 49–52.

Behrenfeld, M. J., J. T. Randerson, C. R. Mcclain, G. C. Feldman, S. O. Los, C. J. Tucker, P. G. Falkowski, C. B. Field, R. Frouin, W. E. Esaias, D. D. Kolber, and N. H. Pollack. 2001. Biospheric primary production during an ENSO transition. Science. **291**: 2594–2597.

Berwald, J., D. Stramski, C. D. Mobley, and D. A. Kiefer. 1995. Influences of absorption and scattering on the vertical changes in the average cosine of underwater light field. Limnol. Oceanogr. **40**: 1347–1357.

Boss, E., and W. S. Pegau. 2001. Relationship of light scattering at an angle in the backward direction to the backscattering coefficient. Appl. Opt. **40**: 5503–5507.

Boss, E., D. Stramski, T. Bergmann, S. Pegau, and M. Lewis. 2004. Why should we measure the optical backscattering coefficient? Oceanography **17**: 44–49.

Boss, E., D. Swift, L. Taylor, P. Brickley, R. Zaneveld, S. Riser, M. J. Perry, and P. G. Strutton. 2008. Observations of pigment and particle distributions in the western North Atlantic from an autonomous float and ocean color satellite. Limnol. Oceanogr. **53**: 2112–2122.

Bot, P. V. M., and F. Colijn. 1996. A method for estimating primary production from chlorophyll concentrations with results showing trends in the Irish Sea and the Dutch coastal zone. ICES J. Mar. Sci. **53**: 945–950.

Boyce, D. G., M. R. Lewis, and B. Worm. 2010. Global phytoplankton decline over the past century. Nature **466**: 591–596.

Bricaud, A., M. Babin, A. Morel, and H. Claustre. 1995. Variability in the chlorophyll-specific absorption coefficients of natural phytoplankton: Analysis and parameterization. J. Geophys. Res. **100**: 13321–13332.

Bricaud, A., A. Morel, M. Babin, K. Allali, and H. Claustre. 1998. Variations of light absorption by suspended particles with chlorophyll a concentration in oceanic (case 1) waters: Analysis and implications for bio-optical models. J. Geophys. Res. **103**: 31033–31044.

Brown, C. A., Y. Huot, M. J. Purcell, J. J. Cullen, and M. R. Lewis. 2004. Mapping coastal optical and biogeochemical variability using an Autonomous Underwater Vehicle (AUV) and a new bio-optical inversion algorithm. Limnol. Oceanogr. Methods **2**: 262–281.

Buck, K. R., F. P. Chavez, and L. Campbell. 1996. Basin-wide distributions of living carbon components and the inverted trophic pyramid of the central gyre of the North Atlantic Ocean, summer 1993. Aquat. Microb. Ecol. **10**: 283–298.

Bukata, R., J. Campbell, R. Doerffer, M. Dowell, H. Gordon, N. Hoepffner, C. Hu, J. Kirk, M. Kishino, O. Kopelevich, H. Krawczyk, A. Neumann, S. Sathyendranath, P. Schlittenhardt, and A. Tanaka. 2000. Reports of the International Ocean-Colour Coordinating Group, IOCCG Report Number 3: Remote sensing of ocean colour in coastal, and other optically-complex, waters. 43p.

Cetinić, I., G. Toro-Farmer, M. Ragan, C. Oberg, and B. H. Jones. 2009. Calibration procedure for Slocum glider deployed optical instruments. Opt. Express **17**: 15420–15430.

Ciotti, Á. M., J. J. Cullen, and M. R. Lewis. 1999. A semi-analytical model of the influence of phytoplankton community structure on the relationship between light attenuation and ocean color. J. Geophys. Res. **104**: 1559–1578.

Cleveland, J. S. 1995. Regional models for phytoplankton absorption as a function of chlorophyll a concentration. J. Geophys. Res. **100**: 13333–13344.

Cleveland, J. S., and M. J. Perry. 1987. Quantum yield, relative specific absorption and fluorescence in nitrogen limited, Chaetoceros gracilis. Mar. Biol. **94**: 489–497.

Cloern, J. E., C. Grenz, and L. Vidergar-Lucas. 1995. An empirical model of the phytoplankton chlorophyll:carbon ratio - the conversion factor between productivity and growth rate. Limnol. Oceanogr. **40**: 1313–1321.

Cullen, J. J. 1982. The Deep Chlorophyll Maximum: Comparing Vertical Profiles of Chlorophyll a. Can. J. Fish. Aquat. Sci. **39**: 791–803.

Cullen, J. J. 2015. Subsurface Chlorophyll Maximum Layers: Enduring Enigma or Mystery Solved? Ann. Rev. Mar. Sci. **7**: 207–239.

Cullen, J. J., and R. F. Davis. 2002. Optical measurements in oceanography: when the blank makes the difference. *Ocean Optics XVI*. 11p.

Cullen, J. J., and R. F. Davis. 2003. The blank can make a big difference in oceanographic measurements. Limnol. Oceanogr. Bull. **12**: 29–35.

Cullen, J. J., and M. R. Lewis. 1988. The kinetics of algal photoadaptation in the context of vertical mixing. J. Plankton Res. **10**: 1039–1063.

Cullen, J. J., and M. R. Lewis. 1995. Biological processes and optical measurements near the sea surface: some issues relevant to remote sensing. J. Geophys. Res. **100**: 13255–13266.

Davis, R. F., C. C. Moore, J. R. V. Zaneveld, and J. M. Napp. 1997. Reducing the effects of fouling on chlorophyll estimates derived from long-term deployments of optical instruments. J. Geophys. Res. **102**: 5851–5855.

Demers, S., S. Roy, R. Gagnon, and C. Vignault. 1991. Rapid light-induced changes in cell fluorescence and in xanthophyll-cycle pigments of Alexandrium excavatum (Dinophyceae) and Thalassiosira pseudonana (Bacillariophyceae): a photo-protection mechanism. Mar. Ecol. Prog. Ser. **76**: 185–193.

Demmig-Adams, B., and W. W. Adams. 1996. The role of xanthophyll cycle carotenoids in the protection of photosynthesis. Trends Plant Sci. **1**: 21–26.

Derenbach, J., H. Astheimer, H. Hansen, and H. Leach. 1979. Vertical Microscale Distribution of Phytoplankton in Relation to the Thermocline . Mar. Ecol. Prog. Ser. **1**: 187–193.

Dickey, T. D. 1991. The emergence of concurrent high-resolution physical and bio-optical measurements in the upper ocean and their applications. Rev. Geophys. **29**: 383–413.

Dickey, T. D., and R. R. Bidigare. 2005. Interdisciplinary oceanographic observations: the wave of the future. Sci. Mar. **69**: 23–42.

Dickey, T. D., E. C. Itsweire, M. Moline, and M. J. Perry. 2008. Introduction to the Limnology and Oceanography special issue on Autonomous and Lagrangian Platforms and Sensors (ALPS). Limnol. Oceanogr. **53**: 2057–2061.

Dickey, T., M. Lewis, and G. Chang. 2006. Optical Oceanography: recent advances and future directions using global remote sensing and in situ observations. Rev. Geophys. **44**: 39p.

Eppley, R. W. 1972. Temperature and phytoplankton growth in the sea. Fish. Bull. **70**: 1063–1085.

Eppley, R. W., F. P. Chavez, and R. T. Barber. 1992. Standing stocks of particulate carbon and nitrogen in the equatorial Pacific at 150°W. J. Geophys. Res. **97**: 655.

Eriksen, C. C., T. J. Osse, R. D. Light, T. Wen, T. W. Lehman, P. L. Sabin, J. W. Ballard, and A. M. Chiodi. 2001. Seaglider: a long-range autonomous underwater vehicle for oceanographic research. IEEE J. Ocean. Eng. **26**: 424–436.

Falkowski, P. G., and D. A. Kiefer. 1985. Chlorophyll a fluorescence in phytopankton: relationship to photosynthesis and biomass. J. Plankt. Res. **7**: 715–731.

Feder, T. 2000. Argo begins systematic global probing of the upper oceans. Phys. Today **53**: 50–51.

Fennel, K., and E. Boss. 2003. Subsurface maxima of phytoplankton and chlorophyll: Steady-state solutions from a simple model. Limnol. Oceanogr. **48**: 1521–1534.

Ferrari, G. M., and M. D. Dowell. 1998. CDOM absorption characteristics with relation to fluorescence and salinity in coastal areas of the Southern Baltic Sea. Estuar. Coast. Shelf Sci. **47**: 91–105.

Finkel, Z. V. 2001. Light absorption and size scaling of light-limited metabolism in marine diatoms. Limnol. Oceanogr. **46**: 86–94.

Foden, J., D. B. Sivyer, D. K. Mills, and M. J. Devlin. 2008. Spatial and temporal distribution of chromophoric dissolved organic matter (CDOM) fluorescence and its contribution to light attenuation in UK waterbodies. Estuar. Coast. Shelf Sci. **79**: 707–717.

Friedrichs, M. A. M., M. E. Carr, R. T. Barber, M. Scardi, D. Antoine, R. A. Armstrong, I. Asanuma, M. J. Behrenfeld, E. T. Buitenhuis, F. Chai, J. R. Christian, A. M. Ciotti, S. C. Doney, M. Dowell, J. Dunne, B. Gentili, W. Gregg, N. Hoepffner, J. Ishizaka, T. Kameda, I. Lima, J. Marra, F. Mélin, J. K. Moore, A. Morel, R. T. O'Malley, J. O'Reilly, V. S. Saba, M. Schmeltz, T. J. Smyth, J. Tjiputra, K. Waters, T. K. Westberry, and A. Winguth. 2009. Assessing the uncertainties of model estimates of primary productivity in the tropical Pacific Ocean. J. Mar. Syst. **76**: 113–133.

Fujii, M., E. Boss, and F. Chai. 2007. The value of adding optics to ecosystem models: a case study. Biogeosciences Discuss. **4**: 1585–1631.

Geider, R. J., H. L. MacIntyre, and T. M. Kana. 1998. A dynamic regulatory model of phytoplanktonic acclimation to light, nutrients, and temperature. Limnol. Oceanogr. **43**: 679–694.

Graff, J. R., A. J. Milligan, and M. J. Behrenfeld. 2012. The measurement of phytoplankton biomass using flow-cytometric sorting and elemental analysis of carbon. Limnol. Oceanogr. Methods **10**: 910–920.

Han, G., C. G. Hannah, J. W. Loder, and P. C. Smith. 1997. Seasonal variation of the three-dimensional mean circulation over the Scotian Shelf. J. Geophys. Res. **102**: 1011.

Hannah, C. G., J. A. Shore, J. W. Loder, and C. E. Naimie. 2001. Seasonal Circulation on the Western and Central Scotian Shelf. J. Phys. Oceanogr. **31**: 591–615.

Hersh, D., and W. S. Leo. 2012. A new calibration method for in situ fluorescence. Bost. Massachusetts Water Resour. Auth. Report 2012–06. 11p.

Holm-Hansen, O., C. J. Lorenzen, R. W. Holmes, and J. D. H. Strickland. 1965. Fluorometric determination of chlorophyll. ICES J. Mar. Sci. **30**: 3–15.

Hovis, W. A., D. K. Clark, F. Anderson, R. W. Austin, W. H. Wilson, E. T. Baker, D. Ball, H. R. Gordon, J. L. Mueller, S. Z. El-Sayed, B. Sturm, R. C. Wrigley, and C. S. Yentsch. 1980. Nimbus-7 Coastal Zone Color Scanner: System description and initial imagery. Science. **210**: 60–63.

Huot, Y., and M. Babin. 2010. Overview of fluorescence protocols: Theory, basic concepts, and practice, p. 31–74. *In* Chlorophyll a Fluorescence in Aquatic Sciences: Methods and Applications. Springer Netherlands.

Huot, Y., M. Babin, F. Bruyant, C. Grob, M. S. Twardowski, and H. Claustre. 2007. Does chlorophyll *a* provide the best index of phytoplankton biomass for primary productivity studies? Biogeosciences Discuss. **4**: 707–745.

Johnson, K. S., W. M. Berelson, E. S. Boss, H. Chase, Z. Claustre, S. R. Emerson, N. Gruber, A. Kortzinger, M. J. Perry, and S. C. Riser. 2009. Observing biogeochemical cycles at global scales with profiling floats and gliders. Oceanography **22**: 216–225.

Karl, D. M. 2014. Contemporary challenge of the sea: Science, society, and sustainability. Oceanography **27**: 208–225.

Kiefer, D. A. 1973a. Fluorescence properties of natural phytoplankton populations. Mar. Biol. **22**: 263–269.

Kiefer, D. A. 1973b. Chlorophyll a fluorescence in marine centric diatoms: Responses of chloroplasts to light and nutrient stress. Mar. Biol. **23**: 39–46.

Kirk, J. T. O. 2011. Light and Photosynthesis in Aquatic Ecosystems: Third Edition, Cambridge University Press.

Kolber, Z., and P. G. Falkowski. 1993. Use of active fluorescence to estimate phytoplankton photosynthesis in situ. Limnol. Oceanogr. **38**: 1646–1665.

Krause, G. H., and E. Weis. 1991. Chlorophyll fluorescene and photosynthesis: the basics. Annu. Rev. Plant Physiol. Plant Mol. Biol. **42**: 313–349.

Kruskopf, M., and K. J. Flynn. 2006. Chlorophyll content and fluorescence responses cannot be used to gauge reliably phytoplankton biomass, nutrient status or growth rate. New Phytol. **169**: 525–536.

Lavigne, H., F. D'Ortenzio, H. Claustre, and A. Poteau. 2012. Towards a merged satellite and in situ fluorescence ocean chlorophyll product. Biogeosciences **9**: 2111–2125.

Lawrenz, E., and T. L. Richardson. 2010. How does the species used for calibration affect chlorophyll a measurements by in situ fluorometry? Estuaries and Coasts **34**: 872–883.

Lehaitre, M., L. Delauey, and C. Compere. 2008. Biofouling and underwater measurements, p. 463–493. *In* Real-time Coastal Observing Systems for Marine Ecosystem Dynamics and Harmful Algal Blooms: Theory, Instrumentation and Modelling. UNESCO.

Lindsey, R., and D. Herring. 2002. MODIS: Moderate-Resolution Imaging Spectrometer. 25p.

Loftus, M. E., and H. H. Seliger. 1975. Some limitations of the in vivo fluorescence technique. Chesap. Sci. **16**: 79–92.

Lorenzen, C. J. 1966. A method for the continuous measurement of in vivo chlorophyll concentration. Deep. Res. **13**: 223–227.

Lorenzen, C. J. 1967. Determination of chlorophyll and pheo-pigments: Spectrophotometric equations. Limnol. Oceanogr. **12**: 343–346.

Lorenzen, C. J. 1972. Extinction of light in the ocean by phytoplankton. J. Cons. int. Explor. Mer. **34**: 262–267.

MacIntyre, H. L., T. M. Kana, T. Anning, and R. J. Geider. 2002. Photoacclimation of photosynthesis irradiance response curves and photosynthetic pigments in microalgae and cyanobacteria. J. Phycol **38**: 17–38.

MacIntyre, H. L., E. Lawrenz, and T. L. Richardson. 2010. Taxonomic discrimination of phytoplankton by spectral fluorescence, *In* Chlorophyll a Fluorescence in Aquatic Sciences: Methods and Applications. Springer Netherlands.

McDougall, T. J., R. Feistel, D. G. Wright, R. Pawlowicz, F. J. Millero, D. R. Jackett, B. A. King, G. M. Marion, S. Seiz, P. Spitzer, and C. T. A. Chen. 2010. The international thermodynamic equation of seawater – 2010: Calculation and use of thermodynamic properties. Intergov. Oceanogr. Comm. Manuals Guid. **56**: 218p.

Mignot, A., H. Claustre, F. D'Ortenzio, X. Xing, A. Poteau, and J. Ras. 2011. From the shape of the vertical profile of in vivo fluorescence to Chlorophyll-a concentration. Biogeosciences **8**: 2391–2406.

Mobley, C. D. 1994. Light and Water: Radiative Transfer in Natural Waters, Academic Press.

Mobley, C., D. Stramski, W. P. Bissett, and E. Boss. 2004. Optical modeling of ocean water: is the Case 1 - Case 2 classification still useful? Oceanography **17**: 60–67.

Moe, A. E., S. Marx, N. Banani, M. Liu, B. Marquardt, and D. M. Wilson. 2005. Improvements in LED-based fluorescence analysis systems. Sensors Actuators, B Chem. **111-112**: 230–241.

Monterey, G. I., and S. Levitus. 1997. Climatological cycle of mixed layer depth in the world ocean. NOAA Atlas NESDIS 14, U.S. Gov. Printing Office.

Morel, A. 1988. Optical modeling of the upper ocean in relation to its biogenous matter content (Case I waters). J. Geophys. Res. **93**: 10,749–10,768.

Morel, A., Y. Huot, B. Gentili, J. P. Werdell, S. B. Hooker, and B. A. Franz. 2007. Examining the consistency of products derived from various ocean color sensors in open ocean (Case 1) waters in the perspective of a multi-sensor approach. Remote Sens. Environ. **111**: 69–88.

Morel, A., and S. Maritorena. 2001. Bio-optical properties of oceanic waters: a reappraisal. J. Geophys. Res. **106**: 7163.

Morel, A., and L. Prieur. 1977. Analysis of variations in ocean color. Limnol. Oceanogr. **22**: 709–722.

Morrison, J. R. 2003. In situ determination of the quantum yield of phytoplankton chlorophyll a fluorescence: a simple algorithm, observations, and a model. Limnol. Oceanogr. **48**: 618–631.

Müller, P., X. P. Li, and K. K. Niyogi. 2001. Non-photochemical quenching. A response to excess light energy. Plant Physiol. **125**: 1558–1566.

Munk, W. M. 2000. Oceanography before, and after, the advent of satellites, p. 1–4. *In* Satellites, oceanography and society. Elsevier.

OTN. 2015. Ocean Gliders and Marine Observation, available at http://gliders.oceantrack.org (last accessed Nov 24 2015).

Perry, M. J., and R. W. Eppley. 1981. Phosphate uptake by phytoplankton in the central North Pacific Ocean. Deep Sea Res. Part A. Oceanogr. Res. Pap. **28**: 39–49.

Perry, M. J., B. S. Sackmann, C. C. Eriksen, and C. M. Lee. 2008. Seaglider observations of blooms and subsurface chlorophyll maxima off the Washington coast. Limno **53**: 2169–2179.

Petrie, B. 2004. The Halifax Section: A Brief History. AZMP Bull. **4**: 26–29.

Pope, R. M., and E. S. Fry. 1997. Absorption spectrum (380-700 nm) of pure water. II. Integrating cavity measurements. Appl. Opt. **36**: 8710–8723.

Preisendorfer, R. W. 1961. Application of radiative transfer theory to light measurements in the sea, p. 11–30. *In* Radiant energy in the Sea.

Proctor, C. W., and C. S. Roesler. 2010. New insights on obtaining phytoplankton concentration and composition from in situ multispectral chlorophyll fluorescence. Limnol. Oceanogr. Methods **8**: 695–708.

Ras, J., H. Claustre, and J. Uitz. 2008. Spatial variability of phytoplankton pigment distributions in the Subtropical South Pacific Ocean: comparison between in situ and predicted data. Biogeosciences Discuss. **4**: 3409–3451.

Roesler, C. S., and A. H. Barnard. 2014. Optical proxy for phytoplankton biomass in the absence of photophysiology: Rethinking the absorption line height. Methods Oceanogr. **7**: 79–94.

Roesler, C. S., and E. S. Boss. 2008. In situ measurement of the Inherent Optial Properties (IOPs) and potential for Harmful Algal Bloom (HAB) detection and coastal ecosystem observations, p. 153–206. *In* Real-time Coastal Observing Systems for Marine Ecosystem Dynamics and Harmful Algal Blooms: Theory, Instrumentation and Modelling. UNESCO.

Roesler, C. S., M. J. Perry, and K. L. Carder. 1989. Modeling in situ phytoplankton absorption from total absorption spectra in productive inland marine waters. Limnol. Oceanogr. **34**: 1510–1523.

Rousseaux, C., and W. Gregg. 2014. Interannual variation in phytoplankton primary production at a global scale. Remote Sens. **6**: 1–19.

Roy, S., C. A. Llewellyn, E. S. Egeland, and G. Johnsen. 2011. Epoxidation, de-epoxidation and the xanthophyll cycles, p. 131–133. *In* Phytoplankton Pigments: Characterization, Chemotaxonomy and Applications in Oceanography. Cambridge University Press.

Ryther, J. H., and C. S. Yentsch. 1957. The estimation of phytoplankton production in the ocean from chlorophyll and light data. Limnol. Oceanogr. **2**: 281–286.

Sackmann, B. S., M. J. Perry, and C. C. Eriksen. 2008. Seaglider observations of variability in daytime fluorescence quenching of chlorophyll-*a* in Northeastern Pacific coastal waters. Biogeosciences Discuss. **5**: 2839–2865.

Sathyendranath, S., V. Stuart, A. Nair, K. Oka, T. Nakane, H. Bouman, M. H. Forget, H. Maass, and T. Platt. 2009. Carbon-to-chlorophyll ratio and growth rate of phytoplankton in the sea. Mar. Ecol. Prog. Ser. **383**: 73–84.

Satlantic. 2011. Operation Manual for OCR-504. 66p.

Schallenberg, C., M. R. Lewis, D. E. Kelley, and J. J. Cullen. 2008. Inferred influence of nutrient availability on the relationship between Sun-induced chlorophyll fluorescence and incident irradiance in the Bering Sea. J. Geophys. Res. **113**: 21p.

Simonetti, P. 1992. Slocum Glider: Design and 1991 field trials. 46p.

Smith, R. C., and K. S. Baker. 1978. Optical classification of natural waters. Limnol. Oceanogr. **23**: 260–267.

Sosik, H. 1996. Bio-optical modeling of primary production:consequences of variability in quantum yield and specific absorption. Mar. Ecol. Prog. Ser. **143**: 225–238.

Stommel, H. 1963. Varieties of oceanographic experience. Science. **139**: 572–576.

Stramski, D., E. Boss, D. Bogucki, and K. J. Voss. 2004. The role of seawater constituents in light backscattering in the ocean. Prog. Oceanogr. **61**: 27–56.

Sullivan, J. M., M. S. Twardowski, J. R. Zaneveld, and C. C. Moore. 2013. Measuring optical backscattering in water, p. 189–224. *In* Light Scattering Reviews 7. Springer Berlin Heidelberg.

Therriault, J., P. B., P. Pepin, J. Gagnon, D. Gregory, J. Helbig, A. Herman, D. Lefaivre, M. Mitchell, B. Pelchat, J. Runge, and D. Sameoto. 1998. Proposal for a northwest Atlantic zonal monitoring program. Can. Tech. Rep. Hydrogr. Ocean Sci. **194**: vii+57p.

Webb, D. C., P. J. Simonetti, and C. P. Jones. 2001. SLOCUM: An underwater glider propelled by environmental energy. IEEE J. Ocean. Eng. **26**: 447–452.

Welschmeyer, N. A. 1994. Fluorometric analysis of chlorophyll a in the presence of chlorophyll b and pheopigments. Limnol. Oceanogr. **39**: 1985–1992.

WETLabs. 2011. Scattering Meter ECO BB User's Guide. 29p.

Woźniak, B., J. Dera, D. Ficek, M. Ostrowska, and S. Kaczmarek. 2003. Modelling light and photosynthesis in the marine environment. Oceanologia **45**: 171–245.

Xing, X., A. Morel, H. Claustre, D. Antoine, F. D'Ortenzio, A. Poteau, and A. Mignot. 2011. Combined processing and mutual interpretation of radiometry and fluorimetry from autonomous profiling Bio-Argo floats: Chlorophyll a retrieval. J. Geophys. Res. **116**: 14p.

Xing, X., A. Morel, H. Claustre, F. D'Ortenzio, and A. Poteau. 2012. Combined processing and mutual interpretation of radiometry and fluorometry from autonomous profiling Bio-Argo floats: 2. Colored dissolved organic matter absorption retrieval. J. Geophys. Res. **117**: 16p.

Yentsch, C. S., and D. A. Phinney. 1989. A bridge between ocean optics and microbial ecology. Limnol. Oceanogr. **34**: 1694–1705.

Zaneveld, J. R., E. Boss, and A. Barnard. 2001. Influence of surface waves on measured and modeled irradiance profiles. Appl. Opt. **40**: 1442–1449.

Zeng, L., and D. Li. 2015. Development of in situ sensors for chlorophyll concentration measurement. J. Sensors **2015**: 16p.

Zhang, X., L. Hu, and M.-X. He. 2009. Scattering by pure seawater at high salinity. Opt. Express **17**: 12685–12691.